Guidelines for Authors

This periodical is a publication of the Academic Publishing and Translation Directorate of Qassim University. Its purpose is to provide an opportunity for scholars to publish their original research.

Manuscripts will be published in on of the following platforms:

i) **Article:** It should be original and has a significant contribution to the field in which the research was conducted.
ii) **Review Article:** A critical synthesis of the current literature in a particular field, or a synthesis of the literature in a particular field during an explicit period of time.
iii) **Brief Article (Technical Notes):** A short article (note) having the same characteristics as an article.
iv) **Innovation and Invention Reports**
v) **Forum:** Letters to the Editor, comments and responses, preliminary results or findings, and miscellany.
vi) **Book Reviews**

The Editorial Board will consider manuscripts in the following fields:

- Electrical Engineering
- Civil Engineering
- Mechanical Engineering
- Chemical Engineering
- Computer Engineering
- Mining and Petroleum Engineering
- Computer Science
- Information Technology
- Information Systems
- Basic Engineering and Computer Sciences

A manuscript should be submitted in English, and, if accepted for publication, it should not be published elsewhere without the written permission of the Editor-in-Chief.

General Instructions

1. **Submission of manuscripts for publication:** Papers must be presented in final page format (not more than 20 pages, A4 size), along with a compact disk (CD) containing the contribution executed on a PC using MS Word or any updated version of it. Manuscripts should be typed using Times New Roman, 12 points font, and one and half space. Pages are to be numbered consecutively and are to include all illustrative material, such as tables and figures, in their appropriate places in the text. If the author does not follow these guidelines, the paper is likely to be rejected or delayed.
2. **Abstracts:** Manuscripts for articles, review articles, and brief articles require both Arabic and English abstracts, using not more than 200 words..
3. **Keywords:** Each article must have keywords before both abstracts (English and Arabic) and they should not exceed 10 words.
4. **Tables and other illustrations:** Tables, figures, charts, graphs and plates should be planned to fit the Journal's page size (A4 incl. running heads). Line drawings are to be presented on high quality tracing paper using black India ink. Copies are not permitted for use as originals. Line quality is required to be uniform, distinct, and in proportion to the illustration. Photographs may be submitted on glossy print paper, in either black and white, or color, or made by using Adobe Photoshop. Tables and other illustrative material must include headings or titles, and captions for figures.

5. **Abbreviations:** The names of periodicals should be abbreviated in accordance with *The World List of Scientific Periodicals.* e.g., *et al., J. of Food Sci.*
For weights and measurements, and where appropriate, abbreviations rather than words are to be used, e.g., cm, mm, m, km, cc, ml, g, kg, min, %, etc., Fig.
Latin abbreviations such as: *op. cit., loc. cit., ibid.,* are to be in italic (if they are used).
6.**References:** References are mentioned numerically [between brackets] in the text and a list of references are provided at the end of the manuscript as follows:
a- Journals: [number] followed by the last name of the author (authors), First name or abbreviation, "paper title" , journal title , volume and issue numbers, (the year of publications between parentheses) , and page numbers.
Example: Sawyer, D. A. "Pounding of Rainwater on Flexible Roof Systems," Proceedings ASCE, Journal of the Structural Division, Vol. 93, No. 1, (1967), pp.127-147.
b- Books: Book references must include author, book title, the publisher's location, and publisher, and the year of publication.
Example: Feld, J., and Carper, K., Construction failure, 2nd Ed., New York, Wiley, 1997.
7. **Content Note or Footnote:** A content note or footnote is a note from the author to the reader providing clarifying information. A content note is indicated in the text by using a half-space superscript number (e.g. … books[3] are …). Content notes are to be sequentially numbered throughout the text. A reference may be cited in a content note by the use of the standard (Author, Date) style in the same way they are used in the text.
Content notes are to be presented below a solid half-line separating them from the text of the page in which the footnote is mentioned (in single column). Use the same half-space superscript number assigned in the content note(s) in the text to precede the content note itself.
8. **Proofs:** No changes, additions or deletions will be allowed in the pageproof stage.
9. **Opinions:** Manuscripts submitted to the Journal for publication contain the author's conclusions and opinions and, if published, do not constitute a conclusion or opinion of the Editorial Board.
10. **Offprints:** Two copies of the journal and twenty reprints of the accepted papers will be sent to the authors.
11. **Correspondence:** All correspondence may be addressed to:

E-mail: quecjour@qec.edu.sa

12. **Frequency:** …Two issues per year…….

Subscription and Exchange:

E-mail: quecjour@qec.edu.sa

In The Name of ALLAH,
Most Gracious, Most Merciful

Journal of Engineering and Computer Sciences, Qassim University, Vol. 3, No. 1, PP 1-71, for English (January 2010/Muharram 1431H.)

Volume (3) **No. (1)**

Journal of Engineering and Computer Sciences

(January 2010) **(Muharram 1431H)**

Qassim University Scientific Publications

(Refereed Journal)

Qassim University

Academic Publishing & Translation

Buraydah - P. O. Box 6666 -51452

EDITORIAL BOARD

Deposif: 1429/2023

Journal of Engineering and Computer Sciences, Qassim University, Vol. 3, No. 1, PP 1-71, for English (January 2010/Muharram 1431H.)

Contents

Page

Journal of Engineering and Computer Sciences, Qassim University, Vol. 3, No. 1, pp. 1-9 (January 2010/Muharram 1431H)

Soil and Groundwater Contamination due to Leaking Underground Fuel Tanks (UFT) in Saudi Arabia

S. M. ElKholy[(1)] and I. S. AlSalamah[(2)]

(1) Associate Professor of Geotechnical Engineering,, Civil Engineering Department, College of Engineering, Qassim University, Saudi Arabia, selkholy@qec.edu.sa,, On leave from: Construction Research Institute, National Water Research Center of Egypt
(2) Associate Professor of Hydrology/Water Resources Engineering, , Civil Engineering Department, College of Engineering, Qassim University, Saudi Arabia, alsalamah@qec.edu.sa.

(Received 4/6/2009; accepted for publication 28/7/2009)

Abstract: Gasoline is a complex contamination agent, which may be originated from a variety of contamination sources. Sources may include, among others, leakage of underground fuel storage tanks in gas stations and large farms. Identifying and quantifying the soil and groundwater contaminations due to leakage from the underground gasoline tanks are of primary importance in providing better regulations to protect the environment. This subject has not received much of researchers' attention in the Gulf area which is recognized by its huge oil production industry.

In AlQassim region of Saudi Arabia, most of the existing gas stations are more than 25 years old when the region started its development era. There were no environmental regulations for constructing the gas stations and the technology used for the underground gasoline tanks is outdated compared with the nowadays technology. Therefore, it is expected that soil and/or groundwater contamination has been taking place for years.

The current research presents an attempt to assess the risks associated with soil and groundwater contamination due to gasoline leakage from underground fuel tanks. A geo-environmental investigation is conducted for two gas stations in the City of Buraidah, the largest in AlQassim region. The results of the study showed that there is an actual case of gasoline leakage which led to soil contamination with gasoline substances. This soil contamination might also threat the groundwater resources in the region due to the leaching phenomenon. The study draws the attention of the authorities to the seriousness of this problem and the importance of starting a remediation process to overcome the problem.

Keywords: Saudi Arabia, AlQassim, soil contamination, groundwater contamination, underground fuel tanks.

1. Introduction

Gasoline is a complex contamination agent, which may be originated from a variety of contamination sources. Sources may include, among others, leakage of underground fuel storage tanks in gas stations and large farms. Identifying and quantifying the soil and groundwater contaminations due to leakage from the underground gasoline tanks are of primary importance in providing better regulations to protect the environment.

In AlQassim region of Saudi Arabia, most of the existing gas stations are more than 25 years old when the region started its development era. Not only that but rural farms in the region depends in its fuel supply on underground fuels tanks. The technology used then for the construction of the stations as well as the underground gasoline tanks are outdated and did not consider the appropriate international standard environment protection regulations. While this subject has received much of the researchers' attention in other countries (US and Europe), it has not yet received the same attention in the Gulf area, which is recognized by its huge oil production industry. Therefore, it is expected that soil and/or groundwater contamination has been taking place and accumulating for years. Following, we will present some of the reported cases of soil/groundwater contamination with gasoline products due to UFT.

In the USA, storage tanks for vehicle fuel and heating oil are common on farms and rural residences nationwide. These underground tanks historically have been constructed of steel, and over the years tens of thousands of the tanks have corroded and leaked petroleum products into soil and groundwater. Underground tanks are also subject to spills when refilling or pumping. Even small leaks can add up to big problems. A significant extensive study (ten years long) in that field sponsored by the California State Water Resources Control Board (SWRCB), Underground Storage Tank (UST) Program was published in 1995 [1]. The goal of the study was to collect data about the fate and transport of Fuel Hydrocarbons (FHC) released into California's diverse hydrogeologic settings and the impacts these releases may have on groundwater resources. The study investigated the FHC plumes, the factors that influence the length and mass of FHC plumes, the extent of the FHC plumes impact on groundwater resources, and the results of the remediation process of the contaminated sites. Plume lengths were defined using a benzene concentration of 10 ppb (parts per billion). The study involved 5700 contaminated sites in the state of California. For each site, a time series of estimated benzene plume lengths, average benzene concentrations, and groundwater data were determined. Borehole logs were used to identify soil lithologic types present at the site. The study showed that Sixty three percent of the sites showed a relationship between increasing TPHg and decreasing O_2 groundwater concentrations. The study showed that plume's geometry tends to change slowly with time. In general, plume lengths change slowly and tend to stabilize at relatively short distances from the FHC release site and an active remediation helps reduce plume mass. The results also indicated that 16% of the well characterized sites were found to have average benzene concentrations greater than 10 ppb, while 42% of the sites had stable plume lengths. This finding may be expected because plume concentrations tend to decrease more rapidly and frequently than plume lengths, and there is a greater probability of finding a stable plume length than a stable plume concentration. The study presented a detailed comprehensive model for detecting, estimating, and remediation of groundwater contamination sites. The study also presented few techniques for remediation such as over-excavation, and pump and treat. Some of the important conclusions drawn from the study were; over-excavation can reduce the likelihood of benzene getting into the groundwater in high concentrations, especially in sites with shallow groundwater. Application of pump and treat technique may increase the chances of significantly decreasing trends in average plume concentration, and over excavation technique may further increase the chances. Plumes at sites with very shallow groundwater almost never show increasing lengths, while those at sites with relatively deep groundwater are more likely to grow; which is the case of groundwater conditions in AlQassim. This study led to overall changes in the technology used to construct underground fuel tanks in the USA and the regulations that control them as well as the remediation procedures.

In a report published by the State of Wisconsin Department of Commerce, it was mentioned that the underground gasoline tanks begin leaking after 12 to 17 years [2]. They also mentioned that a tank leaking one drop every 10 seconds could release 60 gallons per year and it takes only a few quarts of gasoline to severely contaminate soil/groundwater causing environmental and health problems [2]. Figure (1) shows a schematic diagram for a leaking underground fuel tank and the associated potential risk [2]. Figure (2) shows a removed damaged underground tank in the state of California, USA [3]. The two figures clearly show why people and authorities should be very concerned.

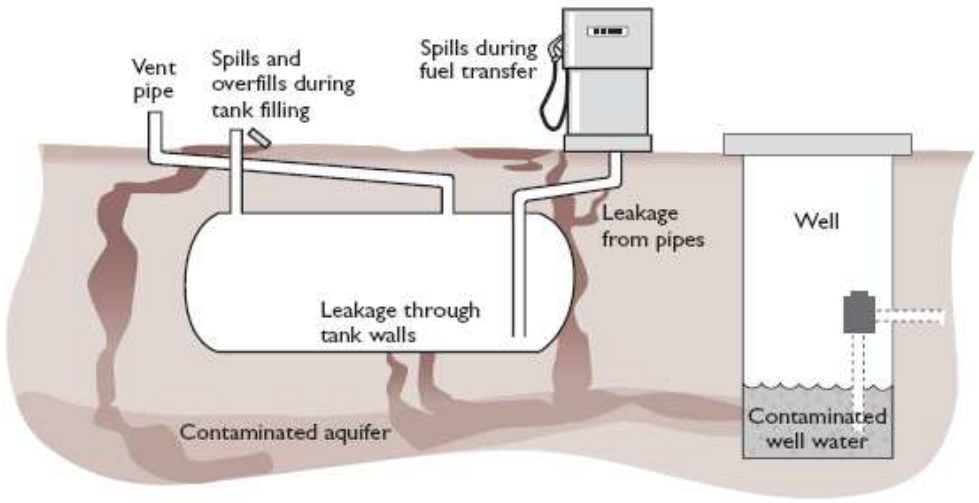

Figure (1). A schematic diagram for a leaking underground fuel tank in a gas station. [2]

Figure (2). A damaged underground fuel tank in California, USA. [3]

The USA Federal Emergency Management Agency (FEMA) has known since at least the 1990s that tanks under its supervision around the country could be leaking fuel into soil and groundwater [3]. The FEMA tanks are part of a larger problem. More than 500,000 leaking storage tanks – most of which are filled with fuel and oil – are buried across the country. Because they're underground, leaking tanks can go undetected for years. If diesel leaks into drinking water, affected people could be at a higher risk of cancer, kidney damage and nervous system disorders. A gallon of fuel can contaminate 1 million gallons of water [3].

The common life expectancy of buried benzene tanks is 10-15 years. At about 20 years, the risk of leaks from buried steel oil tanks becomes significant [4]. Leaks can occur earlier if a tank was damaged at installation or was not properly piped. The same reference presented probable causes for underground fuel tank leaks such as; in-tank corrosion, external rust, corrosive soils, leaking of buried piping connections, and delivery and in-door spills. In the State of New England, for a two year period [1984-5] among customers who have buried

heating oil tanks (16% of total customers) surveyors found an average of 1.7 oil tank leaks per thousand customers. The researchers studying these oil tank leak rates also found 2.5 fuel line leaks per 1000 oil heating customers [5]. Shih *et al*. (2004) investigated the impact of fuel hydrocarbons and oxygenates from leaking underground fuel tanks on groundwater resources [6]. The study evaluated the potential for groundwater resource contamination by fuel hydrocarbons (FHC) and oxygenates (e.g., *tert*-butyl alcohol [TBA], *tert*-amyl methyl ether [TAME], diisopropyl ether [DIPE], ethyl *tert*-butyl ether [ETBE], and methyl tert-butyl ether [MTBE]) by examining their occurrence, distribution, and spatial extent in groundwater beneath leaking underground fuel tank (LUFT) facilities. The data was collected from over 7200 monitoring wells in 868 LUFT sites from the City of Los Angeles, California, USA. The study results demonstrated that MTBE poses the greatest problem, followed by TBA and benzene. Day *et al*. (2001) investigated the fate and transport of fuel components below leaking underground storage tanks (LUFT) in the City of Denver, Colorado, USA [7]. They stated that leak detection is primarily dependent on physical measurement systems that are generally capable of detecting leak rates as small as 0.2 L/h. The risk was evaluated by modeling fate and transport of fuel components from small LUFT leaks. It was found that small leaks do have the potential to impact shallow groundwater. They concluded that routine monitoring of shallow groundwater should be a component of a leak detection program, particularly in high-risk areas. Corapcioglu (1987) and Baehr (1987) introduced compositional multiphase model for groundwater contamination by petroleum products and solved numerically utilizing numerical analysis technique [8], [9].

Several studies were conducted to investigate the mechanism by which the spilled or leaked fuel transports through subsurface soil layers if effective investigative and remedial measures are to be implemented. As mentioned by Rice *et al*. (1995), once liquid FHC are released into the subsurface, they percolate through the unsaturated zone soil pore spaces, at first under the force of gravity. The lithologic heterogeneity, moisture content, and permeability of the soils determine the amount of liquid retained in the soil and the extent of the lateral spreading of liquid and gaseous hydrocarbons. As liquid- and gaseousphase FHC move through the unsaturated zone, they will follow the path of least resistance. When dense, low permeability layers are encountered, the bulk FHC liquid flowing under the force of gravity will tend to spread [10]. A portion of the FHC mass will adhere onto soil particulates [11] or simply lodge in pore throat necks and dead-end pore spaces [12], [13]. The amount of FHC adhered onto soil particulates is dependent on the amount of organic material and type of minerals present in the soil matrix [11].

All the above mentioned literature emphasizes the seriousness of this problem and that it has been under investigations by researches in the USA for years. Therefore it is about time that it gets the appropriate attention in the Meddle East in general and Saudi Arabia and the gulf area in particular. The current study aims only at shading the light on the problem in order to grab the attention of authorities, researchers, and funding agencies to look deeply into the problem. The study is the first step among a series of studies which will be conducted in the future which hopefully shall lead to improving the environmental protection regulations in AlQassim.

2. Methodology of Study

The program of the study involves conducting a field study of the gas stations that exist within the limits of the City of Buraidah, AlQassim. The objective of the field study is to collect data about gas stations including age of the stations, ownership, frequency and method of fuel refilling, type of fuel, and any information about spill accidents. This information is statistically analyzed, and the results are presented in the form of the appropriate tables and figures. Following, two of the oldest gas stations studied were selected to conduct a geo-environmental study in order to determine the status of soil and groundwater within the sites of the selected gas stations. Four boreholes (10 m depth) were executed; two at each site, and soil samples were collected at an interval of 1.0 m or at change of soil nature. The collected soil samples were tested in the laboratory to determine the nature of soil at the sites. The water table couldn’t be reached during the boreholes excavation and consequently there were no collected groundwater samples. The soil samples are then chemically tested in order to examine the existence of any traces of benzene contamination or any of its substances. The concentration of the existing harmful substance, if any, was determined in the form of a percentage by weight of the tested sample. Figures (3) and (4) show the locations of the two selected sites for the study. The figures also show that the two gas stations are constructed nearby residential areas which means that there is an actual environmental threats to the health and of the people living in the area.

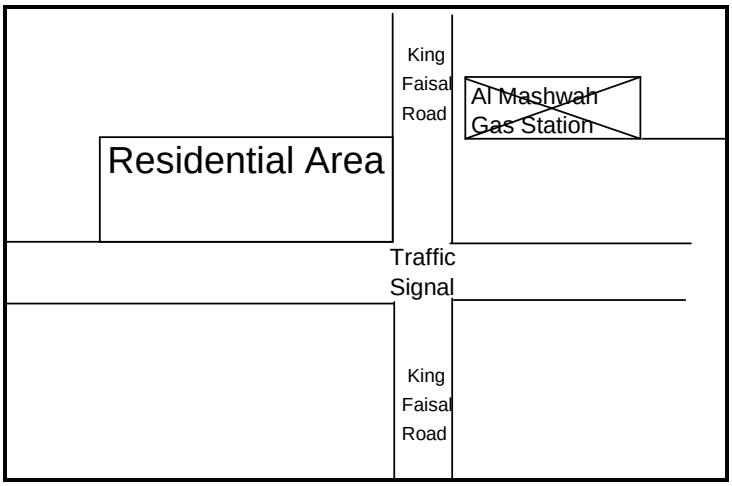

Figure (3). The location of the first gas station in the City of Buraidah.

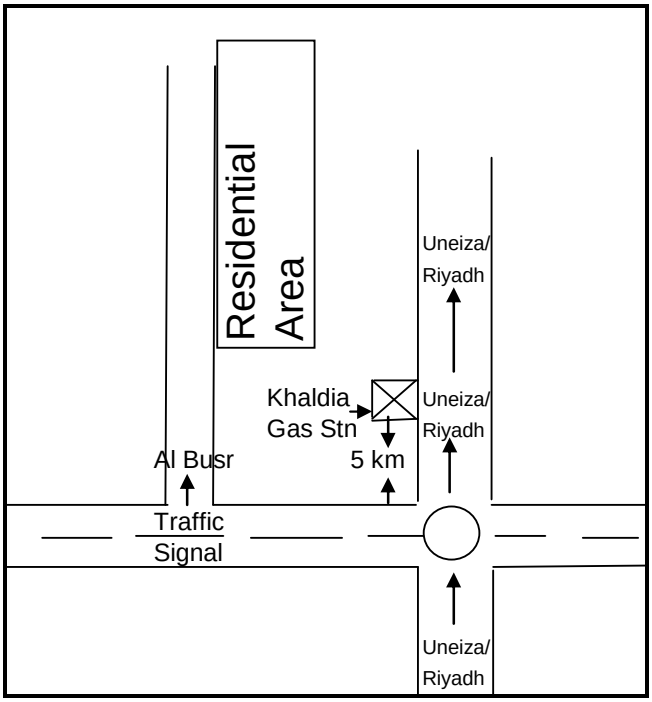

Figure (4). The location of the second gas station in the City of Buraidah.

3. Results and Discussion

3.1 Soil profile

The visual description of the collected soil samples at the two investigated sites showed that the soil profile tends to be of sandy soil with traces of gravel in some areas. The samples were subjected to grain size analysis in order to determine its nature and particle size gradation. The results of the lab tests showed that the soil profile at both sites are composed of surface soil of silt and sand with a varying thickness of 0.5 – 1.0 m. The successive soil layers were found to be graded sand from medium to course with traces of silt and gravel at various depths from ground surface. These soil layers are characterized of high permeability which ranges from 10^{-1} – 10^{-3} cm/s which reflects the high infiltration rate of rain water fall. Figure (5) shows the general soil profile at the investigated sites.

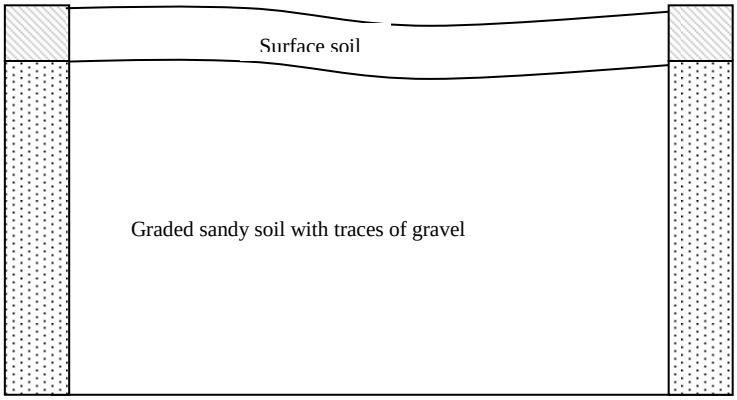

Figure (5). The general soil profile at the sites of investigation.

3.2 Results of chemical tests

The chemical tests were conducted on the soil samples collected at two levels from ground surface (4.0 and 6.0 m). Almost all collected soil samples were observed to have flammable solvents in appreciable amount. In particular samples of BH-03 and BH-04 have high flammable solvents; where as samples of BH-01 and BH-02 have higher hydrocarbons content.

The objectives of the chemical tests were to investigate the existence of any harmful chemical compounds and determine its percentages by weight of the soil samples weight. The investigated harmful compounds include benzene and/or diesel fuel, and any of their substances specially hydrocarbons. Examples of investigated compounds include but not limited to; Dodecane, Tridecane, and Pentadecane which are chemical compounds that consist only of the elements carbon I and hydrogen (H) (i.e., hydrocarbons), wherein these atoms are linked together exclusively by single bonds (i.e., they are saturated compounds) without any cyclic structure (i.e. loops). These compounds are known to be harmful and may cause lung damage if swallowed. They also may be harmful by inhalation or skin absorption, or act as an irritant [14]. Tables (1) and (2) show the results of the chemical tests conducted on the soil samples in the form of % by weight, of the soil sample, of the harmful hydrocarbon compounds.

Table (1). Results of the chemical tests conducted on the soil samples collected at Gas Station (1) at 4.0 and 6.0 m depths.

Test Parameters	% of hydrocarbons by Wt of Soil Samples	
	BH-01 Depth 4.0 m	BH-02 Depth 6.0 m
Dodecane $$ n-Dodecane-C12H26	0.234581	0.685269
Tridecane C13H28	0.785965	1.023695
Tetradecane-C14H30	1.235680	3.263851
Pentadecane-C15H32	2.358640	5.036925
Heptadecane-C17H36	2.012530	6.369810
Heneicosane-C21H44	3.256480	2.023689
Heptadecane-C17H46	2.365810	8.326981
Heneicosane-C21H44	4.359820	8.301200
Hexadecane,2,6,10,14-tetramethyl-C20H42	1.356820	1.235680
Nonadecane-C19H40	3.256980	8.156840
Eicosane-C20H42	4.356958	7.123580
Tetracosane-C24H50	3.356821	6.258680
Tetratriacontane-C34H70	2.359850	5.156380
Octacosane-C28H58	1.985621	2.356450
1-Pentene, 3-methyl-C6H12	15.7908	27.23022
Pentane, 3-methyl	20.50433	34.05188
4-Methyldocosane C23H48	9.90565	16.80349
1-Docosene	1.737667	2.957531

Table (2). Results of the chemical tests conducted on the soil samples collected at Gas Station (2) at 4.0 and 6.0 m depths.

Test Parameters	% of hydrocarbons by Wt of Soil Samples	
	BH-01 Depth 4.0 m	BH-02 Depth 6.0 m
Dodecane $$ n-Dodecane-C12H26	0.586319	0.977198
Tridecane C13H28	1.316936	2.194893
Tetradecane-C14H30	3.201052	5.335087
Pentadecane-C15H32	4.45537	7.42561
Heptadecane-C17H36	5.309717	8.849528
Heneicosane-C21H44	2.169556	3.615927
Heptadecane-C17H46	6.58337	10.97228
Heneicosane-C21H44	6.65061	11.08435
Hexadecane,2,6,10,14-tetramethyl-C20H42	2.347495	3.912491
Nonadecane-C19H40	6.69362	11.15604
Eicosane-C20H42	6.5180	10.8633
Tetracosane-C24H50	5.728577	9.547628
Tetratriacontane-C34H70	4.879555	8.132591
Octacosane-C28H58	3.55985	5.93308
1-Pentene, 3-methyl-C6H12	10.32212	19.23568
Pentane, 3-methyl	15.2354	18.35682
4-Methyldocosane C23H48	8.02563	12.3568
1-Docosene	1.65863	1.89654

3.3 Discussion

The results of the chemical analysis as shown in Tables (1) and (2) show that there is a serious problem that needs to be looked at. The concentrations of the hydrocarbons exist in the collected soil samples poses environmental threats to people living near-by the investigated gas stations. The water table couldn't be reached during the boreholes excavation and consequently there were no collected groundwater samples. The study scope did not include executing deep sampling in order to collect groundwater samples. However, increasing concentrations of hydrocarbons in the soil coupled with the high permeability nature of it would eventually lead to the development of a leaching process of contaminants to reach the groundwater aquifer in the area.

4. Conclusions

The current study focused on the environmental threats of leaking underground fuel tanks of aged gas stations in the City of Buraidiah, AlQassim, Saudi Arabia. Two sites were selected among the oldest constructed gas stations in the city where a geoenvironmental investigation was launched. The investigation showed that the soil profile at these sites is high permeable meaning that any fuel leakage would transport easily through soil layers. The study also showed that there is an actual environmental problem in the investigated sites that requires authorities' attention. The soil at the two sites has high flammable solvents contents and high concentration percentages of hydrocarbons compounds. The hydrocarbon compounds constitute an environmental hazardous problem for the area that must be thoroughly cured. Published research shows that launching a remediation process in the contaminated sites could reverse the contamination hazardous effect. The remediation process is also essential in order to stop propagation of the environmental threat. Although the current study did not elaborate on the status of the groundwater aquifer in the area; the literature review shows that most likely the soil contamination would eventually led to groundwater contamination as well; if it has not already done so. Therefore, it is highly recommended to launch a process of surveying other potential contaminated sites in the city and a remediation process for cleaning the contaminated sites. Generally speaking, USEPA suggests several techniques to be used for detecting leakage from UFT such as; automatic tank gauging systems and statistical inventory reconciliation which monitors the fuel consumption on monthly bases. These are just preliminary recommendations which should be considered by authorities until the necessary regulations for constructing the UFT are updated and set according to the world wide standards.

5. Acknowledgement

This research was funded through the Deanship of Scientific research at Qassim University Grant.

6. References

[1] Rice, D.E., R.D. Grose, J.C. Michaelsen, B.P. Dooher, D.H., Macqueen, S.J. Cullen, W.E. Kastenberg, L.G. Everett, and M.S. Marino. "California Leaking Underground Fuel Tank (LUFT) historical case analyses," California State Water Resources Publication, *UCRL-AR-122207*. (1995).

[2] University of Wisconsin, "Farm & Residential Petroleum Storage Tanks An overview of issues and regulations in Wisconsin," *An Internet Published Report # GWQ030* I-07-00-15M-75-S (1996).

[3] Sullivan, E, "Underground FEMA Fuel Tanks Could Leak", *A visit article original @ the Associated Press, http://www.truthout.org/article/underground-fema-fuel-tanks- could-leak* (2008).

[4] Friedman, D., "Heating Oil Underground & Above ground Oil Storage Tank Leaks, Testing, Problems & Solutions", *http://www.inspect-ny.com/oiltanks/tanks.htm*, (1995).

[5] Friedman, D., "Oil Tank Failure Rates", *http://www.inspect-ny.com/oiltanks/tankfail.htm*, (1995).

[6] Shih, T., Rong, Y., Harmon, T., and Suffet, M., " Evaluation of the Impact of Fuel Hydrocarbons and Oxygenates on Groundwater Resources," *Environmental Science and Technology*, (2004), 38 (1), 42–48.

[7] Day, M. J., Reinke, R. F., and Thomson, J. A., "Fate and Transport of Fuel Components Below Slightly Leaking Underground Storage Tanks," *Environmental Forensics*, (2001), 2, (1), 21-28.

[8] Corapcioglu, M. Yavuz; B., and Arthur L., "A Compositional Multiphase Model for Groundwater Contamination by Petroleum Products 1. Theoretical Considerations," *Water Resources Research*, (1987), 23, (1), 191-200.

[9] Baehr, AL and Corapcioglu, MY, "Compositional Multiphase Model for Groundwater Contamination by Petroleum Products: 2. Numerical Solution," *Water Resources Research*, 23, (1), 201-213, (1987).

[10] Cole, G.M., "*Assessment and Remediation of Petroleum Contaminated Sites*," Lewis Publishers, CRC Press, Boca Raton, Florida. (1994).

[11] Karickhoff, S.W., Brown, D.S., and Scott, T.A., "Sorption of Hydrophobic Pollutants on Natural Sediments," *Water Research*, 13, (1979).

[12] Hunt, J.R., Situ, N., and Udell, K.S., "Nonaqueous Phase Liquid Transport and Cleanup. I. Analysis of Mechanisms," *Water Resources Research*, 24, (8), (1988).

[13] Ahmed, T., "Hydrocarbon Phase Behavior", In "*Contributions in Petroleum Geology and Engineering," Gulf Publishing Company, 7 Houston, Texas* (1989).

[14] U.S. EPA. *Use and distribution of MTBE and ethanol, MTBE Fact Sheet #3*, EPA 510-F-97-016. Washington, D.C.: Office of Underground Storage Tanks, U.S. EPA, (1998).

المخاطر البيئية للتربة والمياه تحت السطحية لخزانات الوقود الأرضية فى المملكة العربية السعودية

شريف عبد الفتاح الخولي[١] **إبراهيم صالح السلامة[٢]**

قسم الهندسة المدنية ، كلية الهندسة ، جامعة القصيم

selkholy@qec.edu.sa[1] .alsalamah@qec.edu.sa[2]

(قدم للنشر في ٢٠٠٩/٦/٤م ؛ قبل للنشر في ٢٠٠٩/٧/٢٨م)

ملخص البحث. أصبح تلوث التربة والمياه الجوفية بالمواد الهيدروكربونية (إحدى مكونات البترول) الناتجة من مستودعات النفط وأماكن حقول البترول ومصانع البتروكيميائية والخطوط الناقلة للبترول وخزانات تخزين الوقود من المواضيع الهامة التي تحتاج إلى دراسة دقيقة لما لها من مخاطر بيئية وصحية علي الإنسان لسميتها. الأبحاث التي أجريت لدراسة مدى انتشار هذه الظاهرة بدول الخليج تكاد تكون معدومة بالرغم من خطورتها علي البيئة وبالرغم من انتشار آبار البترول واعتماد هذه الدول على المياه الجوفية كمصدر أساسي للمياه في هذه المنطقة. تعتبر خزانات الوقود الأرضية الموجودة في محطات التزود بالوقود من أكثر المناطق خطورة على البيئة في حالة تسرب الوقود من الخزانات إلى التربة المحيطة. تبرز خطورة هذا الموضوع على منطقة القصيم كون منسوب المياه تحت السطحية بهذه المنطقة قريبة من سطح الأرض وأن هذه المنطقة تعتمد على هذه المياه في ري المزروعات المختلفة.

وقد ظهر من نتائج عينات التربة المأخوذة من المناطق المحيطة بخزانين من خزانات الوقود الموجودة بمدينة بريدة أنه يوجد تلوث بمواد بترولية بالتربة المحيطة مما يعطي دلالة على خطورة احتمال حدوث تلوث بالتربة والمياه الجوفية بالمواد البترولية على نطاق واسع بمدينة بريدة.

Journal of Engineering and Computer Sciences, Qassim University, Vol. 3, No. 1, pp. 11-25 (January 2010/Muharram 1431H)

Direct Torque Control of Dual Three Phase Inverter Fed Six Phase Induction Motor Drive

S. A. Zaid[*], O. A. Mahgoub, K. Emetwally, and S. E. Abo-Shady

Dept. of Electrical Power and Machines, Faculty of Engineerung,
Cairo University, Giza, Egypt
** sherifzaid@yahoo.com*

(Received 21/1/2009, accepted for publication 1/11/2009)

ABSTRACT. Six-phase induction motor "IM" has advantages over three phase"3-φ"IM like lower harmonics, lower losses, improved reliability, higher torque per ampere, and higher power rating drive. However the control of such motors is more complex than that of the 3-φ motors. The principles of direct torque control "DTC", which is a well-known control method for 3-φ motors, can be utilized to overcome this complexity. This paper introduces the application of the DTC principles to 6-φ IMs drives. The whole 6-φ IM drive system is modeled and simulated in the stationary reference frame. However, it is noted from circuit analysis and Matlab simulations that the use of the conventional 6-φ inverter gives poor performance drive. This is due to the fact that with the conventional inverter only six switching states can give balanced output voltages instead of 64 switching states. This results in lower capability of control, less utilization of the DC supply, and more harmonic distortion as well. However to avoid this demerits, the authors have inferred that the use of a dual 3-φ inverter is the solution to be adapted. Simulation results of a DTC 6-φ IM drive show improved performance compared with the performance of the field orientation trials in the literature.
KEYWORDS: Six-phase "6-φ ", induction motor "IM", direct torque control "DTC", voltage source inverter "VSI".

LIST OF SYMBOLS AND ABBREVIATIONS

A-B-C-D-E-F	The six phases notations
d-q	Direct-quadrature frame (stator frame)
d-q-z_1-z_2-o_1-o_2	The six phases notations after transformation to stationary frame
C, C_1	Constants
C( )	Abbreviation of cosine
i_{ds}, i_{qs}	The stator current components in the stator reference frame
i_{dr}, i_{qr}	The rotor current components in the stator reference frame
[I]	The identity matrix
L_m	Maximum value of the mutual inductance bet. rotor and stator
L_r, L_s	Rotor and stator inductances referred to stator
L_{lr}, L_{ls}	Rotor and stator leakage inductances referred to stator
$[L_{ss}]$	The stator self-inductance matrix
$[L_{rr}]$	The rotor self-inductance matrix referred to stator
$[L_{sr}]$	The stator-rotor mutual-inductance matrix referred to stator
N	The sector number
P	Differentiation w.r.t time
P	Number of poles
R_s, R_r	Stator and rotor resistances referred to stator
S_A, S_B, S_C, S_D, S_E, S_F	6-ϕ Inverter switching logic functions
T	Motor developed torque
T^*	The reference torque
T	Time
T_L	Rated motor torque
[T]	The six phase transformation matrix to stationary frame
$[T_r^s]$	The six phase transformation matrix to a rotating frame
V_{dc}	Inverter DC supply voltage
v_{an}, v_{bn}, v_{cn}	The stator phase voltages
V_{As}, V_{Bs}, V_{Cs}, V_{Ds}, V_{Es}, V_{Fs}	The six inverter phase voltages w.r.t the load neutral point
V_{AN}, V_{BN}, V_{CN}, V_{DN}, V_{EN}, V_{FN}	The six inverter phase voltages w.r.t the DC supply ground
ω^*	The motor reference speed
θ	The rotor angular position w.r.t. the d-axis
ΔT	Torque error
$\Delta\lambda$	Flux error
λ*	The stator flux vector in the stator frame
λ_q,λ_d	The stator flux components in the stator reference frame

1. Introduction

It is generally known that balanced poly-phase voltages applied to a corresponding balanced winding result in a rotating magnetic field. In an ideal machine having a sinusoidal distribution of the air gap flux of a given peak density, the operating c/c's would be identical for any number of phases greater than one. Very early IM's had two phases, but the 3-φ version very soon replaced these. Three-phase version eliminated 3rd harmonic problems and resulted in a motor which was generally better. Increasing the number of phases beyond three has advantages, which might be worth considering for certain applications [1]. Key advantages of multiphase IM drive systems over conventional 3-φ systems are summarized as follows:

1. Reduction of the required inverter phase current permits the use of a single power device for each inverter switch instead of a group of devices connected in parallel. Problems of static and dynamic current sharing among parallel devices, such as bipolar transistors, are thereby eliminated in large drive systems [2].
2. The sixth harmonic pulsating torques, associated with the conventional 3-φ IM drives that fed from six-step VSI, is eliminated by the appropriate choice of a multiphase motor winding configuration [2].
3. Rotor harmonic losses are reduced compared with the level produced in 3-φ systems [2].
4. The total system reliability is improved by providing continued system operation with degraded performance following loss of excitation to one of the machine stator phases [2].
5. The torque per ampere for the same-size machine is increased [3].
6. A high power rating drive can be obtained with standard inverter power modules due to the use of more modules of lower rating [4].

The high phase order drive is likely to remain limited to specialized applications, where high reliability is demanded such as electric/hybrid vehicles, aerospace applications, ship propulsion, and high power drive applications.

However, when a multiphase system is implemented with the conventional voltage source inverter, large harmonic currents have been observed [2], [5], [6], and [7]. This is due to misunderstanding of the inverter modes. Attempts have been made to improve the six phase drive performance by introducing alternative modulation schemes [8-10]. The conventional topology of the 6-φ inverter essentially gives low performance drive and poor utilization of the DC supply. A new topology for the 6-φ inverter will be introduced in the present paper to improve the system performance.

Field orientation control strategy has been applied to multiphase IM [3, 5& 11]. In this paper, the concept of DTC is applied to 6-ϕ IM, as there is no previous attempt in the literature.

2. Machine Model

In a 6-φ IM, the six-stator phases are distributed with a spacing of 60°. The following normal assumptions have been made in deriving the 6-φ IM model:

1. Machine windings are of sinusoidal distribution.
2. Saturation is neglected.
3. Mutual leakage inductances are neglected.

Under these assumptions the voltage equations of the machine, in the original six dimensional space, can be derived.

2.1 Machine Model in the Original Six Dimensional Space

The machine stator and rotor voltage equations can be written as:

$$[V_s] = [R_s]\cdot[I_s] + p\cdot([L_{ss}]\cdot[I_s] + [L_{sr}]\cdot[I_r]) \tag{1}$$

$$[V_r] = [R_r]\cdot[I_r] + p\cdot([L_{rr}]\cdot[I_r] + [L_{rs}]\cdot[I_s]) \tag{2}$$

Where, in these equations, the voltage and current vectors are defined as:

$$[V_s] = \begin{bmatrix} v_{As} \\ v_{Bs} \\ v_{Cs} \\ v_{Ds} \\ v_{Es} \\ v_{Fs} \end{bmatrix}, \quad [I_s] = \begin{bmatrix} i_{As} \\ i_{Bs} \\ i_{Cs} \\ i_{Ds} \\ i_{Es} \\ i_{Fs} \end{bmatrix}, \quad [V_r] = \begin{bmatrix} v_{Ar} \\ v_{Br} \\ v_{Cr} \\ v_{Dr} \\ v_{Er} \\ v_{Fr} \end{bmatrix}, \quad [I_r] = \begin{bmatrix} i_{Ar} \\ i_{Br} \\ i_{Cr} \\ i_{Dr} \\ i_{Er} \\ i_{Fr} \end{bmatrix} \tag{3}$$

The resistance and inductance matrices in Eq.(1) and Eq.(2) are given in Appendix I.

2.2 Transformation of the Voltage Equations to a New Reference Frame

Modeling and control of 6-ϕ machine can be simplified with a proper transformation to a six dimensional frame of reference [5]. The transformation matrix used will be represented by six vectors and referred to as the space "*d-q-z*$_1$*-z*$_2$*-o*$_1$*-o*$_2$" [12].

$$[T]=\frac{1}{\sqrt{3}}\begin{bmatrix} 1 & .5 & -.5 & -1 & -.5 & .5 \\ 0 & \frac{\sqrt{3}}{2} & \frac{\sqrt{3}}{2} & 0 & \frac{-\sqrt{3}}{2} & \frac{-\sqrt{3}}{2} \\ 1 & -.5 & -.5 & 1 & -.5 & -.5 \\ 0 & \frac{-\sqrt{3}}{2} & \frac{\sqrt{3}}{2} & 0 & \frac{-\sqrt{3}}{2} & \frac{\sqrt{3}}{2} \\ \frac{1}{\sqrt{2}} & \frac{-1}{\sqrt{2}} & \frac{1}{\sqrt{2}} & \frac{-1}{\sqrt{2}} & \frac{1}{\sqrt{2}} & \frac{-1}{\sqrt{2}} \\ \frac{1}{\sqrt{2}} & \frac{1}{\sqrt{2}} & \frac{1}{\sqrt{2}} & \frac{1}{\sqrt{2}} & \frac{1}{\sqrt{2}} & \frac{1}{\sqrt{2}} \end{bmatrix} \tag{4}$$

The actual machine phases will be referred to as "*A-B-C-D-E-F*". The transformation transforms the original vector space to a new vector space having the following properties:

- Machine variable components that produce air gap flux are transformed to the *d-q* subspace. The *d-q* subspace, commonly referred to as the *d-q* plane, is electromechanical energy conversion related.
- Those components of machine variables, which will not produce air gap penetrating flux, will be mapped to the subspace z_1-z_2-o_1-o_2 by Eq.(4). These components can be classified as a new type of zero sequence subspace [11].

Applying transformation given by Eqn.(4) to Eqn.(1) and Eqn.(2) yields

$$\begin{bmatrix} v_{ds} \\ v_{qs} \\ v_{z_1s} \\ v_{z_2s} \\ v_{o_1s} \\ v_{o_2s} \end{bmatrix} = [R_s]\cdot\begin{bmatrix} i_{ds} \\ i_{qs} \\ i_{z_1s} \\ i_{z_2s} \\ i_{o_1s} \\ i_{o_2s} \end{bmatrix} + p\cdot\left\{\begin{bmatrix} L_{ls}+3L_m & 0 & 0 & 0 & 0 & 0 \\ 0 & L_{ls}+3L_m & 0 & 0 & 0 & 0 \\ 0 & 0 & L_{ls} & 0 & 0 & 0 \\ 0 & 0 & 0 & L_{ls} & 0 & 0 \\ 0 & 0 & 0 & 0 & L_{ls} & 0 \\ 0 & 0 & 0 & 0 & 0 & L_{ls} \end{bmatrix}\begin{bmatrix} i_{ds} \\ i_{qs} \\ i_{z_1s} \\ i_{z_2s} \\ i_{o_1s} \\ i_{o_2s} \end{bmatrix}\right.$$
$$\left. +3L_m\cdot\begin{bmatrix} cos(\theta) & -sin(\theta) & 0 & 0 & 0 & 0 \\ sin(\theta) & cos(\theta) & 0 & 0 & 0 & 0 \\ 0 & 0 & 0 & 0 & 0 & 0 \\ 0 & 0 & 0 & 0 & 0 & 0 \\ 0 & 0 & 0 & 0 & 0 & 0 \\ 0 & 0 & 0 & 0 & 0 & 0 \end{bmatrix}\begin{bmatrix} i_{dr} \\ i_{qr} \\ i_{z_1r} \\ i_{z_2r} \\ i_{o_1r} \\ i_{o_2r} \end{bmatrix}\right\} \tag{5}$$

$$\begin{bmatrix} 0 \\ 0 \\ 0 \\ 0 \\ 0 \\ 0 \end{bmatrix} = [R_r]\cdot\begin{bmatrix} i_{dr} \\ i_{qr} \\ i_{z_1r} \\ i_{z_2r} \\ i_{o_1r} \\ i_{o_2r} \end{bmatrix} + p\cdot\left\{\begin{bmatrix} L_{lr}+3L_m & 0 & 0 & 0 & 0 & 0 \\ 0 & L_{lr}+3L_m & 0 & 0 & 0 & 0 \\ 0 & 0 & L_{lr} & 0 & 0 & 0 \\ 0 & 0 & 0 & L_{lr} & 0 & 0 \\ 0 & 0 & 0 & 0 & L_{lr} & 0 \\ 0 & 0 & 0 & 0 & 0 & L_{lr} \end{bmatrix}\begin{bmatrix} i_{dr} \\ i_{qr} \\ i_{z_1r} \\ i_{z_2r} \\ i_{o_1r} \\ i_{o_2r} \end{bmatrix}\right.$$
$$\left. +3L_m\cdot\begin{bmatrix} cos(\theta) & sin(\theta) & 0 & 0 & 0 & 0 \\ -sin(\theta) & cos(\theta) & 0 & 0 & 0 & 0 \\ 0 & 0 & 0 & 0 & 0 & 0 \\ 0 & 0 & 0 & 0 & 0 & 0 \\ 0 & 0 & 0 & 0 & 0 & 0 \\ 0 & 0 & 0 & 0 & 0 & 0 \end{bmatrix}\begin{bmatrix} i_{ds} \\ i_{qs} \\ i_{z_1s} \\ i_{z_2s} \\ i_{o_1s} \\ i_{o_2s} \end{bmatrix}\right\} \tag{6}$$

Where θ is the rotor angular position.

As expected it is observed immediately from the above equations that all the electromechanical energy conversion related variable components are mapped into the *d-q* plane, and the non-electromechanical energy conversion related variable components are transformed to the z_1-z_2 and o_1-o_2 planes. Hence, the dynamic equations of the machine are totally decoupled. As a result the analysis and control of the machine can be greatly simplified. In the analysis just completed, *d-q* reference frames were, in effect, separately attached to the stator and rotor, rotating at zero and rotor angular speed, respectively. To express the stator and rotor equations in the same reference frame and thus eliminate the sine and the cosine terms in the above equations, the following relation transformation, which transforms the rotor variables to the stationary reference frame, is appropriate:

$$\left[T_r^s\right]=\begin{bmatrix} cos(\theta) & -sin(\theta) & 0 & 0 & 0 & 0 \\ sin(\theta) & cos(\theta) & 0 & 0 & 0 & 0 \\ 0 & 0 & 0 & 0 & 0 & 0 \\ 0 & 0 & 0 & 0 & 0 & 0 \\ 0 & 0 & 0 & 0 & 0 & 0 \\ 0 & 0 & 0 & 0 & 0 & 0 \end{bmatrix} \tag{7}$$

With this relation transformation applied to Eq.(5) and Eq.(6), the following stator and rotor combined *d-q* plane stationary reference frame equation results:

$$\begin{bmatrix} v_{ds} \\ v_{qs} \\ 0 \\ 0 \end{bmatrix} = \begin{bmatrix} R_s + L_s p & 0 & Mp & \omega M \\ 0 & R_s + L_s p & \omega M & Mp \\ Mp & \omega M & R_r + L_r p & \omega L_r \\ -\omega M & Mp & -\omega L_r & R_r + L_r p \end{bmatrix} . \begin{bmatrix} i_{ds} \\ i_{qs} \\ i_{dr} \\ i_{qr} \end{bmatrix} \tag{8}$$

Where: $p = \frac{d}{dt}, L_s = L_{ls} + 3L_m, L_r = L_{lr} + 3L_m, M = 3L_m$

The electromagnetic torque is given by:

$$T = \frac{6}{2}\frac{P}{2} L_m \left(i_{qs} i_{dr} - i_{qr} i_{ds}\right) \tag{9}$$

3. Inverter Model and Space Vectors

A 6-φ voltage source inverter is shown in Fig.(1). This inverter operates with the same main rules as the 3-φ inverter (i.e. the two switches, or transistors, of any leg are always in opposite operation), and there are always six switches in conduction. The inputs to the inverter, as a control system building block, are the switching functions of the inverter switches (S_A, S_B, S_C, S_D, S_E, S_F). These functions are logic functions, equal '1' when the phase terminal is connected to the positive of the DC side, and equal '0' when the phase terminal is connected to the negative of the DC side. However, the outputs are the motor phase voltages (v_{As}, v_{Bs}, v_{Cs}, v_{Ds}, v_{Es}, v_{Fs}).

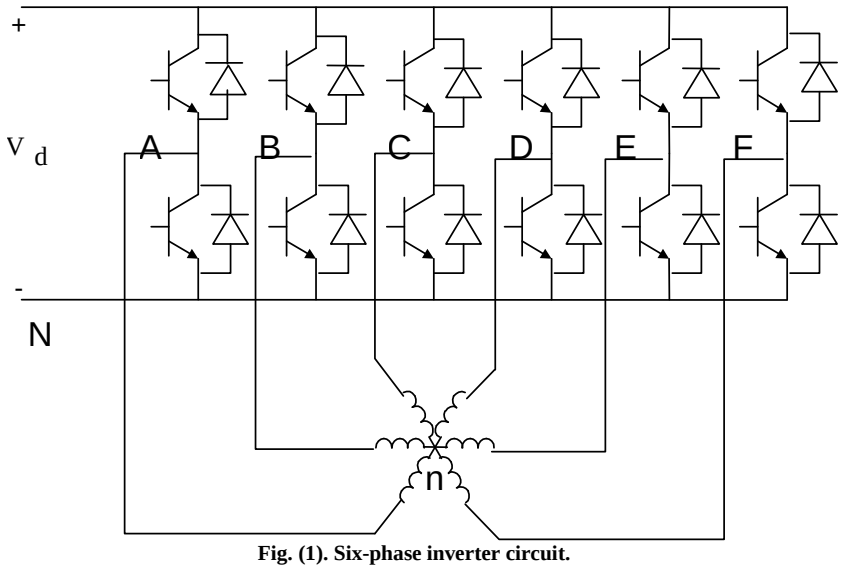

Fig. (1). Six-phase inverter circuit.

The model can be derived as follows. The inverter phase voltages (v_{AN}, v_{BN}, v_{CN}, v_{DN}, v_{EN}, v_{FN}), w.r.t the DC supply ground, can be derived from the switching states using:

$$(v_{AN}, v_{BN}, v_{CN} v_{DN}, v_{EN}, v_{FN}) = V_{dc}(S_A, S_B, S_C, S_D, S_E, S_F) \tag{10}$$

Then the motor phase voltages are derived from the inverter phase voltages by applying Kirchhoff laws to the inverter-motor circuit:

$$\begin{aligned} v_{As} - v_{Bs} &= v_{AN} - v_{BN} \\ v_{As} - v_{Cs} &= v_{AN} - v_{CN} \\ v_{As} - v_{Ds} &= v_{AN} - v_{DN} \\ v_{As} - v_{Es} &= v_{AN} - v_{EN} \\ v_{As} - v_{Fs} &= v_{AN} - v_{FN} \\ v_{As} + v_{Bs} + v_{Cs} + v_{Ds} + v_{Es} + v_{Fs} &= 0 \end{aligned} \tag{11}$$

Solving these equations then using (10)we get the input output relation for the nverter:

$$\begin{bmatrix} v_{As} \\ v_{Bs} \\ v_{Cs} \\ v_{Ds} \\ v_{Es} \\ v_{Fs} \end{bmatrix} = \frac{V_{dc}}{6} \begin{bmatrix} 5 & -1 & -1 & -1 & -1 & -1 \\ -1 & 5 & -1 & -1 & -1 & -1 \\ -1 & -1 & 5 & -1 & -1 & -1 \\ -1 & -1 & -1 & 5 & -1 & -1 \\ -1 & -1 & -1 & -1 & 5 & -1 \\ -1 & -1 & -1 & -1 & -1 & 5 \end{bmatrix} \begin{bmatrix} S_A \\ S_B \\ S_C \\ S_D \\ S_E \\ S_F \end{bmatrix} \tag{12}$$

The 6-φ voltage source inverter has a total of 64 switching states, shown in Table (1).

Table (1). The 6-ϕ single inverter switching states

	S_F	S_E	S_D	S_C	S_B	S_A		S_F	S_E	S_D	S_C	S_B	S_A
V_0	0	0	0	0	0	0	V_{32}	1	0	0	0	0	0
V_1	0	0	0	0	0	1	V_{33}	1	0	0	0	0	1
V_2	0	0	0	0	1	0	V_{34}	1	0	0	0	1	0
V_3	0	0	0	0	1	1	V_{35}	1	0	0	0	1	1
V_4	0	0	0	1	0	0	V_{36}	1	0	0	1	0	0
V_5	0	0	0	1	0	1	V_{37}	1	0	0	1	0	1
V_6	0	0	0	1	1	0	V_{38}	1	0	0	1	1	0
V_7	0	0	0	1	1	1	V_{39}	1	0	0	1	1	1
V_8	0	0	1	0	0	0	V_{40}	1	0	0	0	0	0
V_9	0	0	1	0	0	1	V_{41}	1	0	1	0	0	1
V_{10}	0	0	1	0	1	0	V_{42}	1	0	1	0	1	0
V_{11}	0	0	1	0	1	1	V_{43}	1	0	1	0	1	1
V_{12}	0	0	1	1	0	0	V_{44}	1	0	1	1	0	0
V_{13}	0	0	1	1	0	1	V_{45}	1	0	1	1	0	1
V_{14}	0	0	1	1	1	0	V_{46}	1	0	1	1	1	0
V_{15}	0	0	1	1	1	1	V_{47}	1	0	1	1	1	1
V_{16}	0	1	0	0	0	0	V_{48}	1	1	0	0	0	0
V_{17}	0	1	0	0	0	1	V_{49}	1	1	0	0	0	1
V_{18}	0	1	0	0	1	0	V_{50}	1	1	0	0	1	0
V_{19}	0	1	0	0	1	1	V_{51}	1	1	0	0	1	1
V_{20}	0	1	0	1	0	0	V_{52}	1	1	0	1	0	0
V_{21}	0	1	0	1	0	1	V_{53}	1	1	0	1	0	1
V_{22}	0	1	0	1	1	0	V_{54}	1	1	0	1	1	0
V_{23}	0	1	0	1	1	1	V_{55}	1	1	0	1	1	1
V_{24}	0	1	1	0	0	0	V_{56}	1	1	1	0	0	0
V_{25}	0	1	1	0	0	1	V_{57}	1	1	1	0	0	1
V_{26}	0	1	1	0	1	0	V_{58}	1	1	1	0	1	0
V_{27}	0	1	1	0	1	1	V_{59}	1	1	1	0	1	1

Continued table (1)

	Sf	*Se*	*Sd*	*Sc*	*Sb*	*Sa*		*Sf*	*Se*	*Sd*	*Sc*	*Sb*	*Sa*
V_{28}	0	1	1	1	0	0	V_{60}	1	1	1	1	0	0
V_{29}	0	1	1	1	0	1	V_{61}	1	1	1	1	0	1
V_{30}	0	1	1	1	1	0	V_{62}	1	1	1	1	1	0
V_{31}	0	1	1	1	1	1	V_{63}	1	1	1	1	1	1

By using the transformation matrix of Eq.(4), the inverter phase voltages can be represented in the stationary reference frame as:

$$\begin{bmatrix} v_{ds} \\ v_{qs} \\ v_{z_1 s} \\ v_{z_2 s} \\ v_{o_1 s} \\ v_{o_2 s} \end{bmatrix} = \frac{V_{dc}}{\sqrt{3}} \begin{bmatrix} 1 & .5 & -.5 & -1 & -.5 & .5 \\ 0 & \frac{\sqrt{3}}{2} & \frac{\sqrt{3}}{2} & 0 & -\frac{\sqrt{3}}{2} & -\frac{\sqrt{3}}{2} \\ 1 & -.5 & -.5 & 1 & -.5 & -.5 \\ 0 & -\frac{\sqrt{3}}{2} & \frac{\sqrt{3}}{2} & 0 & -\frac{\sqrt{3}}{2} & \frac{\sqrt{3}}{2} \\ \frac{1}{\sqrt{2}} & -\frac{1}{\sqrt{2}} & \frac{1}{\sqrt{2}} & -\frac{1}{\sqrt{2}} & \frac{1}{\sqrt{2}} & -\frac{1}{\sqrt{2}} \\ 0 & 0 & 0 & 0 & 0 & 0 \end{bmatrix} \begin{bmatrix} S_A \\ S_B \\ S_C \\ S_D \\ S_E \\ S_F \end{bmatrix} \tag{13}$$

The 6-φ voltage source inverter has a total of 64 switching states. There are ten zero voltage states and 54 active voltage states. It must be noted that these numbers depend on the transformation matrix used. The active space voltage vectors can be represented in the *d-q* plane as shown in Fig. (2). It seems that the control flexibility will be better with this large number of states. To operate the inverter using these states, the authors have carried out many trials; however, all the trials lead to a highly distorted inverter output. To discover the core of this problem, let us investigate the circuits of Fig. (3). These five circuits are the only possible circuits of the inverter with the load at any switching state, except the zero states. Therefore, the motor phase voltages can take discrete values $\pm 1/2V_{dc}$, for Fig. (3-a), ($\pm 1/6V_{dc}$, $\pm 5/6V_{dc}$), for Fig. (3-b) & Fig. (3-c), and ($\pm 1/3V_{dc}$, $\pm 2/3V_{dc}$), for Fig. (3-d) & Fig. (3-e). This means that with any inverter switching state the inverter circuit can take one of these five circuits. For the inverter output voltage to be balanced, 60º must shift the six phase voltages. Consequently, three phases are in antiphase with the remaining three. Therefore, with balanced voltages, the instantaneous phase voltages (v_{As}, v_{Bs}, v_{Cs}) should equal the negative of (v_{Ds}, v_{Es}, v_{Fs}), respectively. However, for the 6-ϕ inverter to operate in balanced mode, the only possible switching states are those corresponding to the circuit of Fig. (3-a). Hence, the voltage vectors that can be used for balanced 6-ϕ are (V_7, V_{14}, V_{28}, V_{56}, V_{49}, V_{35}), i.e. the motor phase voltage will be $\pm 1/2V_{dc}$. Therefore, the phase voltages will contain large harmonics and the benefits of the 6-ϕ system will be lost. An improved performance can be obtained with the aid of dual 3-ϕ inverters, as shown in Fig. (3-f).

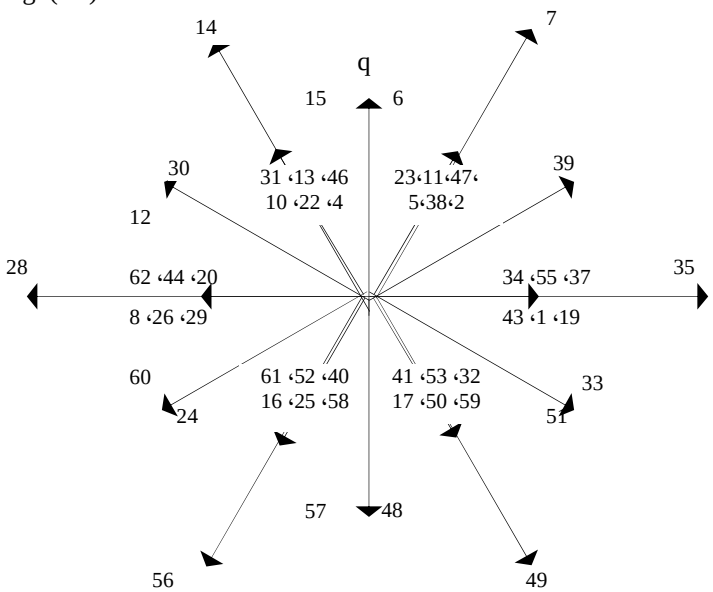

Fig. (2). Six-phase inverter states.

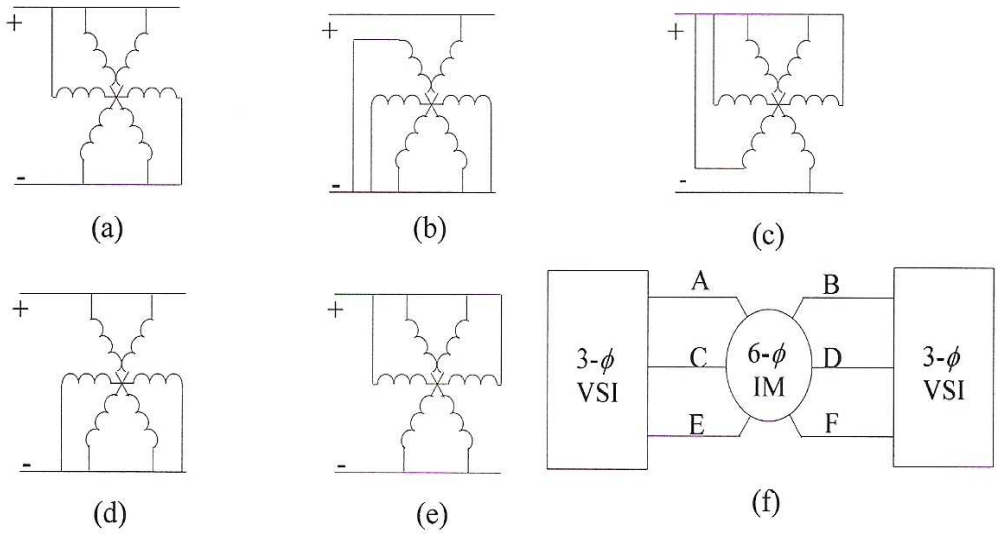

Fig. (3). (a-e)The 6-φ inverter-motor possible circuits,(f) the dual inverter fed 6-φ IM.

The simulated six-step operation of Fig. (4) indicates that for balanced motor operation, the inverter states must take the same previous states (V_7, V_{14}, V_{28}, V_{56}, V_{49}, V_{35}).

However, to achieve these voltage states, there must be synchronization between the two inverters signals. For instance, to get V_7 we must send a control signal to the inverters as (000111) to the legs (*F-E-D-C-B-A*). This means that the 1st inverter (*A-C-E*) must receive a control signal (110), while the 2nd (*B-D-F*) must receive a control signal (100).

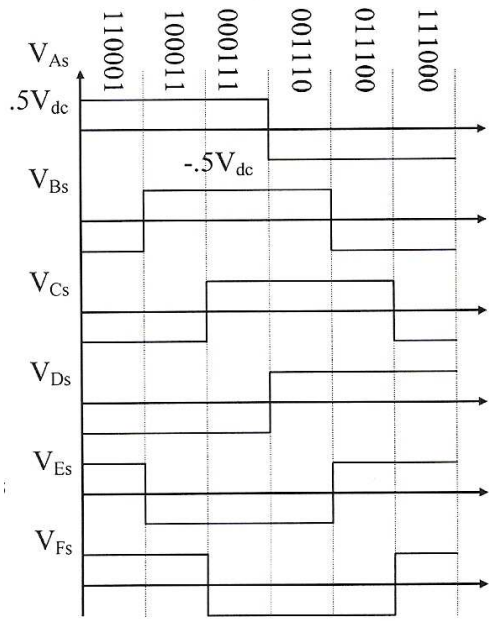

Fig. (4). The six-step operation of the 6-φ inverter.

4. Direct Torque Control of 6-φ IM DRIVE

As the 6-φ IM model in the stationary reference frame is similar to the 3-φ one, then the principles of DTC that are essentially prepared for 3-φ IM, [13–15], can be applied to 6-φ IM. By controlling the relative motion between the stator flux and rotor flux vectors the torque can be controlled. In voltage source inverters (VSI's) that are convenient for DTC drives, the stator flux is a state variable that can be adjusted by the stator voltage and the motion of the stator flux is fully controlled by the proper selection of the stator voltage vector. The aim of DTC is to control both the flux and the torque so as to be in hysteresis band as shown in Fig. (6). For this the motion of the stator flux vector is adjusted by selecting the appropriate voltage vector. The voltage vector is selected according to the following rules:

1. Selecting an active voltage vector will move the stator flux vector, i.e. increase or decrease the flux and the torque.

2. Selecting a zero voltage vector will stop the flux vector motion, the magnitude will not change, and will decrease the torque.

3. The *d*-*q* plane, where the stator flux vector lies, is divided into six regions or sectors [13] as shown in Fig. (5). In each sector the next two adjacent voltage vectors can be selected to increase the torque and increase or decrease the flux respectively. For instance, in sector "1", either vector V_7 or V_{14} can be selected to increase the torque. However, V_7 will increase the stator flux magnitude but V_{14} will decrease the stator flux magnitude.

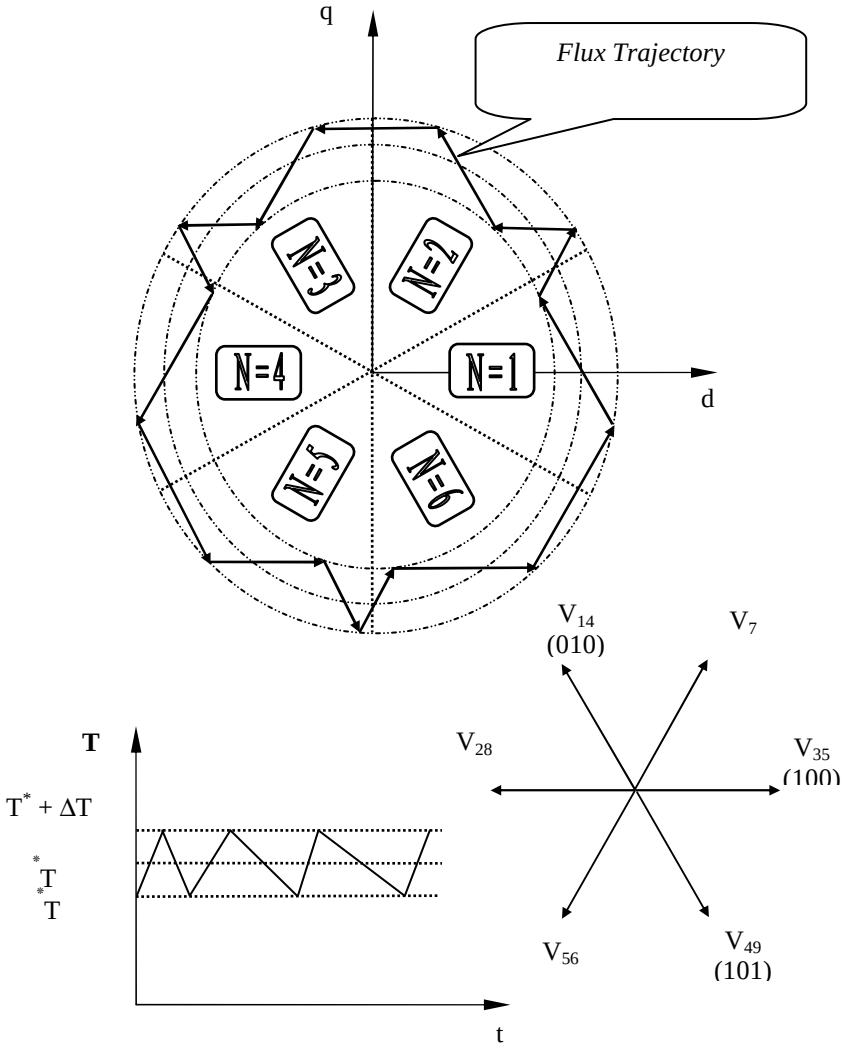

Fig. (5). Typical torque and flux (trajectory) responses with DTC.

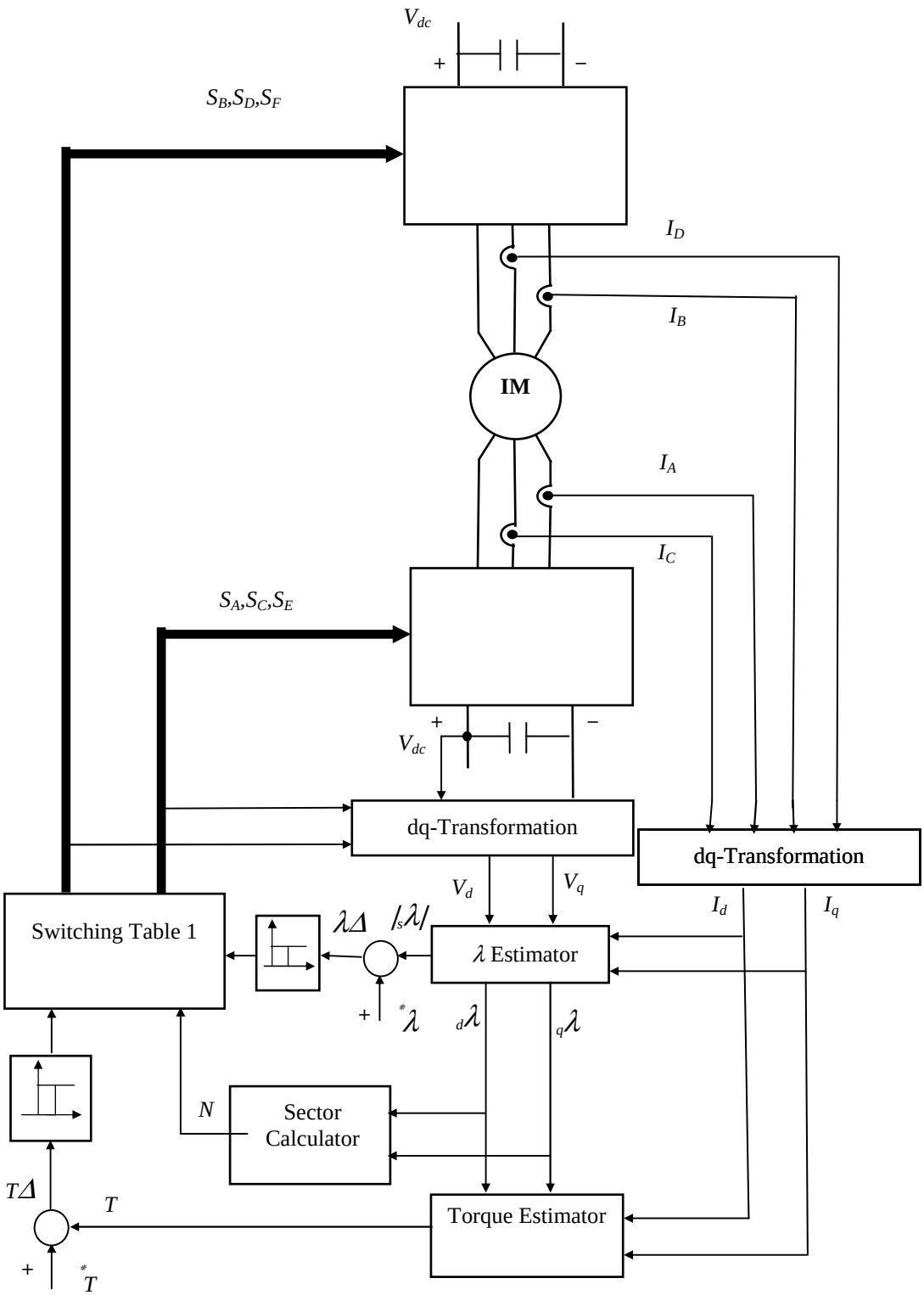

Fig. (6). Block diagram of a 6-φ IM drive controlled with DTC.

Hence, the proper voltage vector, that affects both the flux and torque in a certain sector, is known and the results can be summarized in Table (2).

Table (2). Voltage vector selection with DTC.

$\Delta\lambda$	ΔT	N					
		1	*2*	*3*	*4*	*5*	*6*
$\Delta\lambda = 1$	$\Delta T = 1$	V_7	V_{14}	V_{28}	V_{56}	V_{49}	V_{35}
	$\Delta T = 0$	V_{63}	V_0	V_{63}	V_0	V_{63}	V_0
$\Delta\lambda = 0$	$\Delta T = 1$	V_{14}	V_{28}	V_{56}	V_{49}	V_{35}	V_7
	$\Delta T = 0$	V_0	V_{63}	V_0	V_{63}	V_0	V_{63}

The basic block diagram of DTC system for a voltage source PWM inverter-fed IM drive is shown in Fig.(6). In this system the current and voltage vectors of the stator are measured then the real electric torque and the stator flux vector is estimated through simple estimators. The zone detector detects the sector "*N*=1….6" of the flux vector from its angle. The estimated torque is compared with the reference torque, which is the output of the speed controller, and the estimated flux is compared with the reference flux. The flux and torque controllers are hysteresis controllers which produce digitized output signals "'1' to increase and '0' to decrease".

These signals with the stator flux position signal and the sector number form the digital address to the EPROM that stores the switching Table (1). The output of the EPROM is the switching states of the inverter that form directly the control signals of the drive circuit of the inverter transistors.

5. Simulation Results

A speed control system is simulated using Matlab with a motor that has the parameters given in Table (3) [5]. A five horsepower, four poles IM with thirty-six stator slots was rewound to form a six pole, six phase IM.

Table (3). Motor parameters

N	*1150rpm*	R_s	*.71Ω*	L_s	*.05331H*
v_{ph}	*145V*	R_r	*1.29Ω*	*J*	$.05 N.m.sec^2$
F	*60Hz*	L_m	*.0489H*	λ_s	*0.82Wb*
		L_r	*.05331H*	T_L	*8N.m*

The torque and flux step response are shown in Fig. (7). It is noted that both torque and flux are within the hysteresis bands at steady state. The motor phase currents and voltages are balanced; the phase voltage and current is shown in Fig. (8). The stator flux locus, shown in Fig. (9), nearly resembles a circle. The current spectrum of the 6-φ motor and that of a 3-φ motor of the same rating; at full load; are shown in Fig. (10).

It is noted from the figure that there is a third harmonic component with 6-φ drive, this is a built in disadvantage of the 6-φ IM [1]. However, the total harmonic distortion of the 6-φ drive is less than that of the 3-φ drive. The high order current harmonics appeared in the 6-φ spectrum has no effect on the motor torque as it is absorbed by the motor inertia.

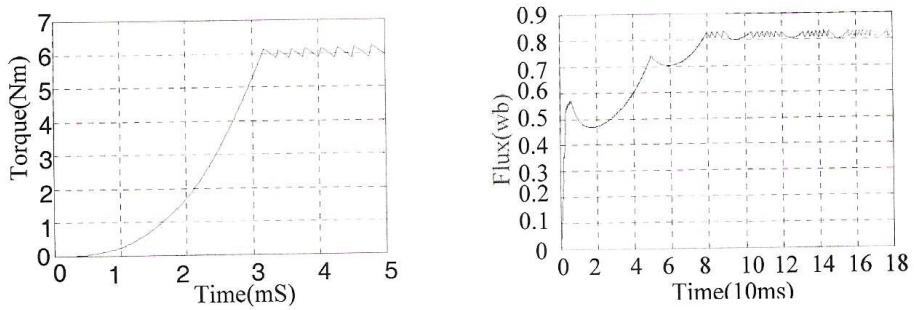

Fig. (7). Flux and torque step responses of 6-φ IM with DTC at starting, the step torque and flux are 75% and 100% respectively.

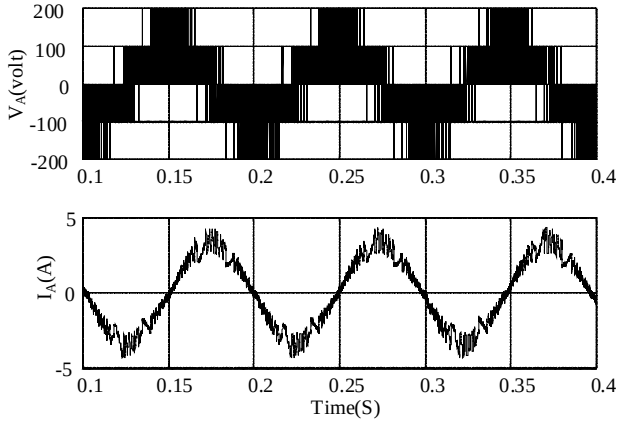

Fig. (8). Phase "A" voltage and current of 6-φ IM with DTC at steady state,no load, and 195 rpm.

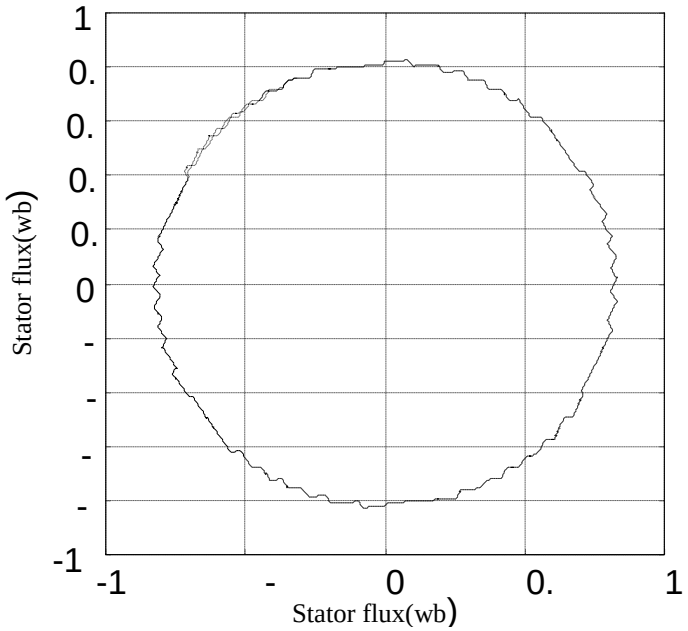

Fig. (9). Stator flux locus of 6-φ IM with DTC.

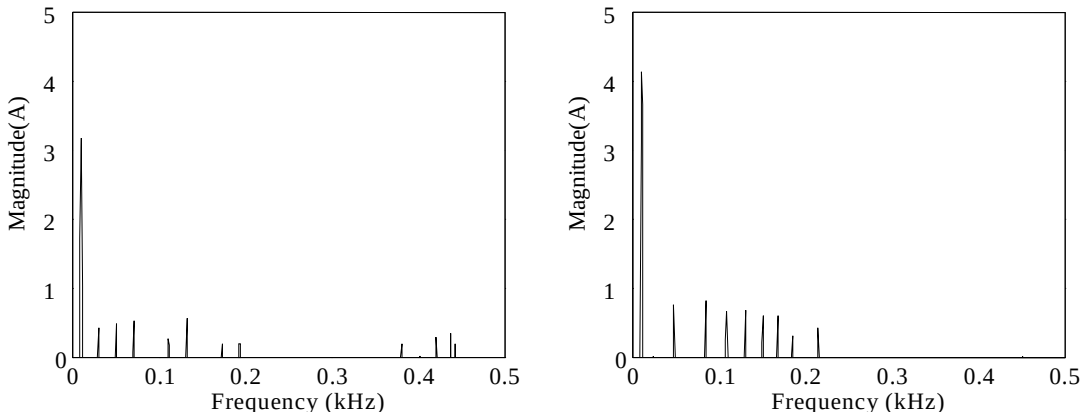

Fig. (10). Current Spectrum of DTC controlled 6-φ IM "left" and 3-φ IM "right".

6. Conclusion

Modeling and simulation of a 6-φ IM drive with DTC has been examined. The salient conclusions that emerged from the study are the following:

1. With the conventional 6-φ inverter there are 64 possible locations for the resultant voltage vector, however only 6 locations can be utilized to generate balanced output.

2. An improved performance over the results of the field orientation trials in the literature has been obtained with the aid of dual 3-φ inverters.

3. Compared to the 3-φ drive, the converter total harmonic distortion of the 6-φ drive is less than that of the 3-φ drive.

7. References

[1] Klingshirn E. A., "High phase order induction motors," *IEEE Trans. on Power Apparatus and Systems*, Vol. PAS-102, No. 1, (1983). 47-59.

[2] Abbas M. A., Christen R., and Jahns T. M., "Six-phase voltage source inverter driven induction motor," *IEEE Trans. on Industry Applicat.*, Vol. IA-20, No. 5, (1984). 1251-1259.

[3] Toliyat H. A., "Analysis and simulation of five-phase variable speed induction motor under asymmetrical connections," *IEEE Trans. on Power Elect.*, Vol. 13, No. 4, (1998). 748-756.

[4] Scholey D., "Induction motors for variable frequency power supplies," *IEEE Trans. on Industry Applicat.*, Vol. IA-18, No. 4, (1982).

[5] Zhao Y., and Lipo T. A., "Space vector PWM control of dual three-phase induction machine using vector space decomposition," *IEEE Trans. on Industry Applicat.*, Vol. 31, No. 5, (1995). 1100-1109.

[6] Gopakumar K., Ranganathan V. T., and Baht S. R., "Split-phase induction motor operation from PWM voltage source inverter," *IEEE Trans. on Industry Applicat.*, Vol. 29, No. 5, (1993). 927-932.

[7] Pavithran K. N., Parimelalagan R., and Krishnamurthy M. R., "Studies on inverter-fed five-phase induction motor drive," *IEEE Trans. on Power Elect.*, Vol. 3, No. 2, (1988). 748-756.

[8] Mohpatra K. K., Gopakumar K., Somasekhar V. T., and Umanand L., "A novel modulation scheme for a six phase induction motor winding," IECON 2002., Vol. 1, (2002). 810-815.

[9] Yazdani D., Khajehoddin S. A., Bakhshai A., and Joos G., "A generalized space vector classification technique for six phase inverters," PESC 2007, (2007). 2050-2054.

[10] Aroquiadassou G., Henao H., Capolino G. A., Boglietti A., and Cavagnino A., "A simple circuit model for predicting six-phase induction machine performances," IECON 06., Vol. 1, (2006). 1441-1446.

[11] Zhao Y., and Lipo T. A, "Modeling and control of a multi-phase induction machine with structural unbalance," *IEEE Trans. On Energy Conversion*, Vol. 11, No. 3, (1996). 570-577.

[12] White D. C., and Woodson H. H., *Electromechanical Energy Conversion*, New York: John Wiley & Sons, (1959).

[13] Takahashi I., and Noguchi T., "A new quick response and high efficiency control strategy of an induction motor," *IEEE Trans. on Industry Applicat.*, Vol. IA-22, No. 5, (1986). 820-827,.

[14] Tiitinen P., Pohjalianen P., and Lalu J., "The next generation motor control method DTC," Revue ABB, (1995) 19-24.

[15] Kazmierkowski M. P., and Kasprowicz A. B., "Improved direct torque and flux vector control of PWM inverter fed induction motor drives," *IEEE Trans. on Industrial Elect.*, Vol. 42, No. 4, (1995). 344-350,.

Appendix I

The resistance and inductance matrices in Eq.(1) and Eq.(2) are defined as follows, according to the machine structure:

The stator and rotor resistance matrices [R_s], [R_r]:

$$[R_s]=\begin{bmatrix} R_s & 0 & 0 & 0 & 0 & 0 \\ 0 & R_s & 0 & 0 & 0 & 0 \\ 0 & 0 & R_s & 0 & 0 & 0 \\ 0 & 0 & 0 & R_s & 0 & 0 \\ 0 & 0 & 0 & 0 & R_s & 0 \\ 0 & 0 & 0 & 0 & 0 & R_s \end{bmatrix},$$

$$[R_r]=\begin{bmatrix} R_r & 0 & 0 & 0 & 0 & 0 \\ 0 & R_r & 0 & 0 & 0 & 0 \\ 0 & 0 & R_r & 0 & 0 & 0 \\ 0 & 0 & 0 & R_r & 0 & 0 \\ 0 & 0 & 0 & 0 & R_r & 0 \\ 0 & 0 & 0 & 0 & 0 & R_r \end{bmatrix} \quad \text{(I-1)}$$

The stator self-inductance matrix [L_{ss}]:

$$[L_{ss}]=L_{ls}\cdot[I]+L_m\cdot\begin{bmatrix} 1 & .5 & -.5 & -1 & -.5 & .5 \\ .5 & 1 & .5 & -.5 & -1 & -.5 \\ -.5 & .5 & 1 & .5 & -.5 & -1 \\ -1 & -.5 & .5 & 1 & .5 & -.5 \\ -.5 & -1 & -.5 & .5 & 1 & .5 \\ .5 & -.5 & -1 & -.5 & .5 & 1 \end{bmatrix} \quad \text{(I-2)}$$

The rotor self-inductance matrix [L_{rr}]:

$$[L_{rr}]=L_{lr}\cdot[I]+\left(\frac{N_r}{N_s}\right)^2\cdot L_m\cdot\begin{bmatrix} 1 & .5 & -.5 & -1 & -.5 & .5 \\ .5 & 1 & .5 & -.5 & -1 & -.5 \\ -.5 & .5 & 1 & .5 & -.5 & -1 \\ -1 & -.5 & .5 & 1 & .5 & -.5 \\ -.5 & -1 & -.5 & .5 & 1 & .5 \\ .5 & -.5 & -1 & -.5 & .5 & 1 \end{bmatrix} \quad \text{(I-3)}$$

Where L_{ls}, L_{lr}, and L_m are the stator leakage, rotor leakage and mutual inductances.

$$[L_{sr}] = L_m \cdot \begin{bmatrix} c(\theta) & c\left(\frac{\pi}{3}+\theta\right) & c\left(\frac{2\pi}{3}+\theta\right) & c\left(\frac{3\pi}{3}+\theta\right) & c\left(\frac{4\pi}{3}+\theta\right) & c\left(\frac{5\pi}{3}+\theta\right) \\ c\left(\frac{5\pi}{3}+\theta\right) & c(\theta) & c\left(\frac{\pi}{3}+\theta\right) & c\left(\frac{2\pi}{3}+\theta\right) & c\left(\frac{3\pi}{3}+\theta\right) & c\left(\frac{4\pi}{3}+\theta\right) \\ c\left(\frac{4\pi}{3}+\theta\right) & c\left(\frac{5\pi}{3}+\theta\right) & c(\theta) & c\left(\frac{\pi}{3}+\theta\right) & c\left(\frac{2\pi}{3}+\theta\right) & c\left(\frac{3\pi}{3}+\theta\right) \\ c\left(\frac{3\pi}{3}+\theta\right) & c\left(\frac{4\pi}{3}+\theta\right) & c\left(\frac{5\pi}{3}+\theta\right) & c(\theta) & c\left(\frac{\pi}{3}+\theta\right) & c\left(\frac{2\pi}{3}+\theta\right) \\ c\left(\frac{2\pi}{3}+\theta\right) & c\left(\frac{3\pi}{3}+\theta\right) & c\left(\frac{4\pi}{3}+\theta\right) & c\left(\frac{5\pi}{3}+\theta\right) & c(\theta) & c\left(\frac{\pi}{3}+\theta\right) \\ c\left(\frac{\pi}{3}+\theta\right) & c\left(\frac{2\pi}{3}+\theta\right) & c\left(\frac{3\pi}{3}+\theta\right) & c\left(\frac{4\pi}{3}+\theta\right) & c\left(\frac{5\pi}{3}+\theta\right) & c(\theta) \end{bmatrix} \tag{I-4}$$

$$[L_{rs}] = L_m \cdot \begin{bmatrix} c(\theta) & c\left(\frac{\pi}{3}-\theta\right) & c\left(\frac{2\pi}{3}-\theta\right) & c\left(\frac{3\pi}{3}-\theta\right) & c\left(\frac{4\pi}{3}-\theta\right) & c\left(\frac{5\pi}{3}-\theta\right) \\ c\left(\frac{5\pi}{3}-\theta\right) & c(\theta) & c\left(\frac{\pi}{3}-\theta\right) & c\left(\frac{2\pi}{3}-\theta\right) & c\left(\frac{3\pi}{3}-\theta\right) & c\left(\frac{4\pi}{3}-\theta\right) \\ c\left(\frac{4\pi}{3}-\theta\right) & c\left(\frac{5\pi}{3}-\theta\right) & c(\theta) & c\left(\frac{\pi}{3}-\theta\right) & c\left(\frac{2\pi}{3}-\theta\right) & c\left(\frac{3\pi}{3}-\theta\right) \\ c\left(\frac{3\pi}{3}-\theta\right) & c\left(\frac{4\pi}{3}-\theta\right) & c\left(\frac{5\pi}{3}-\theta\right) & c(\theta) & c\left(\frac{\pi}{3}-\theta\right) & c\left(\frac{2\pi}{3}-\theta\right) \\ c\left(\frac{2\pi}{3}-\theta\right) & c\left(\frac{3\pi}{3}-\theta\right) & c\left(\frac{4\pi}{3}-\theta\right) & c\left(\frac{5\pi}{3}-\theta\right) & c(\theta) & c\left(\frac{\pi}{3}-\theta\right) \\ c\left(\frac{\pi}{3}-\theta\right) & c\left(\frac{2\pi}{3}-\theta\right) & c\left(\frac{3\pi}{3}-\theta\right) & c\left(\frac{4\pi}{3}-\theta\right) & c\left(\frac{5\pi}{3}-\theta\right) & c(\theta) \end{bmatrix} \tag{I-5}$$

التحكم المباشر فى العزم فى نظام تدوير يستخدام محرك حثى سداسي الأطوار

شريف زيد* أسامة محجوب خالد المتولي سراج الدين أبوشادي

قسم القوى الكهربائيه والمحركات كلية الهندسة جامعة القاهره - الجيزة - مصر

* *sherifzaid@yahoo.com*

(قدم للنشر في ٢٠٠٩/١/٢١م ؛ قبل للنشر في ٢٠٠٩/١١/١م)

ملخص البحث . إن المحركات الحثية سداسية الأطوار تفوق المحركات الحثية ثلاثية الأطوار من ناحية أنها أقل فى المفاقيد و أكثر اعتمادية، كما تسمح بعمل نظام تدوير عالى القدرة إلا أن التحكم فى المحركات الحثية سداسية الأطوار بالغ الصعوبة.و فى هذه المقال تم عمل محاكاة و نمذجة لنظام تدوير يستخدم محركاً سداسي الأطوار وبتطبيق طريقة التحكم المباشر فى العزم على النظام المقترح أثبتت نتائج المحاكاة أن استخدام الشكل التقليدى للعاكس سداسي الأطوار يعطى آداء هابطاً للنظام وهبوطاً في معامل استغلال القدرة[٢]، وحلاً لهذه المشكلات تم اقتراح عاكس سداسي الأطوار مكون من عاكسين من النوع ثلاثى الأطوار، و كانت نتائج المحاكاة تفوق نتائج الأبحاث التي تمت باستخدام توجيه المجال.

Journal of Engineering and Computer Sciences, Qassim University, Vol. 3, No. 1, pp. 27-46 (January 2010/Muharram 1431H)

Voltage Extinction-Angle Control of Grid-Connected Induction Generator

A.F. Almarshoud[*], M.A. Abdel-halim[**], and M. Munawer Shees[***]

College of Engineering, Qassim University, Buraydah
** amarshoud@yahoo.com ** masamie@qec.edu.sa *** munawwarshees@qec.edu.sa*

(Received 21/2/2009, accepted for publication 10/9/2009)

Abstract. This paper presents a complete analysis of an induction generator linked to the power network through an ac voltage controller aiming to control the generated active and reactive power at different speeds. The ac voltage controller uses the extinction angle strategy to control the generator terminal voltage. The generator performance characteristics regarding the harmonic distortion factors, active power, reactive power, power factor, torque ripples and efficiency have been computed at different speeds. These characteristics have been determined with the help of a novel equivalent circuit in the frequency domain.
***Keywords*:** induction generator, ac voltage controller, grid-connected

1. Introduction

Wind energy finds increasing applications as a source of renewable energy in the world. This power may be utilized to generate electrical power using the induction generators [1-2]. The performance of a grid-connected induction generator using a solid state ac voltage controller as an interface between the grid and the stator terminals of the generator is studied in this paper. In this regard a forced-commutated ac voltage controller which utilizes a set of power transistor devices has been used.

Many authors have analyzed the self excited induction generators [3-8] which are utilized in far and isolated sites. The performance of controlled generators using ac voltage controller has been analyzed in previous publications for naturally commutated voltage controllers, and forced commutated voltage controllers [9-11]. The analysis has been determined using numerical techniques based upon a dq-abc reference frame models. In the present paper the steady-state electrical and mechanical performance of the generator has been analyzed through modeling the induction generator and the static converter by novel equivalent circuits in the frequency domain. This is expected to give more accurate results, and enables the iron losses to be taken into consideration which leads to accurate estimation of the generator efficiency.

Simulating programs have been developed to determine the performance characteristics of the uncontrolled grid-connected induction generator and the controlled generator for a wide range of operating conditions and a specified switching strategy of the ac voltage controller. In this regard, the extinction angle control strategy has been used. The computed performance characteristics included the generator current and its distortion factors, the generator active and reactive powers and the generator efficiency. Also, the bus current, its distortion factors, reflected harmonics on the supply, the displacement angle, the bus active and reactive powers, and the power factor has been computed. On the other side the mechanical performance characteristics regarding the unidirectional-developed torque and the pulsating components appearing as a result of the use of the ac voltage controller have been determined.

When using the ac voltage controllers, the active and reactive powers of the grid connected induction generator can be controlled. The bus reactive power is clearly controlled when using the firing angle control strategy.

2. Solid State Control of the Induction Generator

Forced commutated ac voltage controller is suggested to be used as an interface between the grid and the induction generator.

2.1 Control Using a Forced Commutated AC Voltage Controller

The proposed circuit is shown in Fig. (1). Each stator phase has control circuit that contains series and shunt power transistor in bridges of diodes to allow the current to pass in the two directions [10]. The two transistors are operated alternatively, when the series transistor is turned on, the shunt transistor is turned off and vice versa. This control circuit links the induction generator with the network. The terminal voltage as well as the active and reactive power of the generator can be controlled by variation of the on and off periods of the series transistors. The shunt transistor bridge allows the clamped current in the stator phase during the off state of the series bridge to continue flowing as freewheeling path.

The transistorized ac voltage controller may be controlled using different control strategies. In the present paper the extinction angle control strategy is applied. The control of the generator terminal voltage is done by fixing the firing angle (α) at zero degree, while the extinction angle (β) is varied as shown in Fig. (2). One of the advantages of this control strategy is that the switching off of the semiconductor devices is done at small current.

The terminal voltages of the induction generator are as follows:

$$v_a = V_m \sin \omega t \qquad n\pi \leq \omega t \leq (n\pi + \beta),\ n=0, 1,2, .. \qquad (1)$$

v_b and v_c lag behind v_a by $2\pi/3$ and $4\pi/3$ respectively.

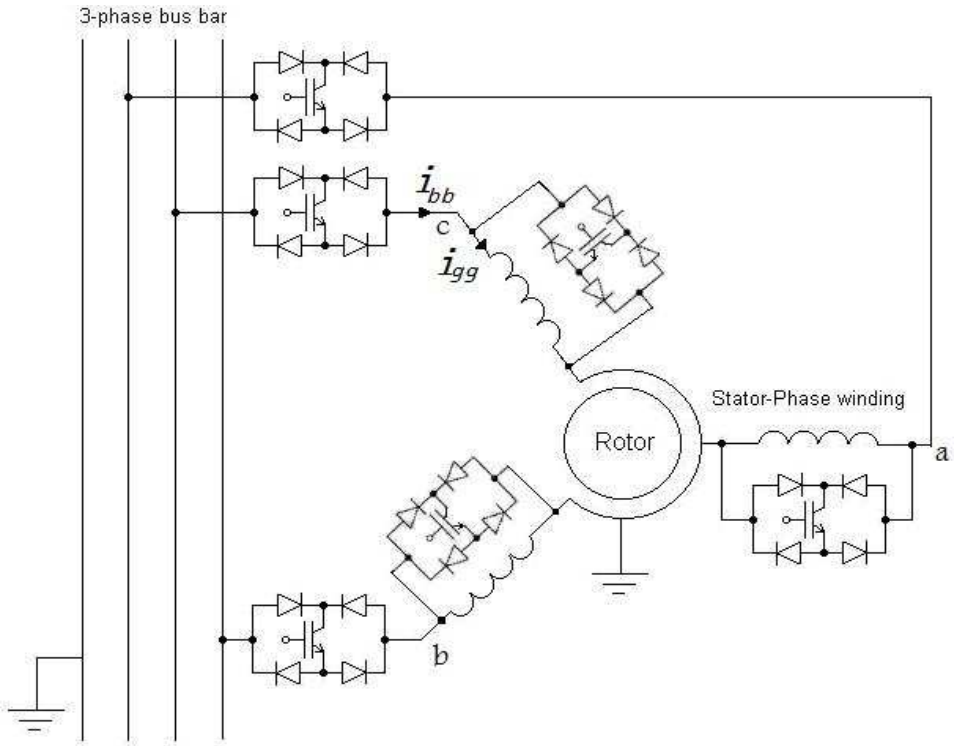

Fig. (1). Induction generator connected to grid via ac voltage controller.

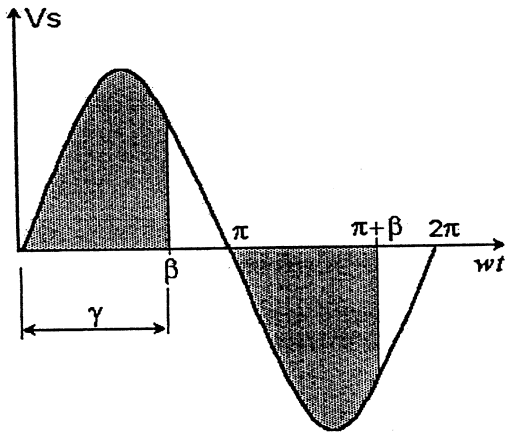

Fig. (2). Extinction angle control strategy.

3. Steady State Modeling

3.1 Frequency Domain Equivalent Circuits

The stator terminal voltage of the induction Generator when using an ac voltage controller is no more pure sinusoidal voltage (Fig. 2). Using Fourier series [12] this voltage can be analyzed to a series of fundamental voltage and higher order voltage harmonics. Let, the bus voltage; v_{bb}, to be

$$v_{bb}(t) = V_m \sin \omega t \quad (2)$$

Then, the generator terminal voltage; v_g, is given by

$$v_g(t) = SF(t).v_{bb} \quad (3)$$

Where SF(ωt) is a switching function that is fully determined according to the control technique such that, in the case of firing angle control technique

SF(t) = 1 $n\pi \le \omega t \le (n\pi + \beta)$; n = 0, 1, 2, .. (4)

Otherwise it is zero.

To get the Fourier series of the generator voltage, SF(θ) is easily analyzed using Fourier series rules, to get

$$SF(\omega t) = a_o + \sum_n c_n \sin(n\omega t + \varphi_n) \tag{5}$$

Where n is even number; n = 2, 4, 6, …

Then,

$$v_g(t) = V_m \sin(\omega t) \{ a_o + \sum_n c_n \sin(n\omega t + \varphi_n) \} \tag{6}$$

which yields the following equation:

$$v_g(t) = \sum_h V_h \sin(h\omega t + \varphi_h) \tag{7}$$

Where h is odd numbers.

V_h and φ_h are given for the extinction-angle control techniques in Appendix A.

The generator applied voltage components, obtained by Fourier series, are classified as follows:

a) Positive sequence voltage components:

Components of order nf = 1 + 6k; where k = 0, 1, 2, 3,…., are called positive sequence voltages. These voltages generate rotating fluxes in the same direction of rotation of the flux produced by the fundamental voltage. The slip w.r.t the flux of any positive sequence voltage is obtained as follows:

$$S_P = \frac{nf \times N_s - N_r}{nf \times N_s} \tag{8}$$

where N_s is the nominal synchronous speed, and N_r is the rotor speed.

b) Negative sequence voltage components:

Components of order nb = 5 + 6k; where k = 0, 1, 2,…., are called negative sequence voltages. These voltages generate rotating fluxes in the opposite direction of rotation of the flux produced by the fundamental voltage. The slip w.r.t the flux of any negative sequence voltage is obtained as follows:

$$S_N = \frac{nb \times N_s + N_r}{nb \times N_s} \tag{9}$$

c) Zero sequence voltage components:

Harmonics of order no = 3 + 6k; where k = 0, 1, 2, 3,…., are called zero sequence or triplex voltages. The net flux of these harmonic components in the air gap is zero. Therefore, they neither contribute to the torque output nor induce currents in the rotor.

The positive and negative sequence equivalent circuits of the slip ring and plain cage induction machines are as shown in Fig. (3a). Fig. (3b) shows the zero sequence equivalent circuit. The zero sequence voltage drives zero sequence currents if the induction generator circuit allows. This happens in case of delta connected generator or four wire system.

It is worth noting that the used equivalent circuits takes into consideration the effect of the fundamental and voltage harmonics upon the stator iron loss, while the effect of these harmonics upon the rotor is neglected. Rotor iron loss is not considered as; firstly the iron loss due to the fundamental flux, which is nearly stationary with respect to the rotor at normal running conditions, is nearly zero. Secondly, the harmonic fluxes decrease drastically with the order of voltage harmonic. Thirdly, the rotor iron size is small compared with the stator iron.

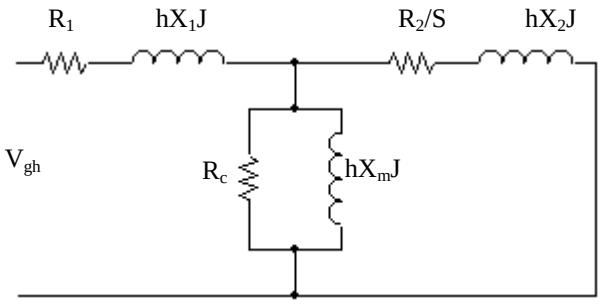

(a)Positive and negative sequence equivalent circuits

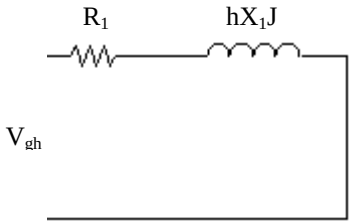

(b) The zero sequence equivalent circuit of the induction machine.

Fig. (3). The generator equivalent circuits.
($S = S_P$ in case of +ve sequence harmonics and $S = S_N$ in case of -ve sequence harmonics).

3.2 Generator Current, Power and Torque Calculations

For each voltage component (of order h) the appropriate equivalent circuit is used to calculate the corresponding stator, magnetizing and rotor currents. Also, the power factor is obtained. Then, the terminal active- and reactive- electrical power, air gap power and the induced torque are calculated as follows:

$$P_{gh} = V_{gh} I_{gh} \cos(\varphi_{gh} - \psi_{gh}) \quad \text{p.u} \tag{10}$$

$$Q_{gh} = V_{gh} I_{gh} \sin(\varphi_{gh} - \psi_{gh}) \tag{11}$$

$$P_{AGh} = I_{gh}^2 R_2/S_h \quad \text{p.u} \tag{12}$$

$$T_{eh} = P_{AGh}/h \quad \text{p.u} \tag{13}$$

Where φ_{gh} is the phase angle of the h^{th} voltage component; V_{gh}, ψ_{gh} is the phase angle of the h^{th} current component; I_{gh}, and S_h is the slip w.r.t the flux of the h^{th} voltage component.

$$THD = \frac{\sqrt{I^2 - I_1^2}}{I_1} \tag{14}$$

THD defines the total harmonic content [13], but it does not indicate the level of each harmonic component. If a filter is used at the output of the converters, the higher-order harmonics would be attenuated more effectively. Therefore, knowledge of both the frequency and the magnitude of each harmonic is important. The distortion factor indicates the amount of the harmonics distortion that remains in a particular waveform after the harmonics of that waveform have been subjected to a second order attenuation (i.e. divided by n^2). Thus, D.F [13] is a measure of effectiveness in reducing unwanted harmonics without having to specify the values of the second order load filter and is defined as [13]

$$D.F = \frac{1}{I_1}\left[\sum_{h=2,3}\left(\frac{I_h}{h^2}\right)^2\right]^{1/2} \tag{15}$$

$$D.F_h = \frac{I_h}{I_1 . h^2}$$

The total generator active- and reactive- electrical power are calculated by

$$P_g = \sum_k P_{gk} \tag{16}$$

$$Q_g = \sum_k Q_{gk} \tag{17}$$

The total steady induced torque is calculated by

$$T_e = \sum_k T_{ek} \tag{18}$$

Where k= 1, 3, 5, …

Interaction between the fluxes that rotate at different speeds results in pulsating torques. The steady and pulsating torque components are calculated in p.u using the following formula [14]:

$$T_{e1} = X_m \sum_{ks} \sum_{kr} (I_{s(ksf)} I_{r(krf)} \sin((ksf - krf)\omega_s t + \psi_{s(ksf)} - \psi_{r(krf)})$$

$$T_{e2} = X_m \sum_{ks} \sum_{kr} (I_{s(ksb)} I_{r(krb)} \sin((ksb - krb)\omega_s t + \psi_{s(ksb)} - \psi_{r(krb)})$$

$$T_{e3} = X_m \sum_{ks} \sum_{kr} (I_{s(ksb)} I_{r(krf)} \sin((ksb + krf)\omega_s t + \psi_{s(ksb)} + \psi_{r(krf)})$$

$$T_{e4} = X_m \sum_{ks} \sum_{kr} (I_{s(ksf)} I_{r(krb)} \sin((ksf + krb)\omega_s t + \psi_{s(ksf)} + \psi_{r(krb)})$$

$$T_e = T_{e1} - T_{e2} + T_{e3} - T_{e4} \tag{19}$$

I_s and I_r are the stator and rotor currents, respectively. Ksf and krf are the stator and rotor harmonic orders which induce forward rotating magnetic fields. ksb and krb are the stator and rotor harmonic orders which induce backward rotating magnetic fields.

3.3 Bus Current and Power Calculations

As at any instant the instantaneous bus power (p_{bb}) equals the instantaneous generator power (p_g), then

$$p_g = p_{bb} \tag{20}$$

which means

$$v_g\, i_g = v_{bb}\, i_{bb} \tag{21}$$

Using Eqns. 3 and 21, leads to

$$i_{bb} = i_g\, SF(t) \tag{22}$$

i_g has components calculated from the equivalent circuits corresponding to the voltage components and SF(t) has its Fourier Series form. Thus the bus current (i_{bb}) could be expressed as a summation of current components as given in Appendix A.

The active- and reactive- electrical powers are calculated, keeping in mind that the bus voltage is a pure sinusoidal voltage, as follows:

$$P_{bb} = V_{bb}\, I_{bb1} \cos(-\psi_{bb1}) \tag{23}$$

$$Q_{bb} = V_{bb}\, I_{bb1} \sin(-\psi_{bb1}) \tag{24}$$

The angle between the fundamental bus current; I_{bb1}, which is measured in the output sense, and the bus voltage is called the displacement angle (DAngl). This angle is calculated as follows:

$$DAngle = \psi_{bb1} + \pi, \tag{25}$$

The bus power factor is calculated from [13]

$$PF = PuF \,.\, DF \tag{26}$$

Where PuF is the purity factor and is given by; $PuF = I_1/I$

The generator efficiency is calculated as follows:

$$\eta = P_e/(T_e\, N_r) \tag{27}$$

The bus current total distortion factor and the individual distortion factors are calculated using the formula applied to the generator current (Eqns. 14, 15).

4. Performance Characteristics of the Controlled Generator

4.1. Generator Performance Characteristics

A simulation program based upon the steady state (frequency domain) equivalent circuits, with the terminal voltage represented as a series of fundamental voltage and higher harmonic voltages has been developed. The terminal voltage is determined using Fourier series analysis (Appendix A.1) which gives the voltage components as a function of the extinction angle. The program has been used to compute the performance characteristics of the generator having the data given in Appendix B. Various performance

characteristics of the generator such as the fundamental current, total current, various distortion factors, the active power, the reactive power and the efficiency of the generator have been computed versus the generator speed at different extinction angles. These characteristics are depicted in Figs. (4-9). These figures indicate that at a certain speed the fundamental current decreases as the extinction angle decreases (Fig. 4). Also, as the extinction angle decreases the harmonic current contents increases. It should be mentioned here that only odd harmonic currents exist (Figs. 5-7). It is obvious from Fig. (8) that the active power decreases as the extinction angle decreases. The reactive power absorbed by the generator increases with the increase of the slip. Over the normal operating slip range (- 0.005 to - 0.02) the reactive power behaves in a fluctuating manner as the extinction angle decreases. The generator efficiency decreases as the extinction angle decreases due to the increase of the harmonic contents (Fig. 10).

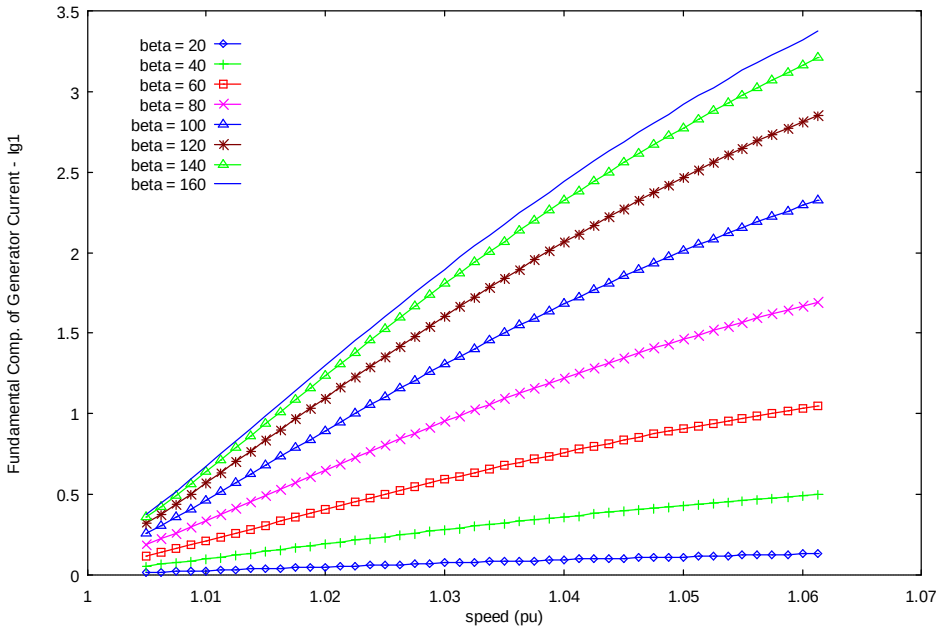

Fig. (4). Relation between fundamental component of generator current and speed.

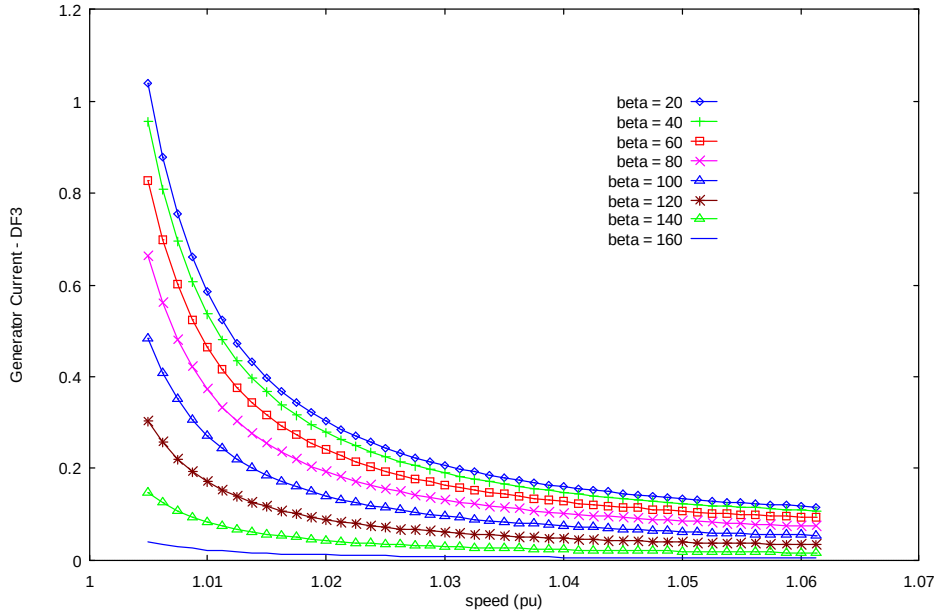

Fig. (5). Relation between distortion factor of the third order harmonic component of generator current and speed.

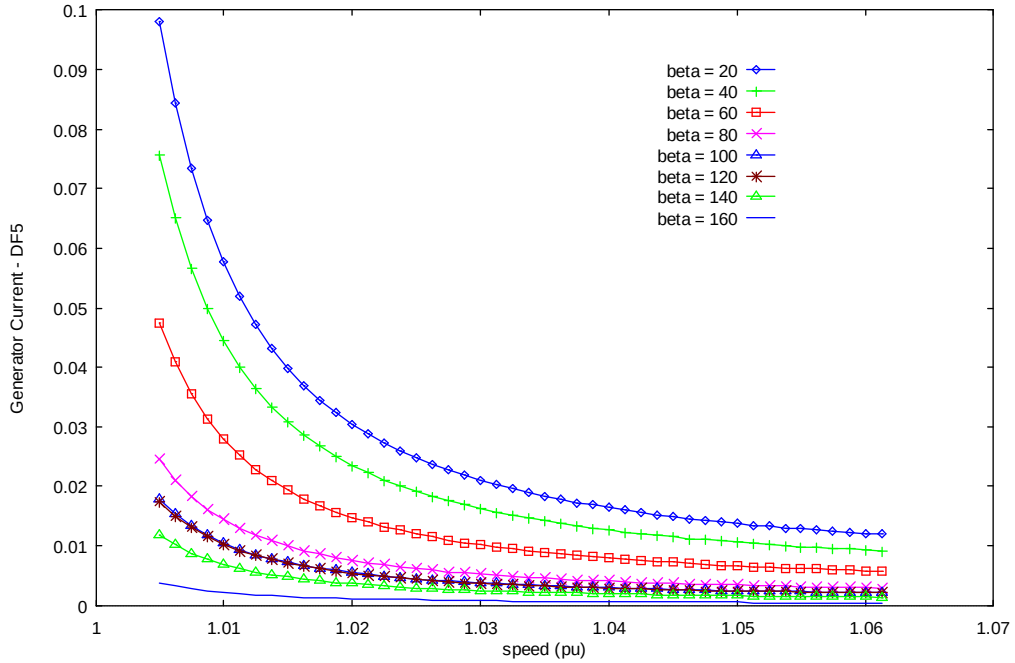

Fig. (6). Relation between distortion factor of the fifth order harmonic component of generator current and speed.

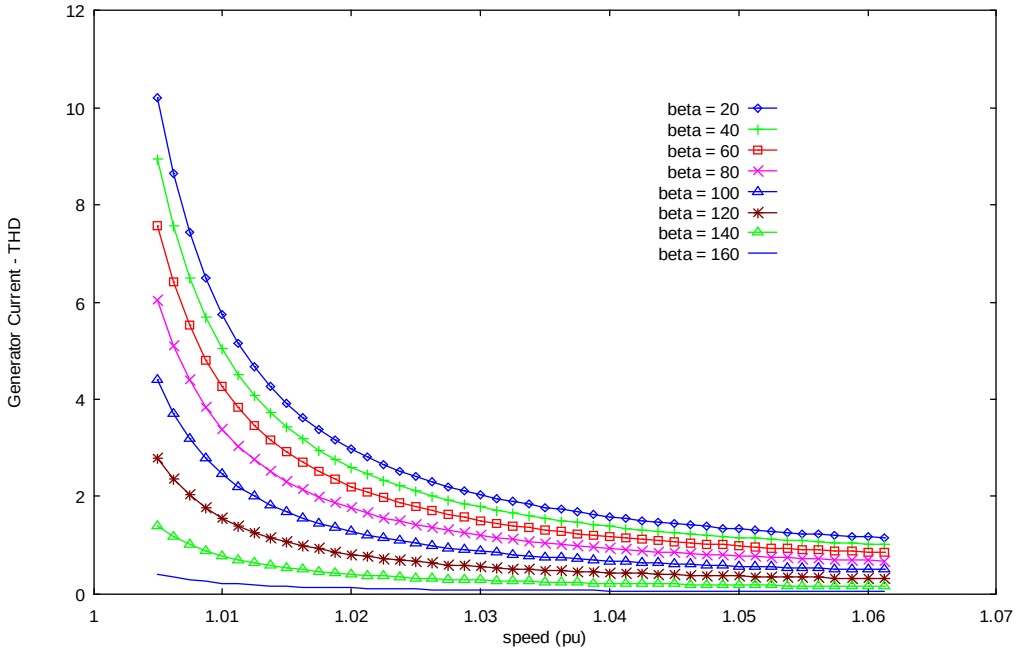

Fig. (7). Relation between total distortion factor of generator current and speed.

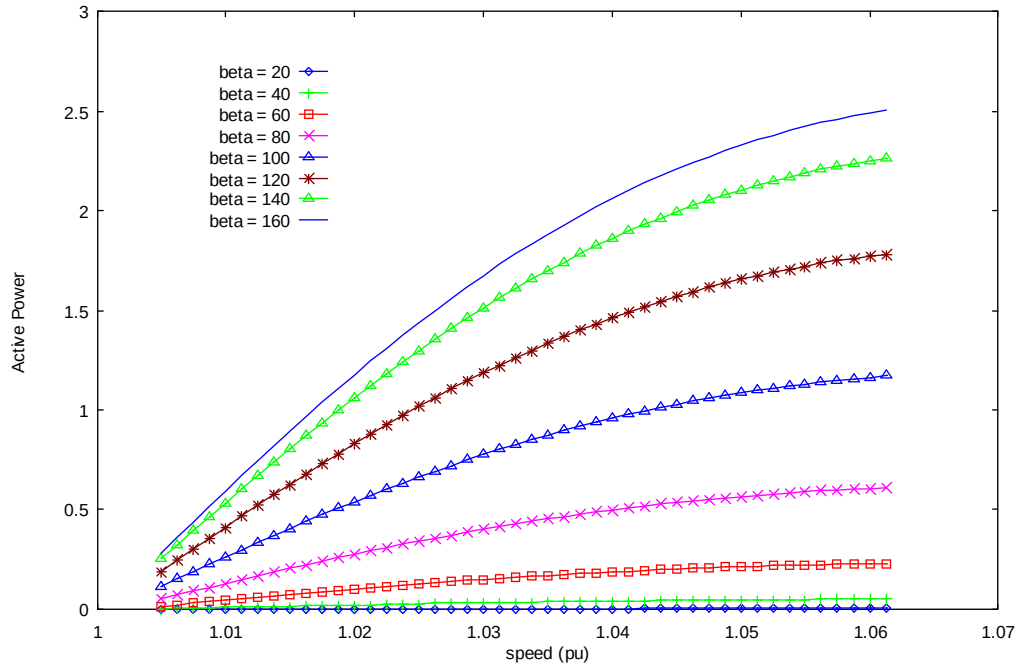

Fig. (8). Relation between the active power of the generator and its speed.

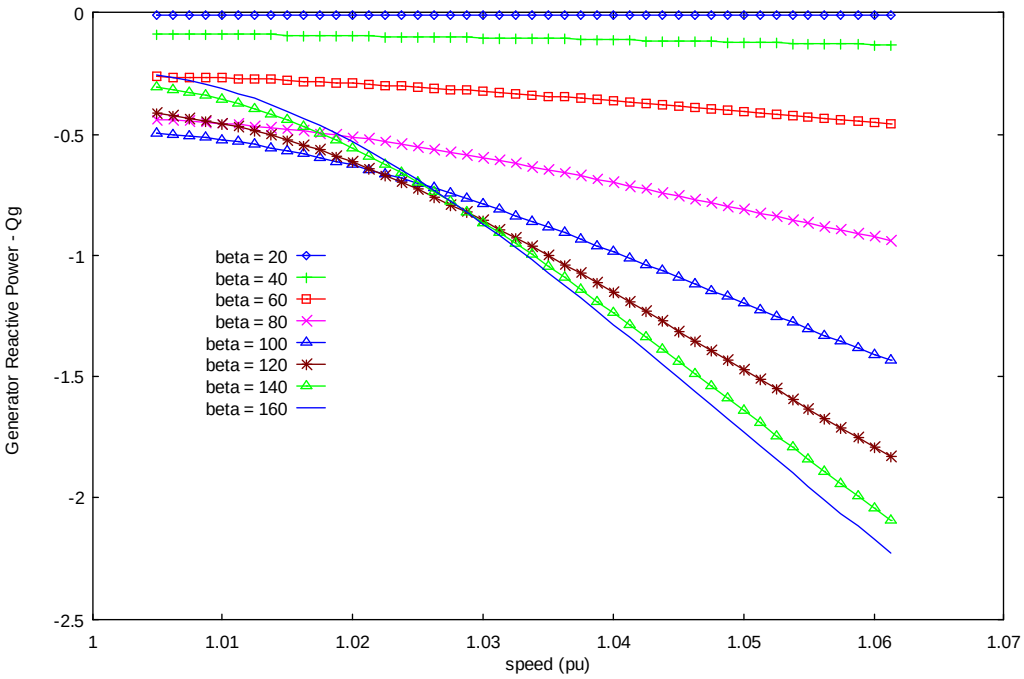

Fig. (9). Relation between the reactive power of the generator and its speed.

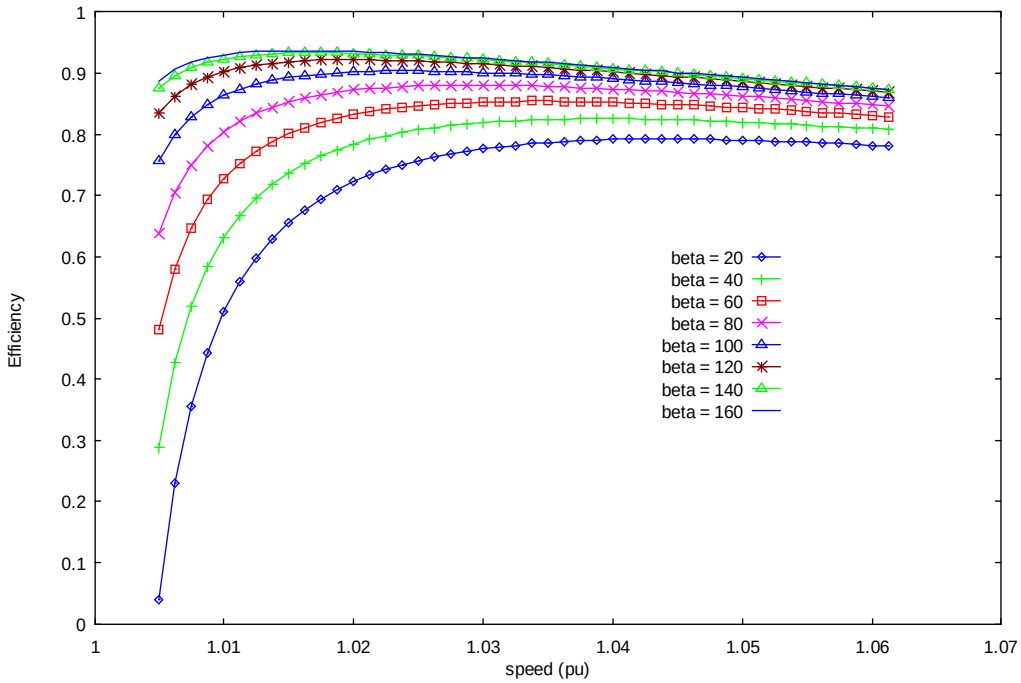

Fig. (10). Relation between efficiency of the generator and its speed.

4.2. Impact Upon the Supply

The effect of using the ac voltage controller when employing the extinction angle-control strategy upon the supply (bus-bar) has been investigated. The concerned quantities include the bus fundamental current, different current distortion factors, the active power, fundamental-current reactive-power, the displacement angle and power factor. The computed results showing the effect of the extinction angle are depicted in Figs (11-17). The bus fundamental current decreases as the extinction angle decreases (Fig. 11). The bus current, like the generator current, contains odd harmonics. As the extinction angle decreases the harmonic contents increase (Figs. 12-14). As the extinction angle decreases, the displacement angle increases in the leading direction, consequently, the generator consumes more fundamental reactive power and delivers less active power (Figs. 15, 16). The power factor shows rapid decrease as the extinction angle decreases (Fig. 17).

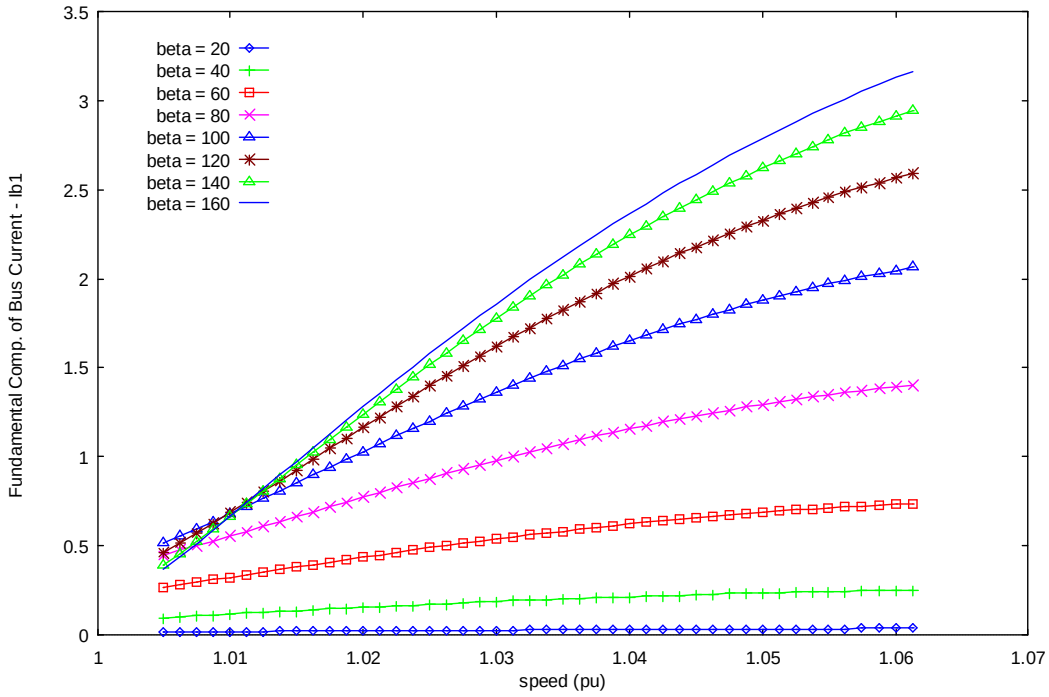

Fig. (11). Relation between fundamental component of bus current and generator-speed.

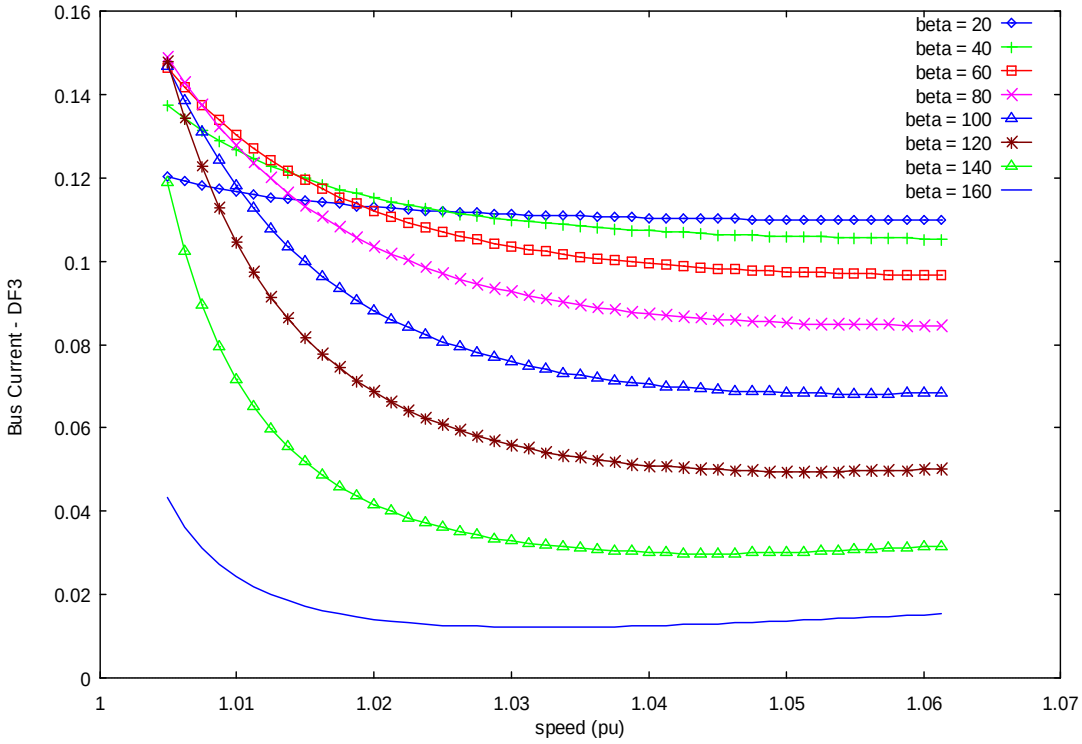

Fig. (12). Distortion factor of third order harmonic component of bus current and generator-speed.

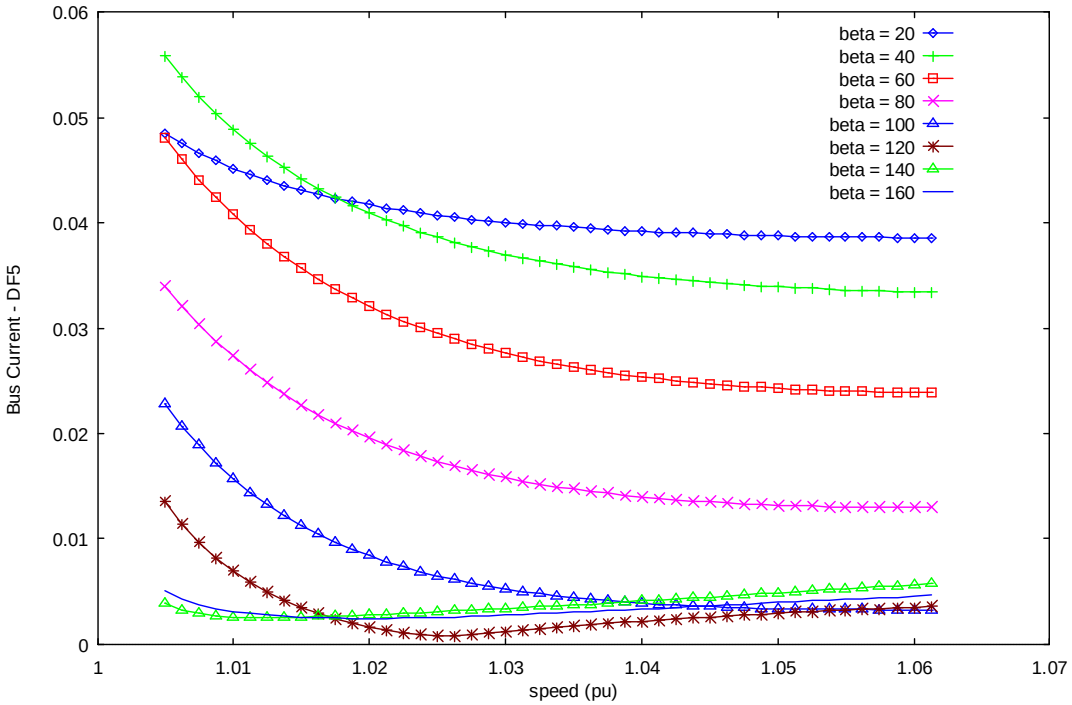

Fig. (13). Distortion factor of the fifth order harmonic component of bus current and generator-speed.

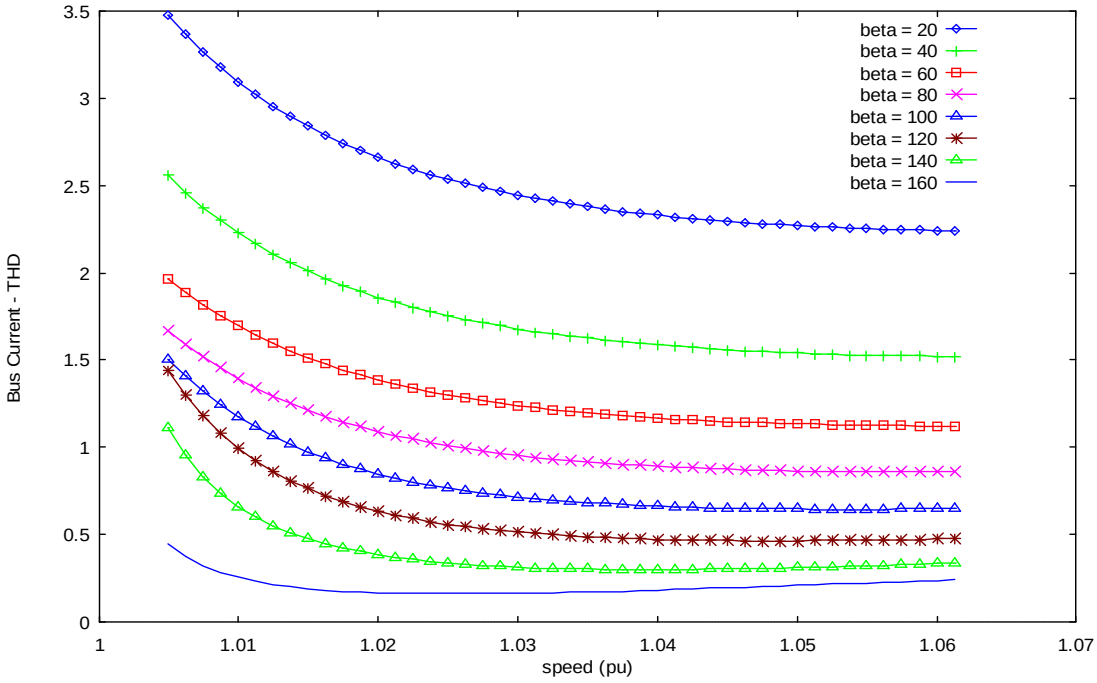

Fig. (14). Relation between total harmonic distortion factor of bus current and generator-speed.

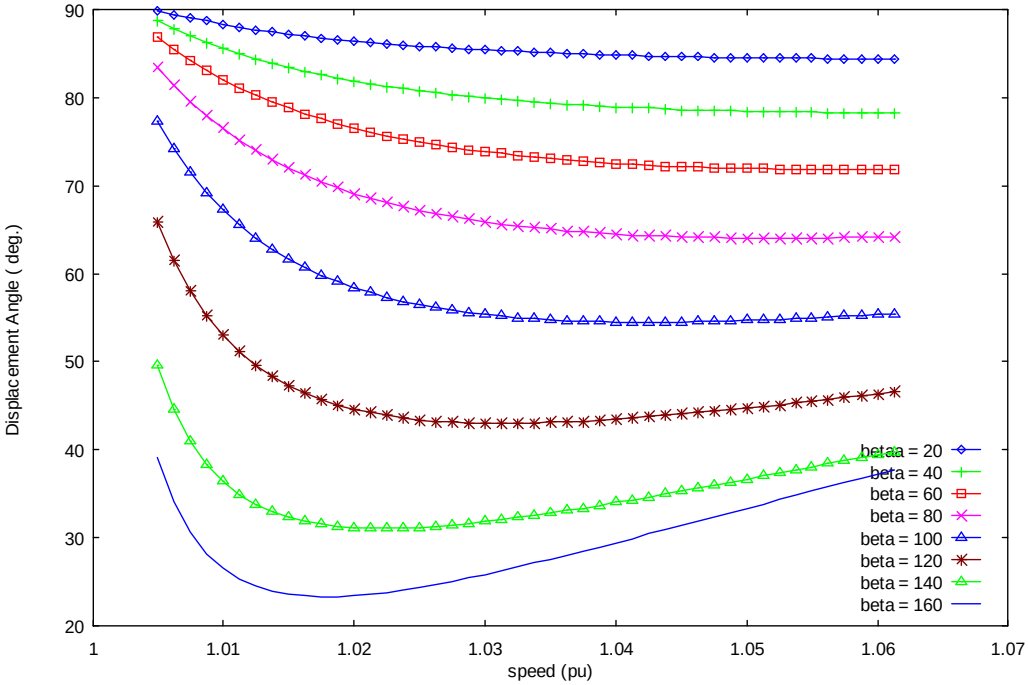

Fig. (15). Relation between displacement angle of bus current and generator-speed.

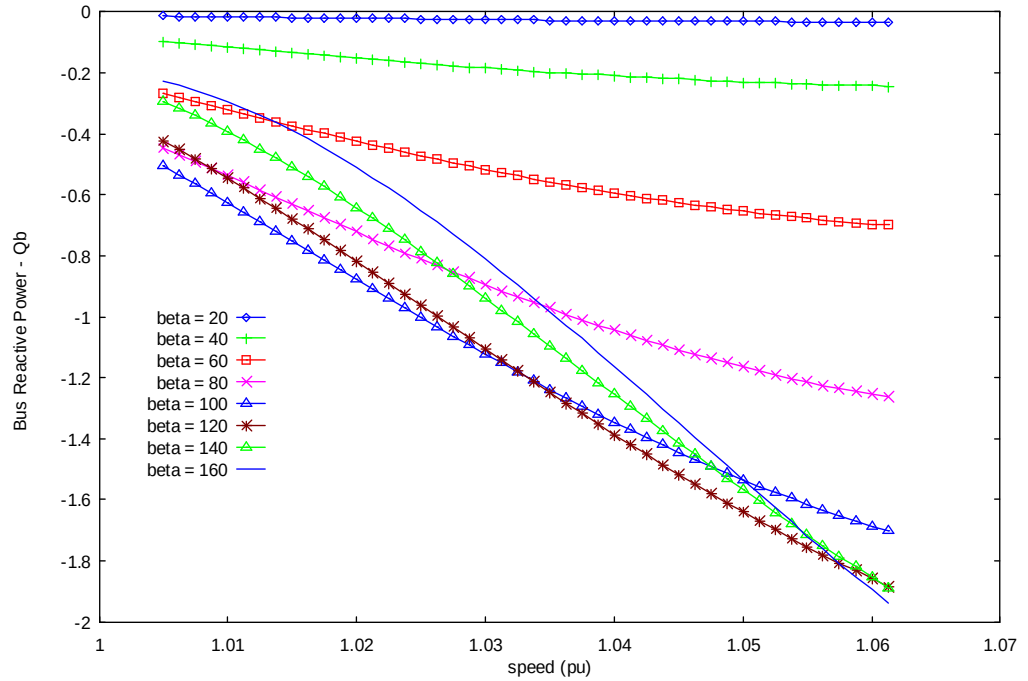

Fig. (16). Relation between bus reactive power and generator-speed.

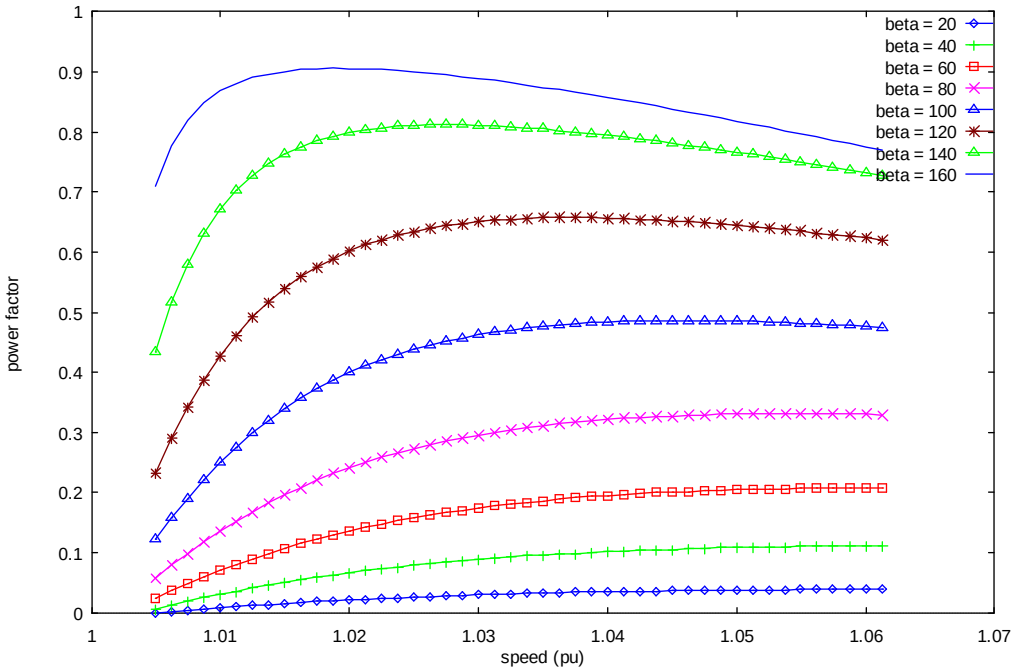

Fig. (17). Relation between bus power factor and generator-speed.

In light of the calculated generator and bus current components, the ratings of the ac voltage controller devices could be determined (see Appendix B). To attenuate the penetration of the resulted harmonic currents into the supply a rejection passive or active filter [13] should be connected between the generator and the bus.

4.3 Mechanical Performance Characteristics of the Controlled- Generator

The effect of using the ac voltage controller upon the induced torque as regarding the produced average torque and the added pulsating torques has been investigated. The computed results are shown in Figs. (18-21). The total average steady torque produced by all the voltage components is shown in Fig. (18) versus the generator speed at different extinction angles. That produced by the fundamental voltage is shown in Fig. (19). The 6^{th} order and 12^{th} order pulsating torques are shown in Figs. (20 and 21) as a percentage of the total steady induced torque. As the extinction angle decreases the 6^{th} order pulsating torque (computed as a ratio of the steady torque) has the tendency to increase but with a fluctuating manner. The 12^{th} order pulsating torque (computed as a ratio of the steady torque) behaves in a fluctuating manner similar to the 6^{th} order pulsating torque.

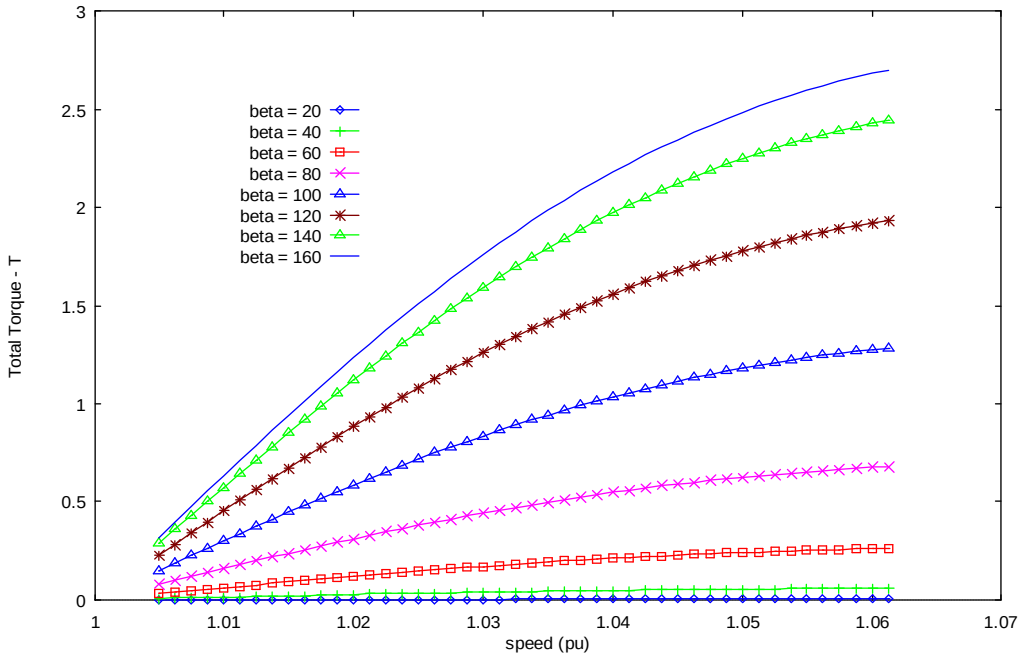

Fig. (18). Relation between the total average induced torque and generator-speed.

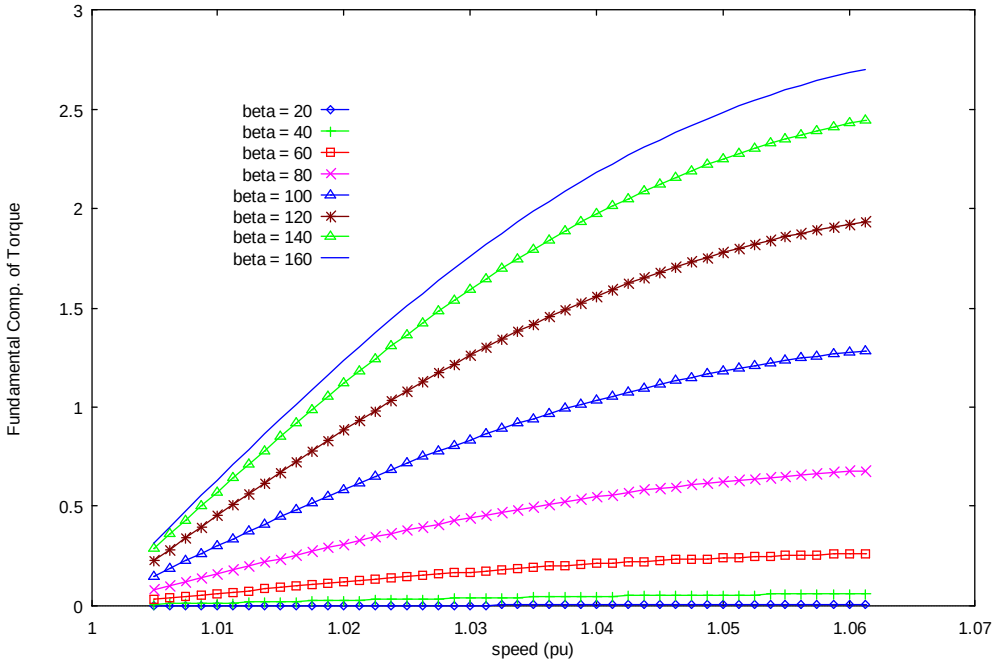

Fig. (19). Relation between average torque induced by the fundamental voltage and generator-speed.

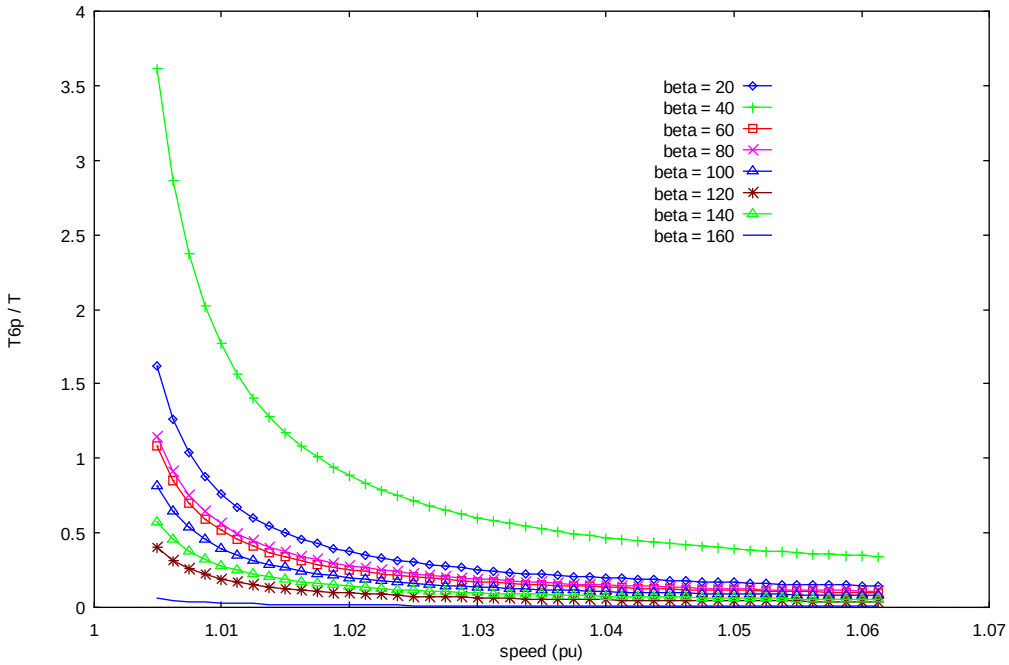

Fig. (20). Relation between sixth order pulsating torque and generator-speed .

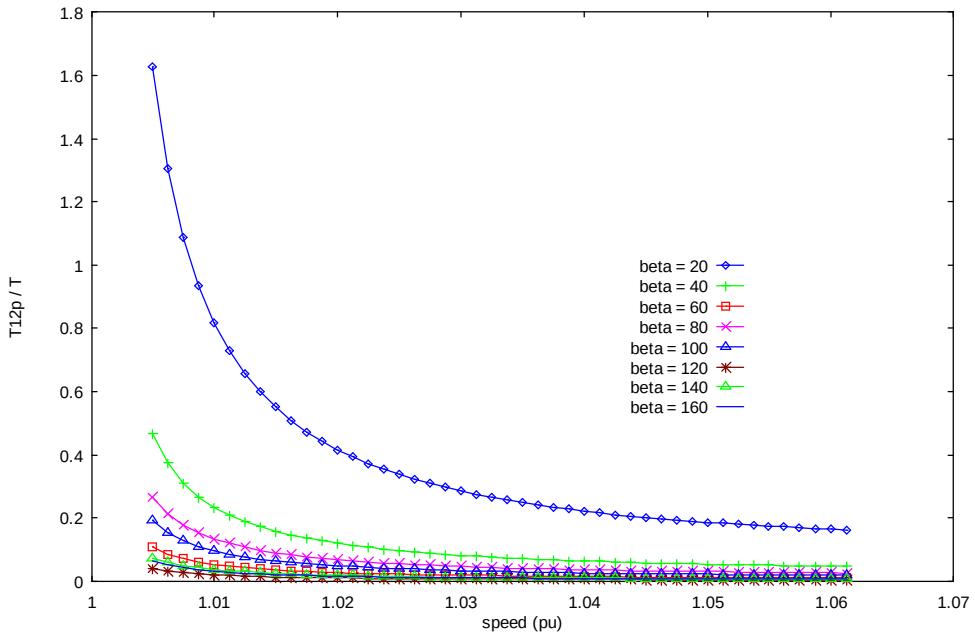

Fig. (21). Relation between twelfth order pulsating torque and generator-speed .

5. Conclusions

The performance of a grid-connected induction generator using a solid state ac voltage controller as an interface between the grid and the stator terminals of the generator has been studied. In this respect forced-commutated ac voltage controller which utilizes a set of power transistor devices has been used.

The steady-state electrical and mechanical performance has been analyzed through modeling the induction generator and the static converter by novel equivalent circuits in the frequency domain. The presented model is more accurate compared with the time domain models, which usually neglect the iron losses. The computed performance characteristics included the generator current and its distortion factors, the generator active and reactive powers and the generator efficiency. Also, the bus current, its distortion factors, reflected harmonics on the supply, the displacement angle, the bus active and reactive powers, and the power factor has been computed. On the other side the mechanical performance characteristics regarding the developed torque and the pulsating components appearing as a result of the use of the ac voltage controller have been determined.

When using the ac voltage controllers, the active and reactive powers of the grid connected induction generator can be controlled. The bus reactive power is clearly controlled when using the extinction angle control strategy.

Using the solid state electronic switches is associated with the existence of current harmonic contents in the generator and harmonic currents reflected on the supply. Only the odd harmonics especially the third harmonics exist extensively.

Acknowledgment
The authors are grateful to the Deanship of Scientific Research for their financial support through this research.

6. References

[1] Fernando D. Bianchi, Herna'n De Battista and Ricardo J. Mantz, "*Wind Turbine Control Systems- Principles, Modelling and Gain Scheduling Design*," Springer, London, (2007).
[2] Singh, B., "Induction generators- A prospective", *Electric Machines and Power Systems*, Vol.23 (1993), 163-177.
[3] Raina, G., and Malik, O. P., "Wind Energy Conversion using a Self-Excited Induction Generator", *IEEE Transactions on Power Apparatus and Systems*, Vol. PAS-102, No. 12 (December 1983), 3933-3936.
[4] Shaltout, A.A., and Abdel-halim, M.A. ,"Solid State Control of a Wind Driven Self-Excited Induction Generator", *Electric Machines and Power Systems*, Vol. 23 (1995) , 571-582.
[5] Shaltout, A. A., and El-Ramahi , A.F. ,"Maximum power tracking for a wind driven induction generator connected to a utility network", *Applied Energy*, Vol.52 (1995), 243-253.
[6] Singh, B., Shridhar, L., and Jha, C.S., "Improvements in the Performance of Self-Excited Induction Generator through Series Compensation", *IEE Proceedings Generation, Transmission and Distribution*, Vol. 146, No. 6 (November 1999), 602-608.
[7] Shaltout, A., Abdel-Halim, M., and Al-Ramahi, A., "Optimised Solid-State Exciter for Wind Powered Pumping Applications", *Proceedings of the Fourth Arab International Solar Energy Conference*, Amman, Jordan, (20-25 November 1993), 233-242.
[8] Brennen, M. B., and Abbondanti, A., "Static Exciters for Induction Generator", *IEEE Transactions on Industry Applications*, Vol. IA-13, No. 5 (September/October 1976), 422-428.
[9] Almarshoud, A. F., Abdel-halim, M. A., Alolah, A. I., "Performance of Grid Connected Induction Generator under Naturally Commutated AC Voltage Controller", *Electric Power Components and Systems*, Vol. 32 (2004), 691-700.
[10] Abdel-halim, M.A., "Solid State Control of a Grid Connected Induction Generator", *Electric Power Components and Systems*, Vol. 29 (2001), 163-178.
[11] Abdel-halim, M. A., Abdel-aziz, M. M. and Mostafa, H. G., "AC chopper controlled grid-connected induction generator", *Qassim University Scientific Journal- Engineering and Computer Sciences*, Vol.1, No. 1 (2008), 1- 19.
[12] Ralaston, A., "*A First Course in Numerical Analysis*", New York, USA, McGraw-Hill, (1995).
[13] Rashid, M. H., "*Power Electronics: Circuits, Devices, and Applications*", Second Edition, Prentice-hall, USA, (1993).
[14] Abdulrahman S. M., Kettleborough, J. G. and Smith, I. R., "Fast Calculation of Harmonic Torque Pulsations in a VSI/Induction Motor Drive", *IEEE Trans. On Industrial Electronics*, Vol.40, No.6 (Dec. 1993), 561-569.

Appendix A: Fourier Series of the Generator Voltage and Bus Current

A.1- Generator Voltage

$v_g = V_m \sin(\omega t)$. SF(t)

where SF(t) is the switching function which is determined according to the control strategy as follows:

SF(t) = 1 $\quad n\pi \leq \omega t \leq (n\pi + \beta)$; n = 0, 1, 2, ..

Otherwise it is zero.

Using Fourier series analysis of the switching function, the generator voltage can be expressed as follows:

$v_g = 0.5V_m [(a_0-a_2) \sin(\omega t) + (a_2-a_4) \sin(3\omega t) + (a_4-a_6) \sin(5\omega t) + (a_6-a_8) \sin(7\omega t) + \ldots\ldots$

$+ b_2 \cos(\omega t) + (b_4-b_2) \cos(3\omega t) + (b_6-b_4) \cos(5\omega t) + (b_8-b_6) \cos(7\omega t) + \ldots\ldots]$

Thus, the fundamental component; $v_{g1} = 0.5V_m (a_0-a_2) \sin(\omega t) + 0.5V_m (b_2) \cos(\omega t)$

$= c_1 \sin(\omega t + \varphi_1)$,

where $c_1 = 0.5V_m [(a_0-a_2)^2 + (b_2)^2]^{1/2}$, $\varphi_1 = \arctan[b_2/ (a_0-a_2)]$

3rd voltage harmonic component; $v_{g3} = 0.5V_m (a_2- a_4) \sin(3\omega t) + 0.5V_m (b_4-b_2) \cos(3\omega t)$

$= c_3 \sin(3\omega t + \varphi_3)$,

where $c_3 = 0.5V_m[(a_2- a_4)^2 + (b_4-b_2)^2]^{1/2}$, $\varphi_3 = \arctan[(b_4-b_2)/ (a_2- a_4)]$

5th voltage harmonic component; $v_{g5} = 0.5V_m (a_4- a_6) \sin(5\omega t) + 0.5V_m (b_6-b_4) \cos(5\omega t)$

$= c_5 \sin(5\omega t + \varphi_5)$,

where $c_5 = 0.5V_m[(a_4- a_6)^2 + (b_6-b_4)^2]^{1/2}$, $\varphi_5 = \arctan[(b_6-b_4)/ (a_4- a_6)]$

and so on.

a_0, a_n and b_n are given, for the extinction angle control strategy as follows:

$a_0 = 2\beta/\pi$

$a_n = \sin(2n\beta)/(n\pi)$, $\quad$ n =2,4,6,,….

$b_n = [1- \cos(2n\beta)]/(n\pi)$, $\quad$ n =2,4,6,…

A.2- Bus Current

$i_{bb} = i_g$ SF(t)

The fundamental bus current is given by

$i_{bb1} = \{0.5\ I_{g1} ((a_0-a_2) \cos(\psi_{g1})+b_2 \sin(\psi_{g1})) + 0.5\ I_{g3} ((a_2-a_4) \cos(\psi_{g3}) + (b_4-b_2)\ \sin(\psi_{g3})) + 0.5\ I_{g5} ((a_4-a_6) \cos(\psi_{g5})+(b_6-b_4) \sin(\psi_{g5})) +\ 0.5\ I_{g7} ((a_6-a_8) \cos(\psi_{g7}) + (b_8-b_6) \sin(\psi_{g7})) +\ldots.\}\times\sin(\omega t)\ + \{0.5\ I_{g1} (b_2 \cos(\psi_{g1}) + (a_0+a_2) \sin(\psi_{g1})) + 0.5\ I_{g3} ((b_4+b_2) \cos(\psi_{g3}) + (a_2+a_4) \sin(\psi_{g3})) + 0.5\ I_{g5} ((b_6+b_4) \cos(\psi_{g5}) + (a_4+a_6) \sin(\psi_{g5}) + 0.5\ I_{g7} ((b_8+b_6) \cos(\psi_{g7}) + (a_6+a_8) \sin(\psi_{g7})) +\ldots.\}\times\cos(\omega t)$

3rd harmonic bus current is given by

$i_{bb3} = \{0.5\ I_{g1} ((a_2-a_4) \cos(\psi_{g1}) + (b_4+b_2) \sin(\psi_{g1})) + 0.5\ I_{g3} ((a_0-a_6) \cos(\psi_{g3}) + b_6 \sin(\psi_{g3})) +\ 0.5\ I_{g5} ((a_2-a_8) \cos(\psi_{g5}) + (b_8-b_2) \sin(\psi_{g5}))\ +\ldots.\}\times\sin(3\omega t)\ +\ 0.5\ I_{g7} ((a_4-a_{10}) \cos(\psi_{g7}) + (b_{10}-b_4) \sin(\psi_{g7})) + \{0.5\ I_{g1} ((b_4-b_2) \cos(\psi_{g1}) + (a_2+a_4) \sin(\psi_{g1})) + 0.5\ I_{g3} (b_6 \cos(\psi_{g3}) + (a_0+a_6) \sin(\psi_{g3})) + 0.5\ I_{g5} ((b_8+b_2) \cos(\psi_{g5}) + (a_2+a_8) \sin(\psi_{g5}) + 0.5\ I_{g7} ((b_{10}+b_4) \cos(\psi_{g7}) + (a_4+a_{10}) \sin(\psi_{g7})) +\ldots.\}\times\cos(3\omega t)$

5th harmonic bus current is given by

$i_{bb5}= \{0.5\ I_{g1} ((a_4-a_6) \cos(\psi_{g1})+(b_6+b_4) \sin(\psi_{g1})) + 0.5\ I_{g3} ((a_2-a_8) \cos(\psi_{g3}) + (b_9+b_2) \sin(\psi_{g3})) + 0.5\ I_{g5} ((a_0-a_{10}) \cos(\psi_{g5})+b_{10} \sin(\psi_{g5})) +\ldots.\}\times\mathrm{Sin}(5\omega t)\ +\ 0.5\ I_{g7} ((a_2-a_{12}) \cos(\psi_{g7}) + (b_{12}-b_2) \sin(\psi_{g7})) + \{0.5\ I_{g1} ((b_6-b_4) \cos(\psi_{g1}) + (a_4+a_6) \sin(\psi_{g1})) + 0.5\ I_{g3} ((b_8-b_2) \cos(\psi_{g3}) + (a_2+a_8) \sin(\psi_{g3})) + 0.5\ I_{g5} (b_{10} \cos(\psi_{g5}) + (a_0+a_{10}) \sin(\psi_{g5})) + 0.5\ I_{g7} ((b_{12}+b_2) \cos(\psi_{g7}) + (a_2+a_{12}) \sin(\psi_{g7})) +\ldots.\}\times\cos(5\omega t)$

where I_{g1} ,I_{g3} ,I_{g5} I_{g7} ..... are the generator harmonic currents.

a_0, a_n and b_n are as given before.

Appendix B: Generator System Particulars, Parameters and Device Ratings

The generator used is a three phase, 500 KVA, Δ/Y, 1830 rpm, 600/1039 V, 475/274 A, 4 pole, 50 Hz, cage induction generator having the following parameters:

$R_1 = R_2 = 0.015$ p.u, $X_1 = X_2 = 0.091$ p.u, $X_m = 4.251$ p.u, $R_c = 30$ p.u.

In the present work the generator has been connected in Y.

The current flowing through any of the series transistors has a uni-directional full wave-form, while that flowing in any of the diodes has a uni-directional half-wave form. Thus the devices are rated as follows:
The transistor ratings are: I (r.m.s rating) = $K_1 K_2$ 274 A,
I_p (peak current rating) = $K_1 K_3 \sqrt{2}$ 274 A,
V_{BO} (forward breakover voltage) = $K_1\sqrt{2}$ 600 V
The diodes ratings are : I (r.m.s rating) = $K_1 K_2$ 274 A,
I_p (peak current rating) = $K_1 K_3 \sqrt{2}$ 274 A,
V_{BD} (reverse breakdown voltage) = $K_1\sqrt{2}$ 600 V
K_1 is a safety factor (1.2 is a suitable value). K_2 is a factor greater than one introduced to account for the effect of the existence of current harmonics upon the r.m.s value (1.3 is a suitable value). K_3 is a factor greater than one introduced to account for the effect of the existence of current harmonics upon the peak value of the current (1.15 is a reasonable value).

التحكم عن طريق زاوية إطفاء الجهد في المولد الحثي المربوط بالشبكة

عبد الرحمن بن فهد المرشود* محمد عبد السميع عبد الحليم محمد مناور شيس*****

قسم الهندسة الكهربائية- كلية الهندسة –جامعة القصيم- بريدة
**** munawwarshees@qec.edu.sa ** masamie@qec.edu.sa * amarshoud@yahoo.com*

(قدم للنشر في ٢٠٠٩/٢/٢١م؛ وقبل للنشر في ٢٠٠٩/٩/١٠م)

ملخص البحث. يقدم هذا البحث تحليلاً لأداء مولد حثي مربوط بالشبكة الكهربائية من خلال حاكم للجهد المتردد، وعن طريق هذا الحاكم يتم التحكم في كل من الطاقة الفاعلة وغير الفاعلة، وفي هذا الصدد تستخدم إستراتيجية التحكم في زاوية الاطفاء لحاكم الجهد المتردد. ويعتمد البحث في التحليل على نموذج جديد للمولد تم تأسيسه باستخدام مبدأ توافقيات الجهد والمركبات التماثلية الموجبة والسالبة والصفرية التتابع، ويتميز هذا النموذج بأنه يعطي نتائج أدق إذا ما قورن بنماذج اطار المحورين المباشر والعمودي، حيث أنه لايستخدم المحاكاة الرقمية والتحليل العددي في ايجاد منحنيات الأداء بما تحويه من تقريب، كما أنه يمثل الفقد في الحديد والذي دائماً ما يهمل في التحاليل السابقة. ويقدم البحث العديد من خصائص الأداء كمنحنيات إجمالي تشوهات التوافقيات وتشوهات المركبات المختلفة لتيار المولد وتيار قضيب التوصيل وكذلك منحنيات كفاءة المولد ومعامل القدرة والعزوم النابضة.

Journal of Engineering and Computer Sciences, Qassim University, Vol. 3, No. 1, pp. 47-57 (January 2010/Muharram 1431H)

Employing Interpolated Wavelets for Hard and Soft Digital Processing of Scintillation Detector Signals

Ashraf Aboshosha, and Mahmoud Sayed

NCRRT, EAEA, 3 Ahmed El-Zomar Str., 8th District, Nasr City, Cairo Egypt. P. O. Box 29,
Fax. 0020-2-24115475, Email: ashraf.shosha@gmail.com

(Received 29/10/2009; accepted for publication 25/1/2010)

Abstract. In this article, hard and soft digital cores have been developed for refining, shaping, counting and multi-channel analysing (MCA) of scintillation detector signals. These cores are implemented to apply the forward wavelet transform for signal decomposition and the back interpolation technique for the reconstruction phase. We aim to de-noise, compress and reconstruct these signals by which the processing speed and storage will be optimized. Moreover, the presented technique deliver all important features of the scintillation signals such as; counting, shaping, pulse height. Also, it performs multichannel analysing from the single channel analyzing results. The new contribution of our framework arises from employing the interpolation techniques to reconstruct the signal where the mother wavelet and details are neglected. Moreover, soft techniques have been applied to evaluate the performance of the nonlinear mother wavelets and interpolation methods. The hardware design is implemented using hardware description language (HDL) and is implemented practically on the FPGA. The performance of the design has been tested in simulation mode on Model Sim benchmark and in real time mode on XC2S 50 Spartan-II FPGA. The soft processing included in this article employs a special purpose digital filter to refine the nuclear pulses and to extract their important features.

1. Introduction

The scintillation detector is one of the most important detectors used in nuclear and particle physics experiments as well as in nuclear medicine. These detectors are used in several radiation detection systems such as detection of mixed ionizing fluxes near nuclear objects, radionuclide control of samples and radiation pollution and in determination of the type and energy of high-energy particles and products of their reactions with targets. Scintillation signals are digitized, consequently quantization noise is added, the loss in signal quality is due to additional noise and shaping or pickup on signal line. Optimum filtering and more complex algorithms are implemented relying on the VHDL core. These algorisms are implemented on field programmable gate arrays (FPGAs). The overall scintillation system presented in this study is shown in figure (1).

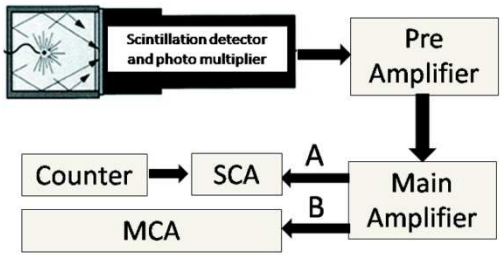

Figure (1). The overall scintillation system.

Throughout this framework the wavelets has been used as base for the pre-processing phase. The wavelet transform has recently emerged as a powerful tool for many applications such as data compression, de-noising, feature detection, and biomedical signal processing. Wavelets have been used in ultrasonic detection [1], in biomedical signals [2], in digital communications channels [3], and in medical images [4]. B. Mahmoud *et al* [5] described an acquisition and treatment system designed for semi-analog Gamma-camera. It consisted of a nuclear medical image acquisition, treatment and scintigraphic image construction in real time.

R. Engels *et al*. [6] developed a data acquisition board, it was a one slot board which received all the temporary information of the detector signals and allowed for complete pulse shape discrimination. A digital acquisition and elaboration system were developed and assembled for the direct sampling of fast pulses from nuclear detectors such as scintillators and diamond detectors [7]. G. Pasqualia *et al*. [8] implemented a DSP equipped fast digitizer. They used a digital signal processor (DSP) online analysis of detector signals. Algorithms have been written and tested on detectors of different types (scintillators, solid-state, gas-filled), implementing pulse shape discrimination, constant fraction timing, semi-Gaussian shaping, and gated integration. S. Zuberi [8] described a series of experiments and technical developments concerning the digital signal processing (DSP) of scintillator pulses in nuclear physics applications. J. Carletta *et al*. [9] designed a field programmable gate array (FPGA)-based digital hardware platform that implements wavelet transform algorithms for real-time signal de-noising of optical imaging signals.

Our proposed digital processor for scintillation detector signals is described as follows, see figure (2);

- De-noising and compression of scintillation signals relying on wavelet transform
- Employing hard and soft interpolations to reconstruct signal patterns
- Shaping signals with respect to threshold level
- Pulse counting
- Multichannel analyzing

The acquired scintillation signals are negative with floating decimal values. To overcome these problems we upscale all signals by large number and raise signals by adding a dc value. Also, we check the synchronization between PC and the FPGA kit to ensure the stability of our integrated system. Our digital processing core has been developed using HDL and it is implemented on an FPGA for denoising, compression, reconstruction based on linear interpolation, shaping and counting of scintillation signals. Moreover the developed technique converts the single channel analyser to multi channel analyser. The proposed solution is illustrated in figure (2).

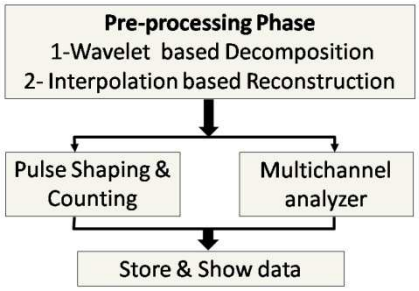

Figure (2). The applied Technique.

The rest of this paper is organized as follows; Section 2 is an overview on scintillation detectors. Section 3 reviews the fundamentals of the pre-processing technique presented in this study where the wavelets decomposition and the interpolation based reconstruction are presented. The FPGA implementation for computing the Haar Wavelets Transform (HWT) and the linear interpolation are presented in section 4. Section 5 presents signal shaping and counting obtained from an online analysis algorithm. In section 6 the concept of the transfer from single channel analyzing to the multi-channel analyzing is presented. Section 7 introduces the soft processing. Finally, Section 8 summarizes the conclusion.

2. Scintillation Detector

A brief overview of the most important parts of the physics behind gamma detection, scintillators and pulse shape analysis (PSA) are needed to fully grasp the content of this research work. A scintillator is a material that emits light, scintillates, when absorbing radiation. When a particle passes through the material it collides with atomic electrons, exciting them to higher energy levels. After a very short period of time the electrons fall back to their natural levels, causing emission of light. There are six different types of scintillators they are; organic crystals, organic liquids, plastics, inorganic crystal, gases and glasses. Pulses of light emitted by the scintillating material can be detected by a sensitive light detector, such as the photomultiplier tube (PMT) or photo diodes. The photocathode of the PMT, which is situated on the backside of the entrance window, converts the light (photons) into so-called photoelectrons. On the other hand in a photodiode, the scintillation photons produce electron-hole pairs that are collected at respectively the anode and the cathode of the diode. Most frequently, reverse biased PIN photodiodes are used having a low capacitance and leakage current. Hence an alternative way to detect the scintillation light from a crystal is the use of a silicon photodiode. The low level noise limitation of photodiode can be overcome by using Avalanche Photodiodes. Avalanche photodiodes (APDs) are photo detectors that can be regarded as the semiconductor analog to photomultipliers [10]. By applying a high reverse bias voltage (typically 100-200 V in silicon), APDs show an internal current gain effect due to impact ionization (avalanche effect).

In scintillators, the efficiency of converting the high-energy radiation into light is typically about 10%, hence the scintillator material must be transparent to the radiation it produces[11]. To accomplish this, the wide-gap material is activated with impurities which represent recombination sites for electrons and holes. Thus produced light has much lower energy than the band gap of the host crystal. Anyhow, PMTs have several merits they are; they are standard devices, large signals can be detected and fast rise times to signals is feasible. Conversely, the quantum efficiency of silicon photodiodes is typically 70 % but its' surface area are limited and noise threshold is low.

3. The Pre-Processing Phase

The pre-processing phase is divided into two steps the first one is the wavelets and the second one is the interpolation.

3.1 The Pre-Processing Phase

The pre-processing phase is divided into two steps the first one is the wavelets and the second one is the interpolation.

3.1.1 Principles of the wavelet based decomposition

Wavelet transforms are associated with multiresolution into different scales, see figure (3).

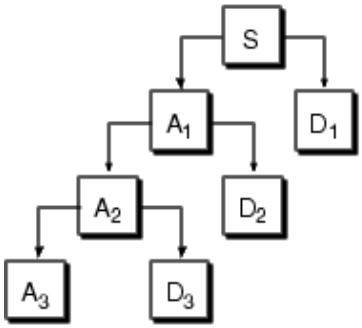

Figure (3). Signal Decomposition.

$$\begin{aligned} s &= A_1 + D_1 \\ &= A_2 + D_2 + D_1 \\ &= A_3 + D_3 + D_2 + D_1 \end{aligned} \quad (1)$$

Wavelet transforms do not have a single set of basis functions like the Fourier transform, which utilizes just the sine and cosine functions. Instead, wavelet transforms have a set of possible basis functions. Thus wavelet analysis provides immediate access to information that can be obscured by other time-frequency methods such as Fourier analysis. Dilations and translations of the Mother function, or analyzing wavelet $\varphi(x)$; define an orthogonal basis, our wavelet basis:

$$\varphi_{(s,l)}(x) = 2^{-\frac{s}{2}}\varphi(2^{-s}x - l) \quad (2)$$

The variables *s* and *l* are integers that scale and dilate the mother function φ to generate wavelets. Hence, the mother functions are rescaled, or dilated by powers of two, and translated by integers. What makes wavelet bases especially interesting is the self-similarity caused by the scales and dilations. To span our data domain at different resolutions, the analyzing wavelet is used in a scaling equation:

$$w(x) = \sum_{k=-1}^{N-1}(-1)^k c_{k+1}\,\varphi(2x - k) \quad (3)$$

Where $w(x)$ is the scaling function for the mother function φ; and c_k are the wavelet coefficients. The wavelet coefficients must satisfy linear and quadratic constraints of the form

$$\sum_{k=0}^{N-1} c_k = 2, \quad \sum_{k=0}^{N-1} c_k c_{k+2l} = 2\delta_{l,0} \quad (4)$$

Where (δ) is the delta function and (l) is the location index. One of the most useful features of wavelets is the ease with which a scientist can choose the defining coefficients for a given wavelet system to be adapted for a given problem. Where the coefficients $\{c_0.....c_n\}$ are filter coefficients. The filters are placed in a transformation matrix, which is applied to a raw data vector. The coefficients are ordered using two dominant patterns, one that works as a smoothing filter (like a moving average), and one pattern that works to bring out the data's detail information. In this paper the signals is filtered in a hierarchical algorithm called a pyramidal algorithm. This algorithm was applied to the original signals, then it is smoothed and decimated by half using down sampler. Just as in the first stage, we repeat to find second wavelet transform. This completes the iteration of the Haar analysis bank, which is graphically represented in figure (3). The mother wavelets (Haar, Daubechies, Coiflet, and Meyer) have been tested to select the best one of them according to the similarity measures as shown in table (1.a). The peak signal to noise ration (PSNR), mean square error (MSE), Eucleadian distance (ED) and the cross correlation (CC) prove that Coiflet is the best mother wavelet. To select the best decomposition level, practical tests have been carried out to find the best one of them. Table (1.b) shows that the third decomposition level is the best one according to the results of the similarity measures

Table (1).a) The statistics of the similarity measure of the different mother wavelets.

Mother Wavelet	CC	ED	MSE	PSNR
Haar	0.9866	12.7990	0.1643	31.926
Daubechies	0.9890	11.8139	0.1418	32.5656
Coiflet	0.9900	11.3834	0.1324	32.8635
Meyer	0.0148	106.878	11.4230	13.5046

Table (1).b) The statistics of the similarity measure of the different decomposition levels.

Level	CC	ED	MSE	PSNR
One	0.9681	20.4778	0.1493	27.8567
Two	0.9830	14.7395	0.1575	30.7084
Three	0.9866	12.7290	0.1443	31.9258
Four	0.7021	18.9554	3.2561	27.0625

3.1.2 The Interpolation based Reconstruction

In the mathematical subfield of numerical analysis, interpolation is a method of constructing new data points within the range of a discrete set of known data points. Interpolation is often recommended for signal de-noising, and would not be much more difficult to implement. We also intend to consider methods that threshold based on estimates of the noise, generated in real time alongside the data. Signals recovered using both hard and soft interpolation; in hard interpolation only linear interpolation is implemented on FPGA. In soft interpolation, several Matlab functions are described, which implement various interpolation algorithms such as nearest neighbor interpolation, linear interpolation, cubic hermite interpolation and cubic spline interpolation. The statistics presented in table (2) prove that the best method was the cubic spline.

Table (2). The statistics of the similarity measure of the different interpolation techniques

Method	CC	ED	MSE	PSNR
Linear	0.9782	16.4669	0.2731	29.7192
Cubic Spline	0.9866	12.7990	0.1643	31.9258
Nearst	0.9307	28.8462	0.8380	27.8501
Cubic Hermit	0.9818	14.8984	0.2226	30.6066

We propose reconstruction method using only approximation coefficient by applying the interpolation technique. Hence, a simple function is applied to calculate new data points. The some of the signal features may be lost but this algorithm is the right manner to remove noise from signals also these signals were stored in economical way by which only approximation coefficients were stored. There are many interpolation methods, in this work we implement linear interpolation on FPGA and the cubic spline in soft techniques.

4. FPGA-based Implementation

In this section, we design and implement the signal pre-processing algorithm on the FPGA

4.1 Design simulation

The proposed architecture is designed using HDL and simulated on Mentor Graphics (Model Sim) to validate its functionality on FPGA. The simulation results are shown in figure (4). The main parameters of this simulation are the master clock "**clk**", the enable signal called "**b**" and ram which use to save intermediate signals "**RAM**", the address of ram is given by signal "**add**". The simulation results and the schematics show the hard wavelets decomposition and the hard interpolation technique.

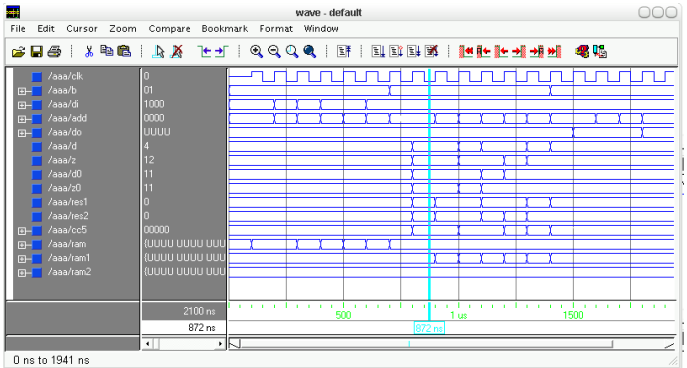

Figure (4). Simulation using Model Sim program.

4.2 Wavelet based Hard Denoising of Scintillation Detector Signals

The hard denoising has been designed and implemented on the FPGA in two phases; the first phase is the down sampling shown in figure (4.a); while the second phase is the interpolation shown in figure (4.b). The device utilization summary, micro statistics and timing summary of the down sampling phase are shown in tables (3-5) while the device utilization summary, micro statistics and timing summary of the interpolation phase are shown in tables (6-8). The original scintillation detector signal, the down sampled one and the reconstructed signal are presented in figure (6). The results shown in figure (6) shows that the compression reaches 50% without scarifying the original signal. The hardware description of the system with the computer interface is shown in figures (7, 8).

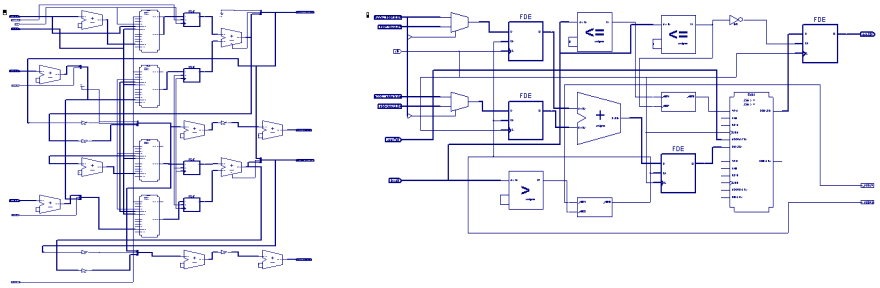

a) Wavelet decomposition phase

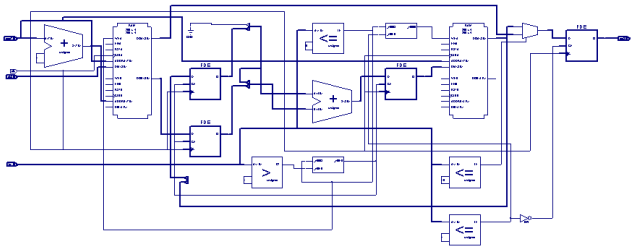

b) Interpolation based reconstruction

Figure (5 a,b). Schematic of the interpolated based Wavelets for scintillation signal denoising.

Table (3).Device utilization summary.

Number of Slices	**374**	**48%**
Number of Slice Flip Flops	32	2%
Number of 4 input LUTs	647	42%
Number of bonded IOBs	18	18%
Number of GCLKs	1	25%

Table (4). macro statistics.

LUT Ram 256x4-bit	**5**
Adders/Subtractors	11
Registers	8
Comparators	3
Multiplexers	2

Table (5). Timing Summary.

Minimum period	**6.536ns**
Minimum input arrival time before clock	26.204ns
Maximum output required time after clock	6.788ns

Table (6). Device utilization summary.

Number of Slices	**176**	**22%**
Number of Slice Flip Flops	16	1%
Number of 4 input LUTs	277	18%
Number of GCLKs	18	185
Number of GCLKs	1	25%

Table (7). macro statistics.

LUT Ram 256x4-bit	**2**
Adders/Subtractors	2
Registers	4
Comparators	4
Multiplexers	1

Table (8). Timing Summary.

Minimum period	**7.022ns**
Minimum input arrival time before clock	23.366ns
Maximum output required time after clock	6.788ns

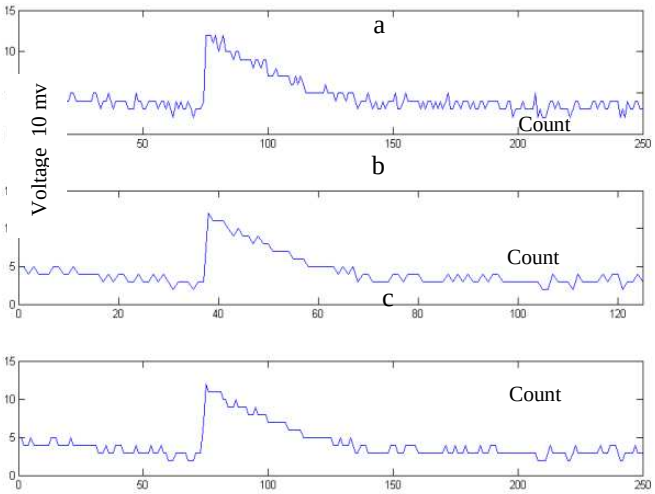

Figure (6). De-noising using wavelet transform and interpolation (a) original signal (b) transformed signal (c) reconstructed signal.

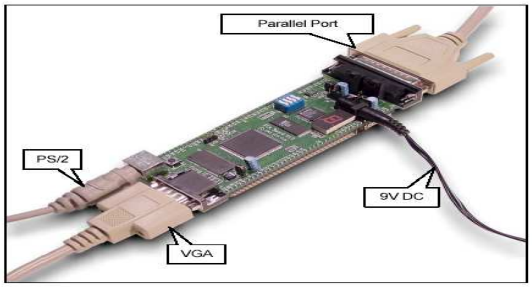

Figure (7). XSA -50 board.

Figure (8). The hardware setup of the system.

5. Signal Shaping and Counting

The previous denoising filtering is an essential step in pulse shaping and counting. Figures (9, 10) show the effect of denoising on pulse shaping and counting. The noise has harmful effect on the digital signal processing. Figure (8) shows the imprecise counting occurred due to presence of noise while the removal of noise led to very precise results as shown in figure (10). Successful results for counting and shaping of series of pulses are presented in figure (11) where (a) is a series of pulses, (b) is the shaping while (c) is the count of nuclear pulses.

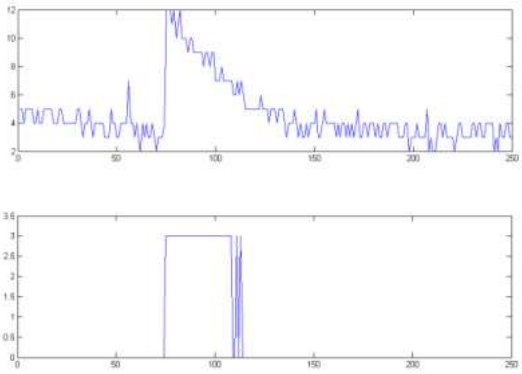

Figure (9).explain the incorrect discrimination.

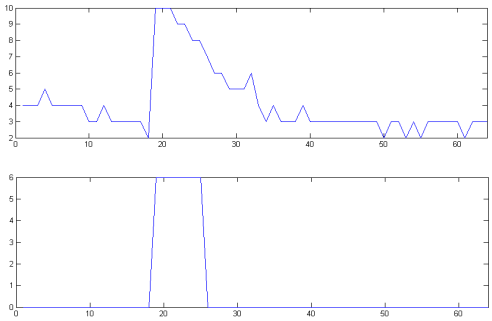

Figure (10). correct pulse shaping.

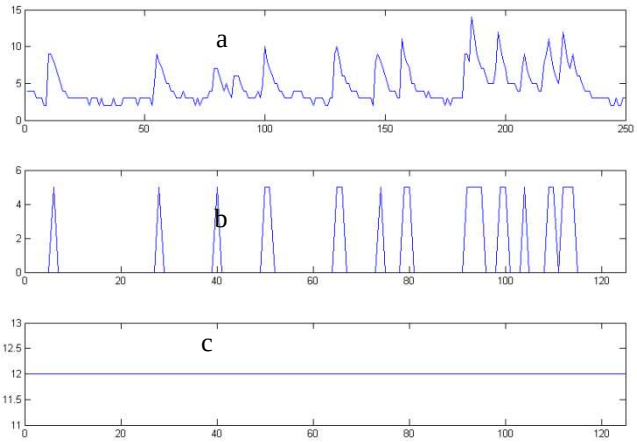

Figure (11).Counting and shaping of scintillation detector signal (a) denoising (b) pulse shaping (c) pulse count.

6. Multi Channel Analyzer

In MCA the pulse height of each input analog signal is digitized as shown in figures (12, 13). The MCA tabulates the voltage pulses on the basis of the output of the ADC by assigning an energy range to each of the detection channel. If a voltage pulse falls within the range represented by one of the channel, a memory location corresponding to that channel has the number of counts in it incremented by one. By performing this operation for all detector events in a given interval the MCA generates a spectrum of the distribution of energy for a measured events (energy histogram) with the y axis representing counts and the x axis representing channel value (relative energy).

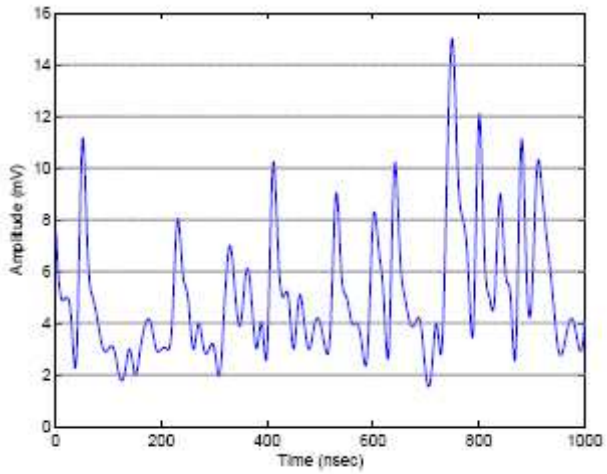

Figure (12). the scintillation signal.

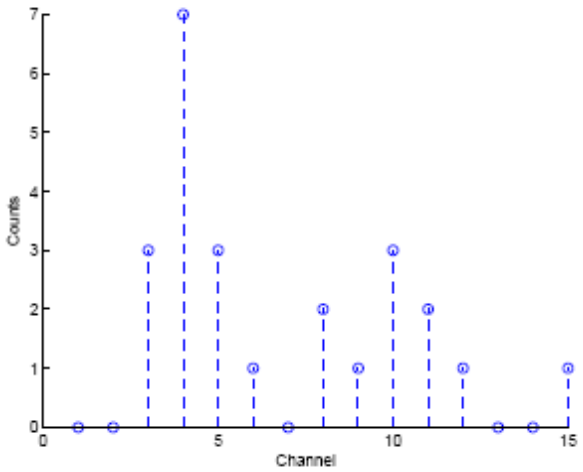

Figure (13). the output of the multichannel analyzer.

Channel Calibration

Energy channel values are converted into kilo electron volts with a channel-to-kilo electron volt conversion factor which is determined from a comparison of photo peak energies and channel location close to the energy of interest.

7. Soft Processing of Scintillation Detector Signals

Throughout this study two modules have been developed; the first one is the hard processing implemented on the FPGA for the real time application and the soft processing for the off line data manipulation. The soft pre-processing includes applying the non-linear wavelets for decomposition and non-linear interpolation

techniques presented in section 3. The comparison between the proposed pre-processing technique presented in this paper and the pre-processing techniques based on the accumulation algorithm presented in [11] and the pre-processing based on median filter proves that the proposed technique is superior to them as shown in table (9).

Table (9). Comparison Statistics of the Preprocessing Techniques .

Method	CC	ED	MSE	PSNR
Accumulation Tech	0.9680	21.3433	0.4555	27.4972
Median filter	0.9831	14.7856	0.2186	30.6856
Proposed Solution.	0.9866	12.7990	0.1643	31.9258

8. Conclusion

This research work presented a qualitative pre-processing, pulse shaping, pulse counting and multichannel analyzing based on hard and soft techniques. One of the most important advantages of this system is the high compression rate using the interpolated wavelets where the mother wavelet and the details have been neglected. FPGAs are visible computational platform for processing of scintillation detector signals with high speed while the high precision has been achieved from the soft processing as well in off-line applications. The wavelet transform and interpolation based reconstruction operation are simultaneously implemented in one processor. The applied techniques achieved high precision denoising, compression, reconstruction, shaping and counting of the signals under study up to (12.5%) without scarifying the original signal. The presented study shows the superiority of the proposed technique compared with the others. The main target of that was the optimization of the overall system by which the storage capacity, precision and speed have been significantly improved.

9. References

[1] S.Shou-peng , Que Pei-wen, Wavelet based noise suppression technique and its application to ultrasonic detection, Ultrasonics, Vol. 44 (2006), 188–193.

[2] F. Javier et al, Haar wavelet based processor scheme for image coding with low circuit complexity,, Computers and Electrical Engineering, Vol. 33 (2007), 109–126.

[3] I. Kilimchuk,et al , Features of scintillation characteristics of CsI:Na and NaI:Tl crystals as the basis for soft gamma radiation detectors, Optical Materials, Vol. 30 (2008), 1800–1802.

[4] S. Antoniou et al , Alpha radiometry of uranium in surface and groundwaters by liquid scintillation counting after separation of the radionuclide by cation exchange, Radiation Measurements, Vol 43 (2008), 1294 – 1298.

[5] Y. Guo et al, Real-time extraction of target_s parameters of sonar by wavelet implemented on TMS320C31, Proceedings of the International Conference on Communication Technology, (1998).

[6] S. Lee and B. Nam, Noise reduction using Haar wavelet and identi.cation of nonlinear channel for QAM using neural network, Proceedings of the IEEE International Symposium on Industrial Electronics, (2001), 488–491.

[7] J.-W. Lin, A.F. Laine, S.R. Bergmann, Improving PET based physiological quantization through methods of wavelet denoising, IEEE Transactions on BiomedicalEngineering, Vol. 48, No. 2 (2001).

[8] B. Mahmoud, et al, Nuclear medical image treatment system based on FPGA in real time, Proceedings of world academy of science, engineering and technolog,yVol. 2, (2005).

[9] Y. Guo et al, Real-time extraction of target_s parameters of sonar by wavelet implemented on TMS320C31, Proceedings of the International Conference on Communication Technology, (998).

[10] S. Antoniou et al , Alpha radiometry of uranium in surface and groundwaters by liquid scintillation counting after separation of the radionuclide by cation exchange, Radiation Measurements, Vol. 43 (2008), 1294 – 1298.

[11] M. Ashour and Ashraf Aboshosha, "Computer-Based Digital Signal Processing for Nuclear Scintillator Detectors", in proceedings of *Seventh Conference of Nuclear Science and Applications*, Cairo, Egypt. February (2000), 6-10.

Journal of Engineering and Computer Sciences, Qassim University, Vol. 3, No. 1, pp. 59-71 (January 2010/Muharram 1431H)

Parametric General Solutions of Boolean Equations Via Variable–Entered Karnaugh Maps

Ali Muhammad Ali Rushdi[*] and Motaz Hussain Amashah

Department of Electrical and Computer Engineering,
King Abdulaziz University,
PO Box 80204, Jeddah 21589, Saudi Arabia,
[*]*arushdi@kau.edu.sa*

(Received 22/6/2009; accepted for publication 7/1/2010)

Abstract. A new method for obtaining a compact parametric general solution of a system of Boolean equations is presented. The method relies on the use of the variable-entered Karnaugh map (VEKM) to implement various steps of the solution procedure and to ensure minimization of the expressions obtained. It is highly efficient as it requires the construction of *natural* maps that are significantly *smaller* than those required by classical methods. Moreover, the method is applicable to general Boolean equations and is not restricted to the two-valued case. As an offshoot, the paper contributes some pictorial insight on the representation of "big" Boolean algebras and functions. It also predicts the correct number of particular solutions of a Boolean equation, and produces a comprehensive list of particular solutions, if desired. Details of the method are carefully explained and further demonstrated via an illustrative example.
Key Words. Boolean equations, Parametric general solutions, Particular solutions, Variable-entered Karnaugh maps.

1. Introduction

The topic of Boolean equations has been a hot topic of research for almost two centuries and its importance can hardly be overestimated. Boolean-equation solving permeates many areas of modern science such as logical design, biology, grammars, chemistry, law, medicine, spectroscopy, and graph theory [1, 2]. Many important problems in operations research can be reduced to the problem of solving a system of Boolean equations. The solutions of Boolean equations serve also as an important tool in the treatment of pseudo-Boolean equations and inequalities, and their associated problems in integer linear programming [3].

To solve a system of n Boolean equations, the equations are usually combined into an equivalent single Boolean equation whose set of solutions is exactly the same as that of the original system of equations. This is conceptually simpler than obtaining the set of solutions for each equation and then forming the intersection of such sets to obtain the set of solutions of the overall system. Typically, general subsumptive or parametric solutions are sought [1-5]. Such general solutions are compact forms from which an exhaustive enumeration of particular solutions can be readily obtained. All types of solutions are obtainable by either algebraic or map methods [1, 2, 6-10].

Both Brown [1, 2] and Tucker and Tapia [6, 7] solved Boolean equations using a Marquand diagram (also called Veitch chart) in which natural binary order is followed, or used a Conventional Karnaugh Map (CKM) in which the rows and columns are arranged according to a reflected binary code. Their methods in [1, 2, 6, 7] are restricted to (or reduce their subject to) two–valued Boolean variables. All these methods state their rules in cell-wise tabular form.

Rushdi [8, 10] developed yet another mapping method for obtaining a subsumptive general solution of a system of Boolean equations. This method is not restricted to the two-valued case and requires the construction of maps that are significantly smaller than those required by earlier procedures. This is because it relies on the use of a more powerful map, namely the variable-entered Karnaugh map (VEKM). The VEKM is an adaptation of the CKM that retains most of its pictorial insight and effectively combines algebraic and mapping techniques. Historically, the VEKM was developed to double the variable-handling capability of the CKM [11]. Later, the VEKM was shown to be the direct or natural map for finite Boolean algebras other than the bivalent or 2-valued Boolean algebra (switching algebra) [1, 8, 10, 12, 13]. These algebras are sometimes called ‘big’ Boolean algebras, and are useful and unavoidable, even if unrecognizable, in many applications [1].

In the present work, we develop a powerful VEKM method to implement an existing procedure [1, 2] for deriving the parametric general solution of a system of Boolean equations. This VEKM method is more efficient than the CKM method in [2], since it requires significantly smaller maps. Another merit of this VEKM is that it produces the solution in the most compact form, thanks to a well-known VEKM minimization procedure [11-13]. As an offshoot, the present work contributes some pictorial insight on the representation of “big” Boolean algebras and functions. Moreover, it correctly predicts the number of particular solutions of the pertinent system of equations, and it identifies a pitfall in an earlier attempt at such a prediction in [2]. If desired, the compact parametric solution obtained is expanded into an exhaustive list of particular solutions.

The rest of this paper is organized as follows. Section II introduces some notation, while Section III reviews pertinent properties of Boolean algebras and addresses the question of pictorial representations of Boolean algebras and functions. Section IV presents a new VEKM method for deriving the parametric solution of a Boolean equation, which is a map adaptation of an existing algebraic procedure. Section V demonstrates the VEKM method via a big-Boolean-algebra example. Section VI addresses the topic of the number of particular solutions and their exhaustive listing. Section VII concludes the paper.

2. Representations of Boolean Algebras and Functions

A Boolean algebra is a quintuple $B = (\mathbf{B}, \vee, \wedge, 0, 1)$ in which **B** is a set, called the carrier; $\vee$ and $\wedge$ are binary operations on **B** and the zero (0) and unit (1) elements are distinct members of **B**, with certain postulates on commutativity, distributivity, binary-operation identities and complementation being satisfied [1-5]. The following facts about a Boolean algebra can be deduced :

1. Every element X of **B** has a unique complement $\overline{X}$.
2. There is a partial-order or inclusion ($\leq$) relation on B that is reflexive, anti-symmetric, and transitive.

3. A Boolean algebra *B* enjoys many useful properties such as associativity, idempotency, absorption, involution, consensus and duality.

4. A Boolean algebra *B* is a complemented distributive lattice with distinct 0 and 1 elements.

5. A nonzero element *Z* of **B** is said to be an atom of **B** iff for every $X \in \mathbf{B}$, the condition $Z \leq X$ implies that $X = Z$ or $X = 0$.

6. Every finite Boolean algebra *B* is atomic, i.e. for every nonzero element $X \in \mathbf{B}$, there is some atom *Z* such that $Z \leq X$.

7. Examples of Boolean algebras include the algebra of classes (subsets of a set), the algebra of propositional functions, the arithmetic Boolean algebra (where $\vee$ and $\wedge$ denote "the least common multiple" and "the greatest common divisor"), as well as the switching or two-element Boolean algebra.

8. Boolean algebras with the same number of elements are isomorphic.

9. Every finite Boolean algebra *B* has 2^m element, where m is the cardinality of (number of elements in) the set of atoms of **B**.

An n-variable function $f: \mathbf{B}^n \rightarrow \mathbf{B}$ is Boolean iff it can be expressed in the minterm canonical form

$$f(\mathbf{X}) = \bigvee f(\mathbf{A})\ \mathbf{X}^{\mathbf{A}}, \tag{1}$$

where the ORing operation $\bigvee$ in (1) extends over all $\mathbf{A} = (a1, a2, \ldots, an) \in \{0, 1\}^n$, and $\mathbf{X}^{\mathbf{A}}$ is defined for $\mathbf{X} = (X_1, X_2, \ldots, X_n) \in \mathbf{B}^n$ as

$$\mathbf{X}^{\mathbf{A}} = X_1^{a1} X_2^{a2} \ldots\ldots X_n^{an}, \tag{2}$$

where for $X \in \mathbf{B}$ and $a \in \{0,1\}$, X^a is defined by

$$X^0 = \overline{X}, \tag{3a}$$
$$X^1 = X. \tag{3b}$$

In (1), the function values $f(\mathbf{A})$, where $\mathbf{A} \in \{0, 1\}^n$ are called the discriminates of $f(\mathbf{X})$.

A dramatic consequence of (1) is that a Boolean function $f: \mathbf{B}^n \rightarrow \mathbf{B}$, where **B** is a carrier of 2^m elements, is uniquely determined by a truth table or map partially representing *f* for the restricted domain $\{0, 1\}^n$ which is a strict subset of the complete domain B^n. Such a representation needs 2^n table or map cells. The complete function table of *f* (which covers the complete domain B^n, and hence requires $(2^m)^n = 2^{mn}$ table lines or map cells) is neither warranted nor needed. In fact, such a complete table should be avoided. Not only does it require tedious work, but it also poses a problem of checking consistency in its $B^n/\{0, 1\}^n$ part.

It is customary to name the elements of **B** in terms of a minimum number of abstract variables $\mathbf{Y} = (Y_1, Y_2, \ldots, Y_k)$. Usually the elements of **B** are taken as the elements of the free Boolean algebra $FB(\mathbf{Y}) = FB(Y_1, Y_2, \ldots, Y_k)$. $FB(\mathbf{Y})$ is isomorphic to the Boolean algebra of switching functions of k variables, and has 2^{2^k} elements. This method works directly when $m = 2^k$. It is also applicable when $2^{k-1} < m < 2^k$, provided that certain constraints are added to nullify some atoms of $FB(\mathbf{Y})$, i.e., some mini-terms of the switching algebra isomorphic to $FB(\mathbf{Y})$.

The first two Boolean carriers are $\mathbf{B}_2 = \{0, 1\}$ and $\mathbf{B}_4 = \{0, 1, a, \overline{a}\}$. Let us temporarily jump to the fourth Boolean carrier $\mathbf{B}_{16} = FB(a, b)$ whose elements constitute the hypercube lattice shown in Fig. (1). This carrier has 4 atoms $\overline{a}\overline{b}, \overline{a}b, a\overline{b}$ and ab which constitute the 4 dimensions of the hypercube. Now, if one of these atoms is nullified (e.g., if we set $\overline{a}b$ to 0), the hypercube in Fig. (1) loses one of its four dimensions, and collapses into the cube of Fig. (2), which constitutes the third Boolean carrier $\mathbf{B}_8$. Similarly, $FB(Y_1, Y_2, Y_3)$ can be used to represent $\mathbf{B}_{256}$ directly, or to represent $\mathbf{B}_{32}$, $\mathbf{B}_{64}$, $\mathbf{B}_{128}$ with 3, 2, and 1 atomic constraints respectively.

We now consider the question: What is the natural map for $f(\mathbf{X}) : \mathbf{B}^n \rightarrow \mathbf{B}$, with **B** having 2^m elements where $2^{k-1} < m \leq 2^k$. The restricted input domain for this function is $\{0, 1\}^n$ representing only the bivalent values of $\mathbf{X} = (X_1, X_2, \ldots, X_n)$. The entries of the map could by any of the 2^{2^k} switching functions of $\mathbf{Y} = (Y_1, Y_2, \ldots, Y_k)$, with possible ORing with don't care terms representing the nullified atoms when $m < 2^k$. The map described this way is nothing but the Variable-Entered Karnaugh Map (VEKM) typically used to represent an incompletely-

specified switching function $f(\boldsymbol{X};\boldsymbol{Y})$: $\{0, 1\}^{n+k} \rightarrow \{0, 1\}$ using n map variables **X** and k entered variables **Y** [8, 10-13].

Note that instead of a conventional map representation of the switching function of (n+k) variables (X; Y) as f (X; Y) $\{0, 1\}^{n+k} \rightarrow \{0, 1\}$ which has constant {0, 1} entries , a VEKM divides the input variables into n map variables **X** and k entered ones **Y**, and therefore represents the function $f(\boldsymbol{X})$: $\{0, 1\}^{n} \rightarrow \{0, 1\}^{k}$ with variable entries belonging to $FB(\mathbf{Y})$. Therefore, a VEKM is the "natural" map for representing $f(\boldsymbol{X})$: $\mathbf{B}^{n} \rightarrow \mathbf{B}$ where **B** has 2^{m} elements and $2^{k-1} < m \leq 2^{k}$. In other words, the VEKM is the natural map for a Boolean function $f(\boldsymbol{X})$, since its input combinations is the restricted domain of f and its entries cover the range of f. An attempt to represent a big Boolean function via a conventional Karnaugh maps (CKM) should be discouraged. Such a representation is a) less efficient, as it produces significantly larger maps, and b) conceptually misleading, as it inadvertently shifts symbols used in describing the output of a function into extraneous inputs, and at the same time conceals the actual nature of this output by reducing it into a bivalent form.

A conventional Karnaugh map is conceptually meaningful however, for solving a switching equation involving the function $f(\boldsymbol{X};\boldsymbol{Y})$: $B_2^{n+k} \longrightarrow B_2$, when it is required to express a set of dependent switching variables **X** in terms of a set of independent switching variables **Y** [14].

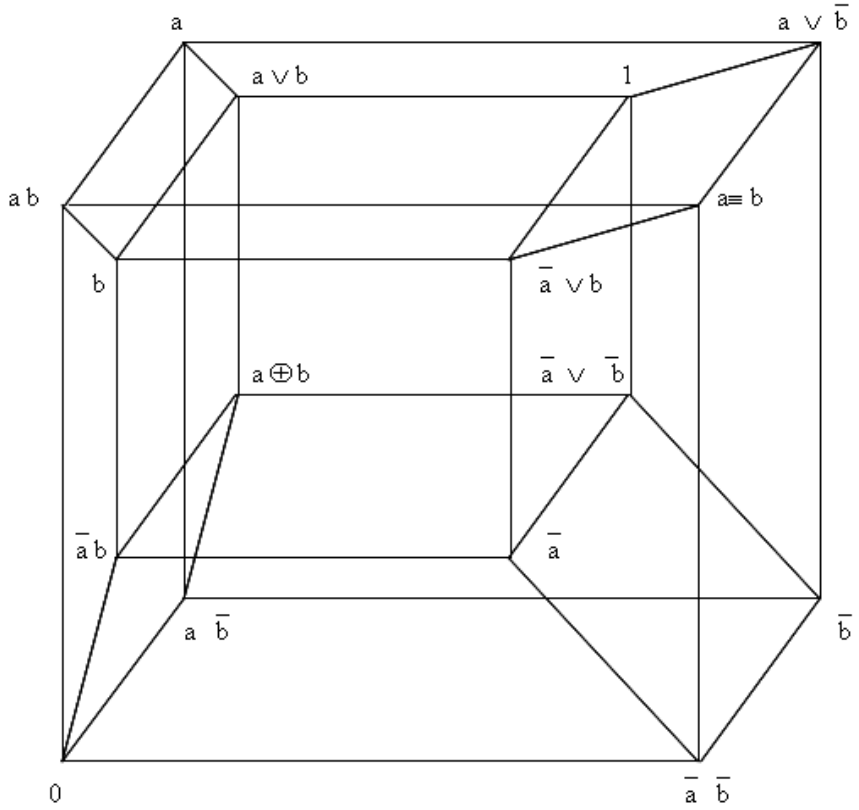

Fig. (1). A lattice indicating the partial ordering among the 16 elements of B_{16}.

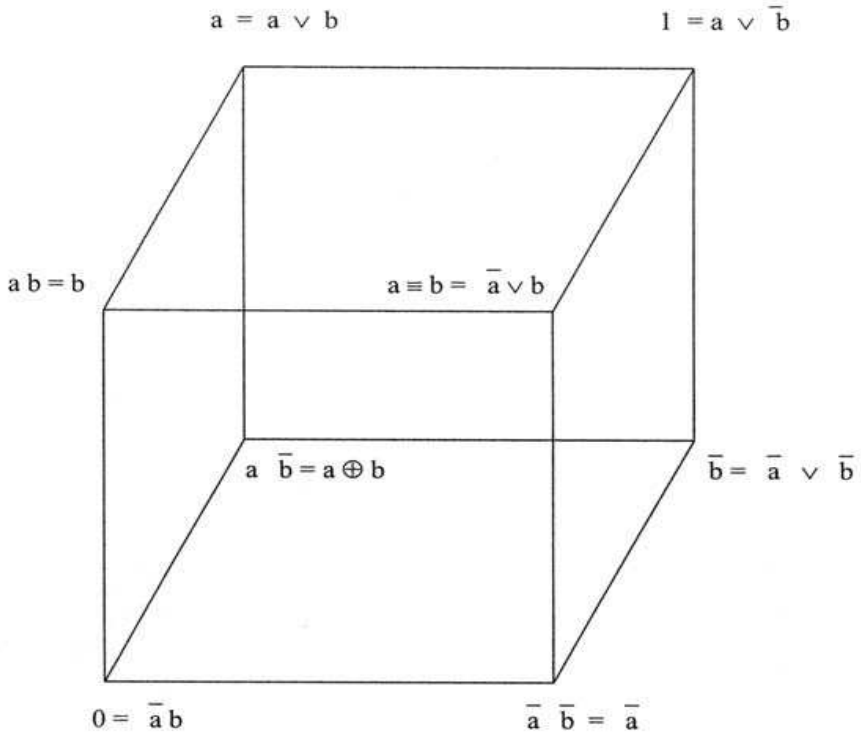

Fig. (2). The lattice in Fig. (1) when collapsed under the condition $\bar{a}\,b = 0$.

3. VEKM Derivation of Parametric Solutions

Brown [1, 2] proved that n parameters are sufficient to construct a parametric general solution of an n-variable Boolean equation $g(\mathbf{X}) = 1$, where g: $\mathbf{B}^n \rightarrow \mathbf{B}$. He proposed a procedure for constructing such a solution using the fewest possible parameters, $p_1, p_2, \ldots, p_k$, which are elements of **B**, where $k \leq n$. We adapt this procedure of Brown into a VEKM procedure as follows:

1. Construct a VEKM representing $g(\mathbf{X})$. Such a construction is achieved via a Boole-Shannon tree expansion [11-13]. If the original Boolean equation is in the dual form $f(\mathbf{X}) = 0$, then construct a VEKM for $f(\mathbf{X})$, and complement it cell-wise [15] to obtain a VEKM for $\bar{f}(X) = g(X)$.

2. Expand the entries of the VEKM of $g(\mathbf{X})$ as ORing of appropriate atoms of the Boolean carrier **B,** or equivalently as a minterm expansion of the free Boolean algebra representing **B.**

3. If certain atoms of **B** do not appear at all in any cell of the VEKM for $g(\mathbf{X})$, then these atoms must be forbidden or nullified. Such nullification constitutes *a consistency condition* for the given Boolean equation.

4. Construct a VEKM for an associated function $G(X_1, X_2, \ldots, X_n; p_1, p_2, \ldots, p_k)$. This VEKM is deduced from that of $g(\boldsymbol{X}_1, \boldsymbol{X}_2, \ldots, \boldsymbol{X}_n)$ through the following modifications:

a) Each appearance of an entered atom in the VEKM of g is ANDed with a certain element of a set of orthonormal tags of minimal size. Table (1) gives examples of such sets as a function of the number of cells in which an atom appears. An orthonormal set consists of a set of terms T_i, i = 1, 2, …, k, which are both exhaustive ($T_1 \vee T_2 \vee \ldots \vee T_k = 1$) and mutually exclusive ($T_i\, T_j = 0$ for $1 \leq i < j \leq k$).

b) Each nullified atom is entered don't care in all the VEKM cells.

5. The parametric solution is

X_i = The sum (ORing) of the 2^{n-1} cells constituting that half of the VEKM in which $\mathbf{X}_i$ is asserted

$$(\mathbf{X}_i = 1), \quad i = 1, 2, \ldots, n. \tag{4}$$

6. Apply an appropriate VEKM minimization procedure [11-13] to recast (4) in a minimal form.

Table (1). Minimal orthonormal sets of tags attached to instances of each atom depending on the number of cells in which it appears (Each orthonormal set consists of exhaustive and mutually exclusive terms).

The No. of cells in which an atom appears	A set of orthonormal tags of minimal size	The minimum number of parameters required
1	{ 1 }	0
2	{ $\overline{p}_1, p_1$ }	1
3	{ $\overline{p}_1, p_1\overline{p}_2, p_1p_2$ }	2
4	{ $\overline{p}_1\overline{p}_2, \overline{p}_1p_2, p_1\overline{p}_2, p_1p_2$ }	
5	{ $\overline{p}_1\overline{p}_2, \overline{p}_1p_2, p_1\overline{p}_2, p_1p_2\overline{p}_3, p_1p_2p_3$ }	
6	{ $\overline{p}_1\overline{p}_2, \overline{p}_1p_2, p_1\overline{p}_2\overline{p}_3, p_1\overline{p}_2p_3, p_1p_2\overline{p}_3, p_1p_2p_3$ }	3
7	{ $\overline{p}_1\overline{p}_2, \overline{p}_1p_2\overline{p}_3, \overline{p}_1p_2p_3, p_1\overline{p}_2\overline{p}_3, p_1\overline{p}_2\overline{p}_3, p_1p_2\overline{p}_3, p_1p_2p_3$ }	
8	{ $\overline{p}_1\overline{p}_2\overline{p}_3, \overline{p}_1\overline{p}_2p_3, \overline{p}_1p_2\overline{p}_3, \overline{p}_1p_2p_3, p_1\overline{p}_2\overline{p}_3, p_1\overline{p}_2\overline{p}_3, p_1p_2\overline{p}_3, p_1p_2p_3$}	

4. A Big Boolean-algebra Illustrative Example

Let us apply the present method in terms of a VEKM representation to find the parametric general solution of an equation of the form $g(X_1, X_2, X_3) = 1$, where g is a Boolean function $g: B_{16}^3 \rightarrow \mathbf{B}_{16}$ and $\mathbf{B}_{16}$ is the Boolean carrier of 16 elements shown in Fig. (1). Note that the complete input space of g consists of $16^3 = 4096$ combinations of **X**, but g is uniquely defined by the values assigned to it on only 8 combinations of **X**, namely those belonging to $\{0, 1\}^3$. Let g be given by the formula

$$g(\mathbf{X}) = \overline{b}\overline{X}_1\overline{X}_2X_3 \vee ab\overline{X}_1X_2 \vee a\overline{b}X_1\overline{X}_2 \vee \overline{a}\overline{b}X_1X_2 \vee a\overline{X}_1\overline{X}_2\overline{X}_3 = 1. \quad (5)$$

Equation (5) has been solved by Brown [2]. His first step is to expand g not only with respect to the 3 variables X_1, X_2, and X_3 but further with respect to the "constants" a and b thereby producing a 5-variable 32-cell Karnaugh map. In our present procedure, however, we expand g only with respect to the true variables X_1, X_2, and X_3, thereby representing g by the 8-cell VEKM in Fig. (3) which has X_1, X_2, and X_3 as map variables and has a and b as entered "variables". Since a and b are actually constants, this VEKM is a natural map for g. Now, Fig. (4) shows each of the entries of the map of g in Fig. (3) being expanded as ORing of appropriate atoms of $\mathbf{B}_{16}$, or equivalently as a sum of certain minterms of $FB(a, b)$. Out of the 4 atoms of $\mathbf{B}_{16}$, three atoms, namely, $\overline{a}\overline{b}, a\overline{b},$ and ab appear somewhere in the cells of the map of Fig. (4), while the fourth atom ($\overline{a}b$) does not appear at all therein. This means that the atom $\overline{a}b$ is nullified or forbidden ($\overline{a}b = 0$). In Fig. (5), the function $g(X_1, X_2, X_3)$ is replaced by an associated function $G(X_1, X_2, X_3, p_1, p_2)$, where each appearance of an entered atom in Fig. (4) is ANDed with a certain element of a set of orthonormal tags of minimal size (See Table 1). The atom $a\overline{b}$ appears in 4 of the 8-cells of the map in Fig. (4), so each of these 4 appearances is tagged with a particular element of the orthonormal set { $\overline{p}_1\overline{p}_2, \overline{p}_1p_2, p_1\overline{p}_2, p_1p_2$ }, respectively. The atom ab appears in 3-cells of the map of Fig. (4), and hence each of these 3 appearances is ANDed with its own tag selected from the orthonormal set **{** $\overline{p}_1, p_1\overline{p}_2, p_1p_2$ **}.** Finally, the atom $\overline{a}\overline{b}$ made its appearance 3 times in the cells of the map of Fig. (4), and utilized a set of orthonormal tags equivalent to that of the atom ab. In assigning tags to various instances of various atoms, slight simplifications are achieved if adjacent tags are located in adjacent cells whenever possible. The map in Fig. (5) is now completed by adding the nullified atom ($\overline{a}b$) as a don't-care entry in each of the 8-cells of the map.

Now, the parametric solution can be readily deduced from Fig. (5). For i = 1, 2, and 3, the variable X_i is equal to the sum (ORing) of the 4-cells constituting half of the map for which X_i is asserted, i.e., for which $X_i = 1$. This means that

$$X_1 = a\bar{b}\,p_1p_2 \vee a\bar{b}\,p_1\bar{p}_2 \vee \bar{a}\bar{b}\,p_1p_2 \vee \bar{a}\bar{b}\,p_1\bar{p}_2 \vee d(\bar{a}b)\,, \tag{6a}$$

$$X_2 = ab\,p_1p_2 \vee ab\,p_1\bar{p}_2 \vee \bar{a}\bar{b}\,p_1p_2 \vee \bar{a}\bar{b}\,p_1\bar{p}_2 \vee d(\bar{a}b)\,, \tag{6b}$$

$$X_3 = a\bar{b}\,p_1p_2 \vee ab\,\bar{p}_1p_2 \vee \bar{a}\bar{b}\,p_1p_2 \vee \bar{a}\bar{b}\,\bar{p}_1 \vee ab\,p_1p_2 \vee d(\bar{a}b)\,, \tag{6c}$$

The expressions (6) can be minimized by any algebraic or map method, such as the VEKM minimization procedure in [11-13]. Due to space limitations, we do not elaborate on this procedure herein, though we give the reader a glimpse of its details in Fig. (6) and Fig. (7). Each of these two figures shows pictorially and succinctly how the VEKM minimization procedure achieves minimal expressions for X_1, X_2, and X_3. These minimal expressions are

$$X_1 = p_1\bar{b}\,, \tag{7a}$$

$$X_2 = p_1(\bar{a} \vee b)\,, \tag{7b}$$

$$X_3 = p_2\bar{b} \vee p_1p_2 \vee \bar{p}_1\bar{a}\,, \tag{7c}$$

In the general solution (7), the two parameters p_1 and p_2 are independently chosen elements of the underlying Boolean algebra, i. e., of the $\mathbf{B}_{16}$ carrier in Fig. (1) that collapsed into a $\mathbf{B}_8$ carrier in Fig. (2). Since each of p_1 and p_2 can assume one out of eight possible values, the total number of combinations of values for p_1 and p_2 is 8^2 or 64 values. This number is an upper bound on the number of particular solutions of Equation (5). The actual number of particular solutions of Equation (5) is strictly less than this upper bound, since there are different combinations of (p_1, p_2) that produce identical particular solutions of Equation (5). For example, each of the parameter assignments (p_1, p_2) = (*0*, *0*) and (p_1, p_2) = (*0*, *b*) produces the particular solution (X_1, X_2, X_3) = (*0*, *0*, $\bar{a}$).

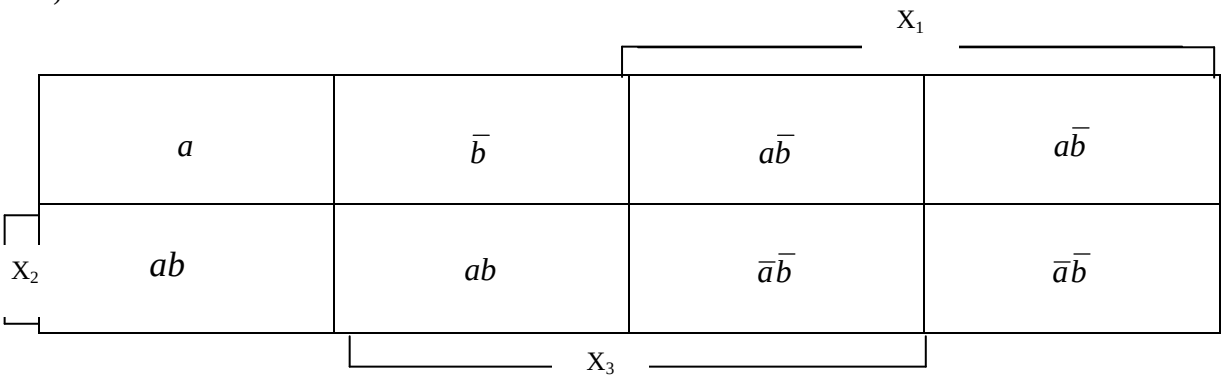

$g\,(X_1, X_2, X_3)$

Fig. (3). A natural map representation of the Boolean function g given by (5).

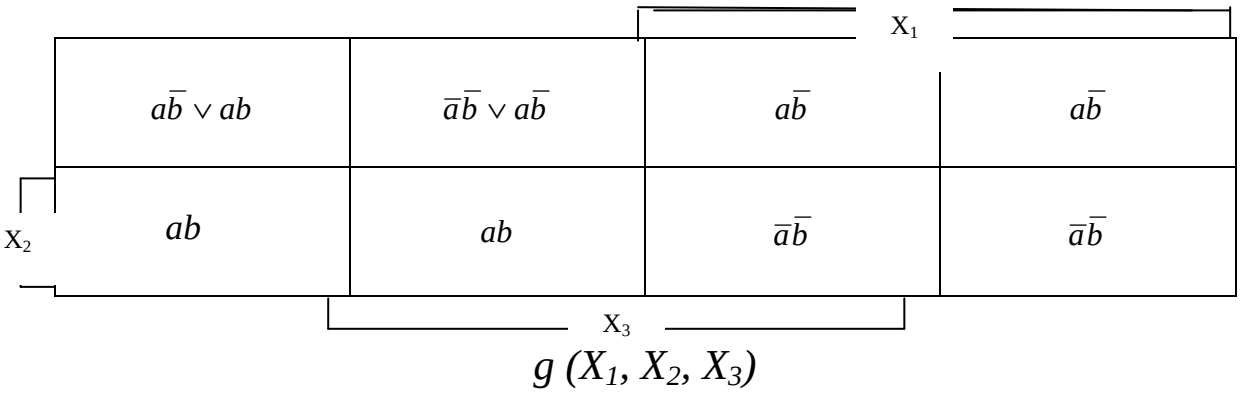

$g\,(X_1, X_2, X_3)$

Fig. (4). Entries of the map for the function g in Fig.(3) expanded in terms of atoms of $\mathbf{B}_{16}$ or minterms of *FB(a , b)*.

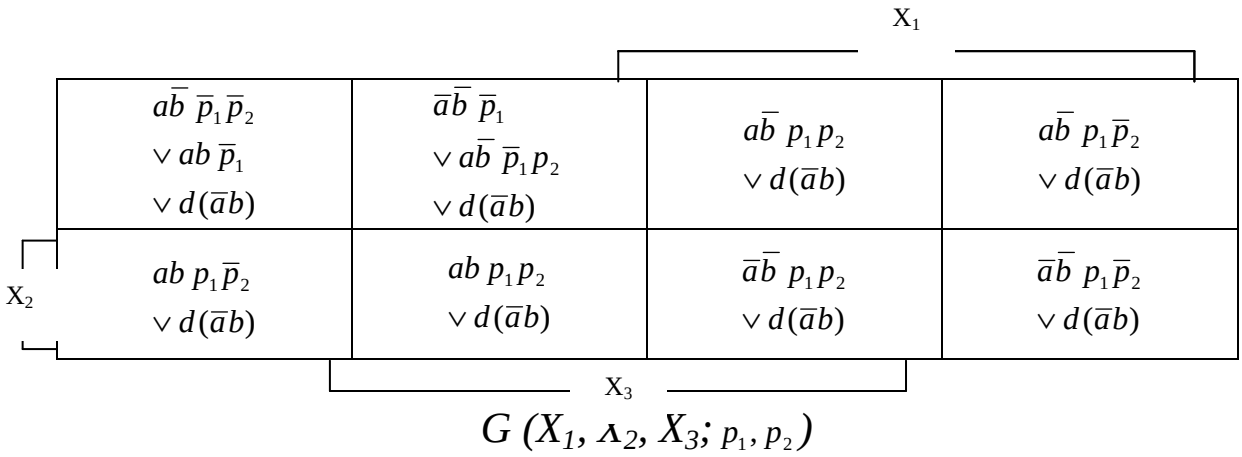

Fig. (5). Each appearance of an entered atom in Fig.4 is ANDed with a certain element of a set of orthonormal tags, while the atom $\bar{a}b$ that appears nowhere in Fig. 4. is entered don't care.

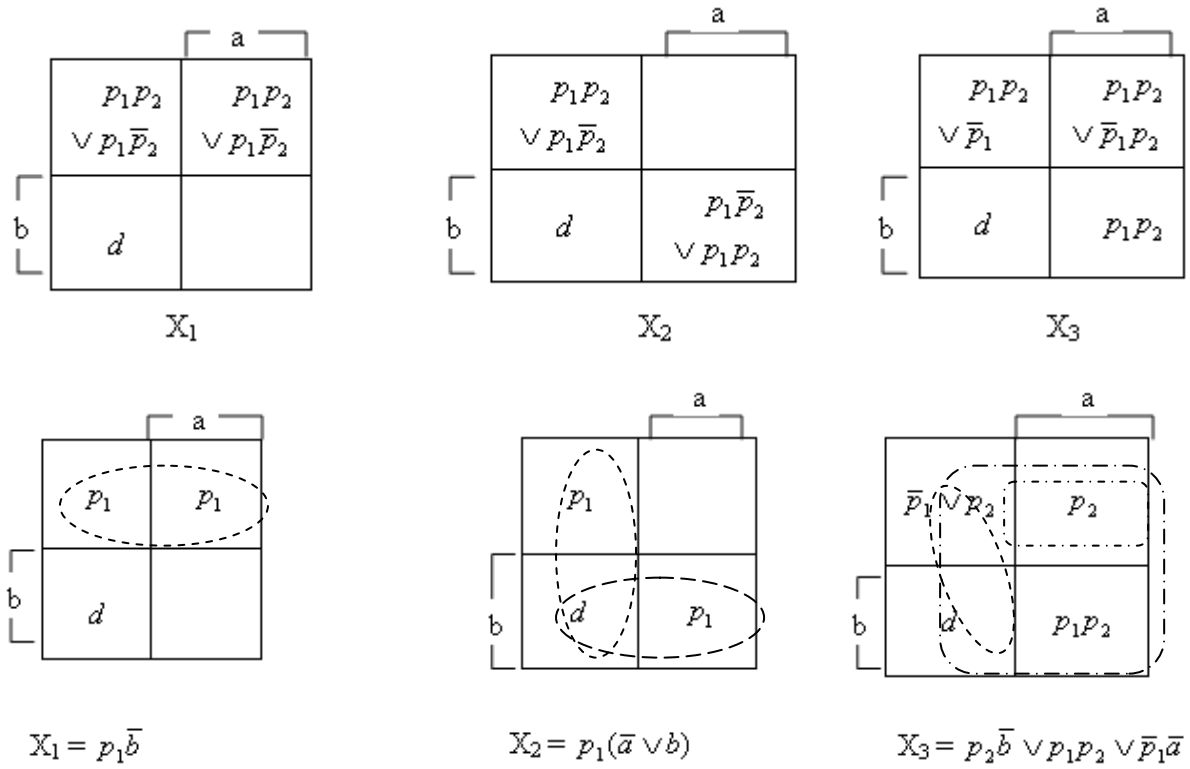

Fig. (6). VEKM expression of the parametric solution.

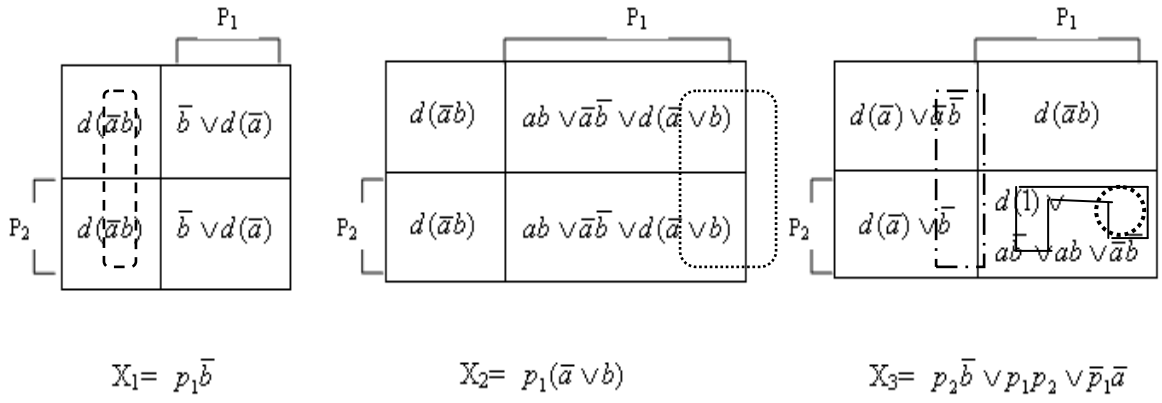

Fig. (7). An alternative VEKM expression of the parametric solution.

5. Direct Derivation of Particular Solutions

Any particular solution is obtained by randomly retaining a single instance of each of the entered atoms in the map of Fig. (3). Figure (8) shows the case where the atom $a\bar{b}$ is retained in the $\bar{X}_1\bar{X}_2\bar{X}_3$ cell, the atom ab is kept in the $\bar{X}_1X_2X_3$ cell, and the atom $\bar{a}\bar{b}$ is retained in the $X_1X_2\bar{X}_3$ cell. Note that the atom $\bar{a}b$ was not entered in Fig. (3) and hence is not retained in Fig. (8).

As stated earlier, the consistency condition is $\bar{a}b = 0$, which means that the atom $\bar{a}b$ is a forbidden or cannot – happen entity, and hence it appears don't-care in each cell of Fig. (8). In the particular solution obtained, the value of the X_i variable is the disjunction of entries in the X_i half map, augmented by a don't-care $\bar{a}b$, i.e.,

$$X_1 = \bar{a}\bar{b} \vee d(\bar{a}b) = \bar{a}, \tag{8a}$$

$$X_2 = ab \vee \bar{a}\bar{b} \vee d(\bar{a}b) = \bar{a} \vee b, \tag{8b}$$

$$X_3 = ab \vee d(\bar{a}b) = b. \tag{8c}$$

The number of particular solutions for this case = 3 x 3 x 4 = 36, a number which is well below the upper bound of 64.

Brown [2, pp. 192-193] obtained a particular solution using a 5–variable Karnaugh map representation in which he used the parameters *a* and *b* as extra map variables. His solution is similar to the present one, with the exception that he did the equivalent of randomly adding the forbidden atom $\bar{a}b$ to the cell $X_1\bar{X}_2X_3$. Therefore, he obtained the particular solution

$$X_1 = \bar{a}\bar{b} \vee \bar{a}b = \bar{a}, \tag{9a}$$

$$X_2 = ab \vee \bar{a}\bar{b}, \tag{9b}$$

$$X_3 = ab \vee \bar{a}b = b, \tag{9c}$$

which is not different from (8) if the consistency condition is invoked . However, the freedom of adding $\bar{a}b$ arbitrarily asserted to one of 8 cells produced the erroneous prediction of 388 particular solutions [2, p. 192], an overestimation by a multiplicative factor of 8, and also a violation of the pertinent upper bound.

In general, the number of particular solutions for any big Boolean-algebra equation $g(\mathbf{X})=1$ can be obtained by drawing the natural Karnaugh map for $g(\mathbf{X})$ and observing the number of times each entered atom of $g(\mathbf{X})$ makes its appearance in the cells of the map, i.e.,

Number of particular solutions =

Π (Number of times an atom appears in the map of g(**X**)), (10)

where the product operator (**Π**) in (10) runs over every entered atom in the map of $g(\mathbf{X})$.

If desired, a complete listing of all particular solutions can be obtained in a variety of ways such as (a) exhaustively and directly enumerating particular solutions by repeatedly following the strategy of this section, i. e., by noting every instance in which each entered atom is retained once in the natural map of the function *g*, (b) assigning independent values to the parameters in a parametric general solution, and (c) expanding a tree of sub-cases for a subsumptive general solution [1, 2, 8, 10].

Table (2) explicitly lists all the particular solutions of the equation g =1 in (5). These solutions are all the valid solutions (and nothing else) produced individually without any kind of overlapping or repetition. For each of these solutions g can be shown to equal $a \vee \bar{b}$ which is 1 according to the consistency condition ($\bar{a}b = 0$). However, Table (1) is not the recommended form for a solution representation since it details a large number of solutions and obscures regularities in their form.

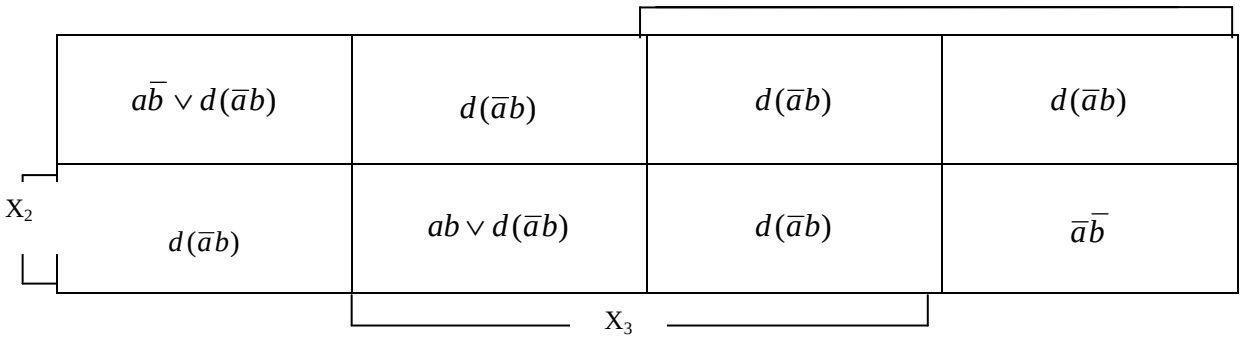

Fig.(8). Pertaining to the derivation of one particular solution.

Table (2). Listing of particular solutions of equation (5):

X_1	X_2	X_3	X_1	X_2	X_3
0	0	$\bar{a}$	$a\bar{b}$	0	$\bar{a}$
0	0	$\bar{b}$	$a\bar{b}$	0	$\bar{b}$
0	b	$\bar{a}$	$a\bar{b}$	b	$\bar{a}$
0	b	$\bar{a} \vee b$	$a\bar{b}$	b	$\bar{a} \vee b$
0	b	$\bar{b}$	$a\bar{b}$	b	$\bar{b}$
0	b	1	$a\bar{b}$	b	1
$\bar{a}$	$\bar{a}$	0	$\bar{b}$	$\bar{a}$	0
$\bar{a}$	$\bar{a}$	$\bar{a}$	$\bar{b}$	$\bar{a}$	$\bar{a}$
$\bar{a}$	$\bar{a}$	$a\bar{b}$	$\bar{b}$	$\bar{a}$	$a\bar{b}$
$\bar{a}$	$\bar{a}$	$\bar{b}$	$\bar{b}$	$\bar{a}$	$\bar{b}$
$\bar{a}$	$\bar{a} \vee b$	0	$\bar{b}$	$\bar{a} \vee b$	0
$\bar{a}$	$\bar{a} \vee b$	b	$\bar{b}$	$\bar{a} \vee b$	b
$\bar{a}$	$\bar{a} \vee b$	$\bar{a}$	$\bar{b}$	$\bar{a} \vee b$	$\bar{a}$
$\bar{a}$	$\bar{a} \vee b$	$\bar{a} \vee b$	$\bar{b}$	$\bar{a} \vee b$	$\bar{a} \vee b$
$\bar{a}$	$\bar{a} \vee b$	$a\bar{b}$	$\bar{b}$	$\bar{a} \vee b$	$a\bar{b}$
$\bar{a}$	$\bar{a} \vee b$	a	$\bar{b}$	$\bar{a} \vee b$	a
$\bar{a}$	$\bar{a} \vee b$	$\bar{b}$	$\bar{b}$	$\bar{a} \vee b$	$\bar{b}$
$\bar{a}$	$\bar{a} \vee b$	1	$\bar{b}$	$\bar{a} \vee b$	1

6. Conclusions

This paper presents a new method for obtaining the most compact form of the parametric general solution of a system of Boolean equations. The method is based on the use of the variable-entered Karnaugh map and hence is an effective combination of mapping and algebraic methods. The method starts by reducing a Boolean system of equations into a single equation of the form g(**X**) = 1, expressing g(**X**) in appropriate VEKM form and then modifying this VEKM by augmenting its atomic entries by appropriate elements of sets of orthonormal tags which are products of the parameters used. The method then proceeds by constructing small VEKMs for the pertinent variables **X.** Each of these latter functions is an ISBF that appears in a form suitable for VEKM minimization. The technique proposed herein is not restricted to two-valued Boolean algebras as clearly attested to by the illustrative example in Section V. As an offshoot, the paper contributes some pictorial insight on the representation of "big" Boolean algebras and functions. It also predicts the correct number of particular solutions of a Boolean equation, and produces a comprehensive list of particular solutions.

The concepts and method developed herein can be utilized in various application areas of Boolean equations [1-10, 16]. In particular, an automated version of the present Boolean-equation solver can be applied in the simulation of gate-level logic. However, such an application must handle the incompatibility between the lattice structure of 'big' Boolean algebras, which are only partially ordered, and multi-valued logics, which are totally ordered [17]. The ideas expressed herein can also be incorporated in the automated solution of large systems of Boolean equations [18]. They can also be extended to handle quadratic Boolean equations [19], Boolean ring equations [4, 5, 20], and Boolean differential equations [21].

List of Symbols

n number of input variables **X** for a Boolean function $f(\mathbf{X})$.
m cardinality of the set of atoms of a Boolean algebra *B*.
k minimum number of symbols used in a free Boolean algebra to represent the elements of a Boolean carrier **B**.
A/B the set difference of sets A and B = $\{ X \mid X \in A, X \notin B\}$.
X an n-tuple $(X_1, X_2, \ldots, X_n)$ of Boolean variables $X_i \in$ **B.**

7. References

[1] Brown, F. M., Boolean Reasoning: The logic of Boolean Equations, Kluwer Academic Publishers, Boston, MA, USA (1990).
[2] Brown, F. M., Boolean Reasoning: The logic of Boolean equations, 2nd Ed., Dover Publications, Mineola, NY, USA (2003).
[3] Hammer, P. L. and S. Rudeanu, Boolean Methods in Operations Research and Related Areas, Springer Verlag, Berlin, Germany (1968).
[4] Rudeanu, S., Boolean Functions and Equations, North-Holland Publishing Company & American Elsevier, Amsterdam, the Netherlands (1974).
[5] Rudeanu, S., Lattice Functions and Equations, Springer Verlag, London, UK (2001).
[6] Tucker, J. H., and M. A. Tapia, Using Karnaugh Maps to Solve Boolean Equations by Successive Elimination, Proceedings of IEEE Southeastcon 92, Birmingham, AL, USA, 2 (1992), 589-592.
[7] Tucker, J. H. and M. A. Tapia, Solution of a Class of Boolean Equations, Proceedings of IEEE Southeastcon 95, New York, NY, USA, 1 (1995), 106-112.
[8] Rushdi, A. M., Using Variable-Entered Karnaugh Maps to Solve Boolean Equations, International Journal of Computer Mathematics, Vol. 78, No. 1 (2001), 23-38.
[9] Rudeanu, S., Algebraic Methods versus Map Methods of Solving Boolean Equations, International Journal of Computer Mathematics, Vol. 80, No. 7 (2003), 815-817.
[10] Rushdi, A. M., Efficient solution of Boolean equations using variable-entered Karnaugh maps, Journal of King Abdul-Aziz University: Engineering Sciences, Vol. 15, No. 1 (2004),115-131.
[11] Rushdi, A. M., Improved Variable-Entered Karnaugh Map Procedures, Computers and Electrical Engineering, Vol. 13, No. 1 (1987), 41-52.

[12] Rushdi, A. M. and H. A. Al-Yahya, A Boolean Minimization Procedure Using the Variable-Entered Karnaugh Map and the Generalized Consensus Concept, International Journal of Electronics, Vol. 87, No. 7 (2000), 769-794.
[13] Rushdi, A. M. and H. A. Al-Yahya, Further Improved Variable-Entered Karnaugh Map Procedures for Obtaining the Irredundant Forms of an Incompletely-Specified Switching Function, Journal of King Abdulaziz University: Engineering Sciences, 1Vol. 3, No. 1 (2001), 111-152.
[14] Baneres, D., J. Cortadella, and M. Kishinevsky, A Recursive Paradigm to Solve Boolean Relations, IEEE Transactions on Computers, Vol. 58, No. 4 (2009), 512-527.
[15] Rushdi, A. M., Map derivation of the minimal sum of a switching function from that of its complement, Microelectronics and Reliability, Vol. 25, No. 6 (1985), 1055-1065.
[16] Bochmann, D., A. D. Zakrevskij and Ch. Posthoff, Boolesche Gleichungen: Theorie, Anwendungen und Algorithmen (Boolean Equations: Theory, Applications and Algorithms, Sammelband-Verlag, Berlin, Germany (1984).
[17] Woods, S. and G. Casinovi, Multiple-Level Logic Simulation Algorithm, IEE Proceedings on Computers and Digital Techniques, 1Vol. 48, No. 3 (2001), 129-137.
[18] Woods, S. and G. Casinovi, Efficient Solution of Systems of Boolean Equations, Proceedings of the IEEE/ACM International Conference on Computer-Aided Design, (1996), 542-546.
[19] Rudeanu S., On quadratic Boolean Equations, Fuzzy Sets and Systems, Vol. 75, No. 2 (1995), 209-213.
[20] Rudeanu S., Unique Solutions of Boolean Ring Equations, Discrete Mathematics, Vol. 122, No. 1-3 (1993), 381-383.
[21] Serfati, M., Boolean Differential Equations, Discrete Mathematics, Vol. 146, No. 1-3 (2003), 235-246.

حلول عامة معلمية للمعادلات البولانية باستخدام خرائط كارنوه متغيرة المحتويات

علي بن محمد على رشدي*، ومعتز بن حسين عماشة

قسم الهندسة الكهربائية وهندسة الحاسبات ، جامعة الملك عبدا لعزيز ، ص.ب. ٨٠٢٠٤ ، جدة ، المملكة العربية السعودية

*arushdi@kau.edu.sa

(قدم للنشر في ٢٠٠٩/٦/٢٢م ؛ وقبل للنشر في ٢٠١٠/١/٧م)

ملخص البحث. يتم تقديم طريقة جديدة للحصول على حل عام معلمي ملموم لنظام من المعادلات البولانية. وتعتمد هذه الطريقة على استعمال خريطة كارنوه متغيرة المحتويات (خ ك غ ح) في تنفيذ مختلف خطوات إجراء الحل وفي تحقيق التصغير الأعظمي للتعبيرات الناتجة. تتمتع هذه الطريقة بكفاءة عالية حيث إنها تتطلب إنشاء خرائط طبيعية تقل في الحجم كثيرا عن تلك التي تتطلبها الخرائط التقليدية. وفضلا عن ذلك يمكن تطبيق الطريقة على المعادلات البولانية العامة دون التقيد بالحالة ثنائية القيمة. وتسهم هذه الورقة أيضا بثمرة جانبية هي توفير مزيد من التبصر ووضوح الرؤية حول كيفية تمثيل الأنواع "الكبيرة" للجبر البولاني والمعادلات البولانية. تتنبأ هذه الورقة أيضا بالعدد الصحيح للحلول الخاصة لمعادلة بولانية كما توضح كيف يمكن سرد مجموعة الحلول الخاصة سردا مستنفدا عند الحاجة. يجري شرح طريقة الحل بعناية كما يعززبيان تفصيلاتها من خلال مثال توضيحي.

قواعد النشر

أهداف المجلة

تهدف المجلة إلى نشر إنتاج الباحثين من داخل الجامعة وخارجها في جميع تخصصات العلوم الهندسية وعلوم الحاسب، والمجالات الرئيسية التي تشملها المجلة هي:

- الهندسة الكهربائية
- الهندسة المدنية
- الهندسة الميكانيكية
- الهندسة الكيميائية
- هندسة التعدين والبترول
- هندسة الحاسب
- علوم الحاسب
- تكنولوجيا المعلومات
- نظم المعلومات
- العلوم الهندسية الأساسية

لغة المجلة:

تقبل المجلة البحوث باللغة الإنجليزية.

أ) المواد التي تقبلها المجلة للنشر:

١- البحث: وهو عمل أصيل للمؤلف (أو المؤلفين) يضيف جديداً للمعرفة في مجال تخصص (فرع المجلة).

٢- المقالة المرجعية: وتتناول العرض النقدي والتحليلي للبحوث والكتب ونحوها التي سبق نشرها في ميدان معين والرسائل العلمية المتميزة.

٣- المقالة القصيرة (تعليق تقني): مقالة قصيرة تحوي تطبيقاً تقنياً.

٤- الابتكارات العلمية المتميزة وبراءات الاختراع.

٥- المراسلات: وتتناول عرض فكرة أو رأي علمي أو اقتراح بحثي.

٦- انتقادات الكتب

ب) شروط النشر:

١- أن يكون البحث متسماً بالأصالة والابتكار والمنهجية العلمية وسلامة الاتجاه وصحة اللغة وجودة الأسلوب.

٢- أن لا يكون البحث قد سبق نشره أو قدم للنشر لجهة أخرى.

٣- جميع البحوث المقدمة للنشر في المجلة خاضعة للتحكيم.

ج) تعليمات النشر:

عند تقديم البحث للنشر يشترط الآتي:

١- أن يقدم الباحث طلباً بنشر بحثه، ويوضح فيه العنوان الالكتروني للمراسلات.

٢- لا يجوز إعادة نشر أبحاث المجلة في أي مطبوعة أخرى إلا بإذن كتابي من رئيس التحرير.

٣- يرسل الباحث بحثه باللغة الانجليزية عن طريق البريد الالكتروني على العنوان الالكتروني المذكور في فترة المراسلات، وكذلك ملخص باللغتين العربية والإنجليزية بحيث لا تزيد كلماته عن ٢٠٠ كلمة.

٤- يكتب البحث باستخدام برنامج (Microsoft word) ويستخدم font 12 Times New Roman في كتابة المتن، مع ترك مسافة ونصف بين الأسطر.

٥- يجب ألا يزيد عدد صفحات البحث شاملا الرسومات والجداول عن ٢٠ صفحة حجم A4.

٦- أن يكتب عنوان البحث واسم الباحث وعنوانه ولقبه العلمي والجهة التي يعمل بها على الصفحة الأولى مستقلة.

٧- توضع هوامش كل صفحة أسفلها.

٨- يشار إلى المراجع داخل المتن بالأرقام حسب تسلسل ذكرها وتثبت في فهرس يلحق بآخر البحث.

أ) الدوريات: يشار إليها في المتن بأرقام داخل أقواس مربعة على مستوى السطر. أما في قائمة المراجع فيبدأ المرجع بذكر رقمه داخل قوسين مربعين فاسم عائلة المؤلف ثم الأسماء الأولى أو اختصاراتها فعنوان البحث (بين علامتي تنصيص) فاسم الدورية (تحته خط) فرقم المجلد، فرقم العدد فسنة النشر (بين قوسين) ثم أرقام الصفحات.

مثال: الحميدي، إبراهيم عبدالله. "الهجرة الداخلية في المملكة العربية السعودية حجمها واتجاهاتها." مجلة كلية الآداب، جامعة الملك سعود، م١٦، ع١ (٢٠٠٤م)، ١٠١-١٥١.

ب) الكتب: يشار إليها في المتن داخل قوسين مربعين مع ذكر الصفحات، مثال ذلك [٨، ص١٦]. أما في قائمة المراجع فيكتب رقم المرجع داخل قوسين مربعين متبوعاً باسم عائلة المؤلف ثم الأسماء الأولى أو اختصاراتها فعنوان الكتاب (تحته خط) فمكان النشر ثم الناشر فسنة النشر.

مثال: اليوسف، صالح سليمان. المشقة تجلب التيسير: دراسة نظرية وتطبيقية، الرياض: المطابع الأهلية للأوفست، ١٩٨٨م.

٩- ترفق جميع الصور والرسوم المتعلقة بالبحث في ملف مستقل.

١٠- ترقم الجداول والرسومات ترقيماً مستقلاً عن ترقيم البحث ويعنون الجدول بعنوان فوق الجدول والرسم بعنوان تحت الرسم.

١١- لا يعاد البحث إلى صاحبه سواء نشر أو لم ينشر.

١٢- يعطى الباحث نسختين من المجلة وعشرين مستلة من بحثه المنشور.

١٣- يلزم الباحث إجراء التعديلات المنصوص عليها في تقارير المحكمين، مع تعليل ما لم يعدل.

١٤- تعبر المواد المنشورة في المجلة عن آراء ونتائج مؤلفيها فقط.

عناوين المراسلة

E-mail: quecjour@qec.edu.sa

مجلة علوم الهندسة والحاسب، جامعة القصيم، المجلد (٣)، العدد (١)، ص ص ١-٧١ بالإنجليزية (يناير ٢٠١٠م / محرم ١٤٣١هـ)

المجلد الثالث العدد (١)

مجلة علوم الهندسة والحاسب

(يناير ٢٠١٠م) (محرم ١٤٣١هـ)

المجلة العلمية لجامعة القصيم

(مجلة محكمة)

Qassim University

جامعة القصيم

النشر العلمي والترجمة

بريدة - ص.ب. ٦٦٦٦ - ٥١٤٥٢

هيئة التحرير

رقم الإيداع : ٢٠٢٣ / ١٤٢٩

مجلة علوم الهندسة والحاسب، جامعة القصيم، المجلد (٣)، العدد (١)، ص ص ١-٧١ بالإنجليزية (يناير ٢٠١٠م / محرم ١٤٣١هـ)

المحتويات

صفحة